Received: 1 November 2021 | Revised: 8 December 2021 | Accepted: 22 December 2021

DOI: 10.1002/pol.20210810

REVIEW

JOURNAL OF POLYMER SCIENCE WILEY

Manning condensation in ion exchange membranes: A review on ion partitioning and diffusion models

David Kitto[1] | Jovan Kamcev[1,2]

[1]Department of Chemical Engineering, University of Michigan, North Campus Research Complex B28, Ann Arbor, Michigan, USA

[2]Macromolecular Science and Engineering, University of Michigan, North Campus Research Complex B28, Ann Arbor, Michigan, USA

Correspondence
Jovan Kamcev, Macromolecular Science and Engineering, University of Michigan, North Campus Research Complex B28, Ann Arbor, Michigan 48109 USA.
Email: jkamcev@umich.edu

Funding information
Basic Energy Sciences, Grant/Award Number: DE-SC0022040; Office of Science; U.S. Department of Energy; National Science Foundation, Grant/Award Number: DGE-1841052

Abstract

The rational design of ion exchange membranes (IEMs) is becoming more pertinent as their usage becomes broader and as their staple applications (i.e., electrodialysis, flow batteries, and fuel cells) improve in commercial viability. Such efforts would be catalyzed by an improved fundamental understanding of ion transport in IEMs. This review discusses recent progress in modeling ion partitioning and diffusion in IEMs in an effort to relate IEM performance metrics to fundamental membrane properties over which researchers and membrane manufacturers possess direct and sometimes precise control. Central focus is given to the Donnan-Manning model for ion partitioning and the Manning-Meares model for ion diffusion in IEMs. These two frameworks, which are derived from Manning's counter-ion condensation theory for polyelectrolyte solutions, have been widely used within the IEM literature since their recent introduction. To explore this topic, the mathematical derivation of both models is revisited, followed by a survey of experimental and computational discussions of counter-ion condensation in IEMs. Alternative models which fulfill similar roles in predicting IEM transport properties are compared. This review concludes by highlighting the uniquely favorable positions of the Donnan-Manning and Manning-Meares models and discussing their prospects as leading predictors of IEM partitioning and diffusive properties.

KEYWORDS

counter-ion condensation, ion activity, ion diffusion, ion exchange membranes, ion partitioning

1 | INTRODUCTION

Ion exchange membranes (IEMs) are an important class of polymeric materials which primarily see industrial use in water purification and energy storage/generation applications, such as electrodialysis (ED), reverse electrodialysis (RED), redox flow batteries (RFBs), and fuel cells.[1–7] IEMs have also been implemented in more diverse areas including drug delivery devices, food processing lines, and (bio)chemical reactors.[5,8,9] In all of these applications, IEMs are valued for their ability to enhance or impede the transport of species based not only on their size, but also on their ionic state. IEMs feature polymer backbones with covalently attached ionizable functional groups, which serve to expedite the transport of ions with opposing charge (counter-ions) while impeding that of those with similar charge (co-ions).

The usefulness of a single IEM is not universal. The various applications mentioned above have different performance needs, and so IEMs which prioritize the transport of different species are necessary.[3] For example, ED utilizes alternating cation and anion exchange membranes (CEMs and AEMs) to desalinate water; the cations

and anions must transport through the designated membrane but not the other.[3,5] Thus, ED requires membranes that enable counter-ion/co-ion selectivity. Comparatively, vanadium RFBs employ IEMs which allow catholyte and anolyte solutions to exchange charge balancing species (e.g., protons for CEMs and sulfate/bisulfate for AEMs) but not the redox active vanadium ions.[3,6] Vanadium RFBs therefore require AEMs with counter-ion/co-ion selectivity and CEMs with counter-ion/counter-ion selectivity. Beyond just ionic species, controlling the transport of neutral solutes can be important, such as with IEMs used in electrolysis cells. In one such case, electrocatalytic CO_2 reduction processes utilize AEMs to promote hydroxide transport but control the exchange of solvents and products such as water and ethanol.[7,9] Thus, these AEMs must exhibit both counter-ion/counter-ion selectivity and broader uncharged solute rejection. With such diverse necessities of IEMs, it has become essential that researchers parse these complex requirements down to fundamental membrane properties, which allow membrane scientists to understand how various desirable or undesirable behaviors arise.[10–14] Further developing this fundamental understanding will enable the rational design of new materials with improved performance and efficiency for any given application.

This review focuses on the interactions between IEMs and mobile ions, which is applicable in each of the situations mentioned above, and indeed in nearly every application involving IEMs. The membrane performance for the diverse systems employing IEMs can be quantified via several different metrics related to the transport rate and selectivity of the membrane. One may consider ion transport through IEMs as belonging to one of two categories: electrically-driven and concentration-driven. In a real system, both driving forces are present, but researchers typically simplify their experiments by applying just one primary motivator.[15] When the driving force for ion transport is an electric potential gradient, transport in IEMs is discussed in terms of ionic conductivity, κ, which is defined for a single electrolyte system as:

$$\kappa = \frac{-I}{\frac{\partial \Psi}{\partial x}} = \frac{F^2}{RT}\left(z_g^2 C_g^{m,t} D_g^m + z_c^2 C_c^{m,t} D_c^m\right) \quad (1)$$

Here, I is the current density, $\partial\Psi/\partial x$ is the electric potential gradient across the membrane, F is Faraday's constant, R is the ideal gas constant, T is the absolute temperature, and the remaining values are defined for either the counter-ion, $i = g$, or co-ion, $i = c$, in the membrane. These ionic properties are the ion valence, z_i, the ion diffusivity in the membrane, D_i^m, and the ion concentration in the membrane, $C_i^{m,t}$. Since the geometric area of the membrane is commonly used for flux calculations in experimental methods, the concentrations that appear in transport equations are similarly defined per the total membrane volume (t).[16] It is generally preferred that IEMs possess high ionic conductivities, which minimize any ohmic losses incurred by the membrane.

For applications with concentration gradient driving forces, the salt permeability coefficients of IEMs are generally discussed. Oppositely charged ions which diffuse down a concentration gradient will generate an electric field if they travel at different speeds, so the counter-ion and co-ion transport across the membrane is coupled through electroneutrality. The single salt (s) membrane permeability coefficient, P_s, defined as the steady-state salt flux normalized by the membrane thickness and the concentration difference across the membrane, is given by[15,17]:

$$P_s = K_s D_s^m = \left(\frac{C_s^{m,t}}{C_s^s}\right)\left(\frac{D_c^m D_g^m\left(z_c^2 C_c^{m,t} + z_g^2 C_g^{m,t}\right)}{z_c^2 C_c^{m,t} D_c^m + z_g^2 C_g^{m,t} D_g^m}\right) \quad (2)$$

where K_s is the salt partition coefficient, D_s^m is the salt diffusion coefficient in the membrane, C_s^s is the concentration of salt in the upstream solution, $C_s^{m,t}$ is the concentration of mobile salt in the membrane, and the remaining variables have already been defined. For fundamental studies of ion transport in membranes, the salt permeability is a useful tool to extract transport data.[17] However, in applied situations, the concentration gradient-driven permeation of salts (a process dominated by the minority/rejected species, the co-ion) is not prioritized; rather, it is preferable to minimize the salt permeability.

The second metric dictating the performance of IEMs is their transport selectivity. Perhaps the most common metric for quantifying IEM selectivity is the membrane permselectivity (Π). In ED, Π refers to the enhancement of counter-ion transport over co-ion transport due to the membrane[3,18]:

$$\Pi \equiv \frac{t_g^m - t_g^s}{t_c^s} \quad (3)$$

Here, Π is defined in terms of the transport numbers of species i in phase j, t_i^j (the phases being m for membrane and s for solution). The transport number refers to the fraction of current attributed to the conduction of species i. Defined per Equation (3), a membrane with $\Pi = 0$ conducts counter-ions and co-ions in the same proportion as in an aqueous solution, while a membrane with $\Pi = 1$ exclusively transports counter-ions. Because Π refers only to counter-ion/co-ion selectivity, a more general membrane selectivity α may be utilized[18]:

$$\alpha_{i/j} \equiv \frac{z_i^2 C_i^{m,t} D_i^m}{z_j^2 C_j^{m,t} D_j^m} = \frac{t_i^m}{t_j^m} \tag{4}$$

Here i and j can represent any two ionic species, with species i being the more permeable species. Similarly to the transport numbers defined above, $\alpha_{i/j}$ represents the ratio of current carried by species i to that carried by species j. When considering nonionic species or when the current is not the transport metric of interest, one may use the separation factor, $SF_{i,j}$[10]:

$$SF_{i/j} \equiv \frac{J_i^m / C_i^s}{J_j^m / C_j^s} \tag{5}$$

In this equation, J_i^m refers to the total cross-membrane flux of species i. As the broadest of these three selectivities, the separation factor enables applications like a CO_2 electrolysis module to consider the hydroxide to ethanol selectivity. Regardless of which metric is being used, membrane applications require IEMs with greater selectivity for their species of interest.

The motivation for modeling or correlating structure–property relationships lies in the complexity of IEM design. Researchers have targets in terms of conductivities and selectivities, which are related to the ionic concentrations and diffusivities in the membrane through the equations defined above. However, researchers can only directly modulate structural parameters like the charge density and the effective crosslinking density. Empirical trends have been established in the past, but this can lead to complex results and potentially mask the underlying fundamental phenomena. For example, higher ion exchange capacities (IECs) have been correlated with increased salt permeability coefficients,[19,20] but controlled studies have demonstrated that this permeability increase can be attributed to the elevated water content caused by adding such hydrophilic charge groups to the polymer backbone—when controlling for the water content, the trend is reversed.[21] A fundamental model based on the underlying physics of transport phenomena would pierce deeper than surface-level correlations and give confidence in predicting extrapolated data or saturation effects. This demand has motivated studies focused on the conceptual modeling of IEMs from a fundamental picture of membrane-ion interactions, which aim to replace empirical correlations based on studies of uncontrolled commercial membranes. Yet, for much of this field's history, a complete molecular understanding of ion partitioning and diffusion in IEMs has been elusive, and models have neither been entirely predictive nor quantitative.[10,11,13,14]

A model recently adapted from the adjacent polyelectrolyte literature has become promising for producing quantitative predictions of IEM partitioning and diffusion behavior: Manning's theory of counter-ion condensation.[15,17,22] Manning's model has been a staple in theoretical treatments of polyelectrolyte solutions since the 1970s, when the equations put forth by Manning succeeded in accurately describing the behavior of a wide range of dilute polyelectrolyte solutions and quantifying the critical-onset trends observed throughout the field.[23–28] Manning's limiting laws still see success in describing the behavior of polyelectrolytes today. Although not an obviously quantitative comparison, the behavior of IEMs has been frequently compared with that of polyelectrolytes. Many researchers had put forth ideas about counter-ion condensation as an explanation for some unintuitive behavior in IEMs.[29–37] The quantitative predictive power for IEMs was demonstrated only recently when Manning's equations were applied directly to ion partitioning data for several commercial IEMs.[38] This study exemplified good agreement between the membrane ion activity coefficients described by Manning's framework and those obtained from experimental ion partitioning data. Surprisingly, the thermodynamic behavior of densely charged IEMs appeared to be approximated well by the theory of dilute polyelectrolyte solutions, with only minor adjustments (which will be discussed in detail in the following section).

The IEM ion partitioning and ion diffusivity frameworks developed by Kamcev et al. have now been utilized widely and applied to a diverse set of materials. Some materials are indeed described poorly by the framework, and there is some dissent as to the use case and validity of the model, but many studies have also reported success in predicting experimental data using these frameworks. With the past 6 years of wider use in the field, some broader statements may now be made regarding the utility of Manning's counter-ion condensation model for IEMs. This review aims to analyze the predictive capabilities of the Donnan-Manning and Manning-Meares frameworks, highlight further developments made to these models (and still lacking in the models), and discuss their place among alternative models for quantifying ion concentrations and diffusion coefficients in IEMs. To do this, we will examine both the ion partitioning and ion diffusion frameworks of Manning's theory. We first reconstruct the mathematics and assumptions of the polyelectrolyte and IEM models, then turn to the broader literature's successes, failures, critiques, additions, and replacements for Manning's theory of counter-ion condensation as applied to IEMs.

2 | THE DONNAN-MANNING MODEL FOR ION PARTITIONING IN IEMS

2.1 | Model development

Manning's counter-ion condensation theory for polyelectrolyte solutions will be presented below, with abbreviated derivations but explicit equations. Manning's framework considers just two effects in polyelectrolyte solutions: long-range point-to-line electrostatic forces and the condensation of counter-ions directly resulting from those long-range forces.[23,26] With only these effects, Manning's theory predicts the colligative properties of dilute polyelectrolyte solutions remarkably well.[27] As per the subsequent discussion, the model also describes the ion activity and diffusion coefficients in IEMs, sometimes without adjustable parameters. This discussion follows the original works of Manning and then Kamcev et al. so that both the model and the adaptations may be highlighted.

2.1.1 | Manning's polyelectrolyte theory for counter-ion condensation

Before introducing the governing equations, we will highlight the assumptions used by Manning when developing the theory.[23] The polyelectrolyte solution is first simplified by applying a mean-field approximation. The counter- and co-ions are represented as point charges, and the polymer as a series of linear point charges. Finally, the solvent between polyelectrolyte chains is considered to provide enough shielding such that interactions between distant polymer chains are negligible. That is, relevant electrostatic forces on counter- and co-ions stem only from the closest polymer chain; mathematically, the spacing between polymer chains is greater than one Debye length,[39] $\kappa^{-1} = \left(4\pi\lambda_B \sum z_i^2 C_i\right)^{-1/2}$ (here λ_B refers to the Bjerrum length, which is discussed in greater detail at Equation (6)). In this way, the theory is analogous to the Debye-Hückel limiting law, which is considered to be exact for dilute aqueous salt solutions.[40] As a simplifying condition more than an assumption, the discussion is also limited to charged polymers with a single species of counter-ion and a single species of co-ion, though later publications have provided additional analyses which consider more complicated cases.[41,42]

Manning's theory is centralized about the reduced linear charge density of the polymer, ξ, and a critical value of such, ξ_{crit}.[23] Taken together, these two values quantify the extent to which nearby polymer fixed charge groups collaborate at attracting counter-ions. At $\xi/\xi_{crit} = 1/2$, nearest neighbors work in concert to attract a specific counter-ion; at $\xi/\xi_{crit} = 1$, next-nearest neighbors do; at $\xi/\xi_{crit} = 3/2$, this partnership reaches third nearest neighbors, and so forth (Figure 1). The two parameters may be defined for a polyelectrolyte per the following equations, based upon the polymer's mean linear charge-to-charge distance (b), the medium's dielectric constant (ε), the polymer fixed charge valence (z_A), and the counter-ion valence (z_g).

$$\xi = \frac{\lambda_B}{b} = \frac{e^2}{4\pi\varepsilon_0\varepsilon k_B T b} \tag{6}$$

$$\xi_{\text{crit}} = \frac{1}{|z_A z_g|} \tag{7}$$

In Equation (6), we define the Bjerrum length, λ_B, the protonic charge, e, the permittivity of free space, ε_0, the Boltzmann constant, k_B, and the absolute temperature, T. Because Manning's model was intended for dilute

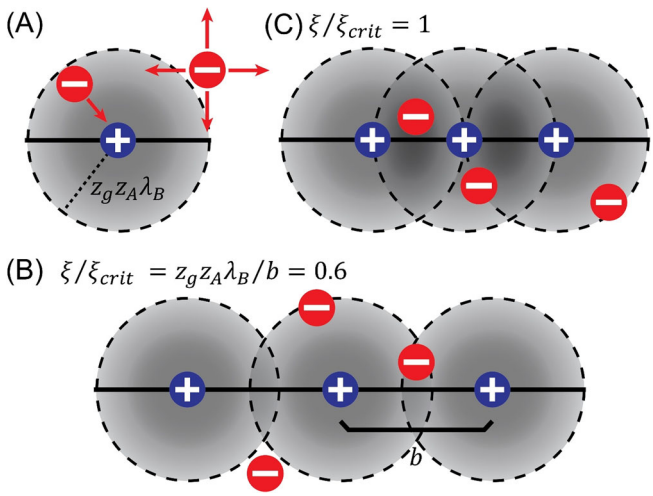

FIGURE 1 Simplified illustrations of cooperative counter-ion attraction by adjacent fixed charge groups on a polyelectrolyte chain. (A) Within a distance of $z_A z_g \lambda_B$, counter-ions must escape the attractive force of a fixed ion to diffuse away. In an isolated two-ion system, this energy barrier is not insurmountable, but does increase as the counter-ion approaches the fixed charge group. (B) When considering adjacent fixed charge groups along a polyelectrolyte, separated by a distance b, the system may exhibit regions of overlapping electrostatic influence. Beyond $\xi/\xi_{crit} = 0.5$, these overlapped regions create local minima of energy away from the fixed charge groups. (C) Beyond $\xi/\xi_{crit} = 1$, the region of adjacent electrostatic influence no longer overlaps away from the fixed charge groups, but at the location of the fixed charges. This implies that the local energy minima created by the overlap have intersected the absolute energy minima, deepening the energy well for counter-ions and resulting in condensation

systems, the value of ε was left as that of pure water at 25 °C, 78.5.[23] The Bjerrum length represents the separation distance at which electrostatic forces between two elementary charges are comparable in magnitude to the thermal energy scale,[40] which is how ξ derives the meaning of cooperative behavior described above. Because electrostatic forces scale with ion valences, ξ_{crit} is necessary to correct for the Bjerrum length's assumption of elementary (monovalent) species. With these parameters established, Manning's theory describes the consequence of more than two like-charged fixed ions acting together on a single point in space, $\xi > \xi_{crit}$. When this condition is met, some counter-ions condense onto the polymer backbone; that is, they become localized to a region extremely close to the polymer, no longer exhibit osmotic activity, and reduce the effective charge density of the polyelectrolyte.

Manning noted how prior studies identified this charge-overlap-density as a threshold beyond which infinitely many energy states come into existence along the polymer backbone—that is, the system becomes unstable (Figure 2).[23] This was accompanied by an abrupt shift in experimentally observed behavior: a critical onset phenomenon.[27] To negate this excess of polyelectrolyte charge, an oppositely charged polyelectrolyte must be superimposed atop the polymer, such that the net result is a system that does not exceed the unstable condition of $\xi > \xi_{crit}$; these opposing charges are comprised of the counter-ions. It is therefore based on this charge density instability that a fraction of counter-ions (f_c) condense, exiting the solution phase in favor of the polymer phase. The remaining fraction of counter-ions (f_u) are uncondensed and remain in the solution phase to maintain electroneutrality for a polymer at the net charge density of ξ_{crit}.

$$f_u = \frac{\frac{X\xi_{\text{crit}}}{\xi} + \nu_g\left|\frac{z_g}{z_A}\right|}{X + \nu_g\left|\frac{z_g}{z_A}\right|} \text{ for } \xi \geq \xi_{\text{crit}} \tag{8}$$

$$f_c = \frac{X\left(1 - \frac{\xi_{\text{crit}}}{\xi}\right)}{X + \nu_g\left|\frac{z_g}{z_A}\right|} \text{ for } \xi \geq \xi_{\text{crit}} \tag{9}$$

In these equations, ν_g is the number of counter-ions per added salt molecule and X is the ratio of the fixed charge group concentration to the added salt concentration ($X = C_A/C_s$). The equations are defined as fractions such that $f_u + f_c = 1$. In addition to merely avoiding the energy state instability, which was the methodology used in the original discussion (Figure 2),[23] Manning later defined these fractions in a process of free energy minimization.[26,43] The results are identical. From these equations,

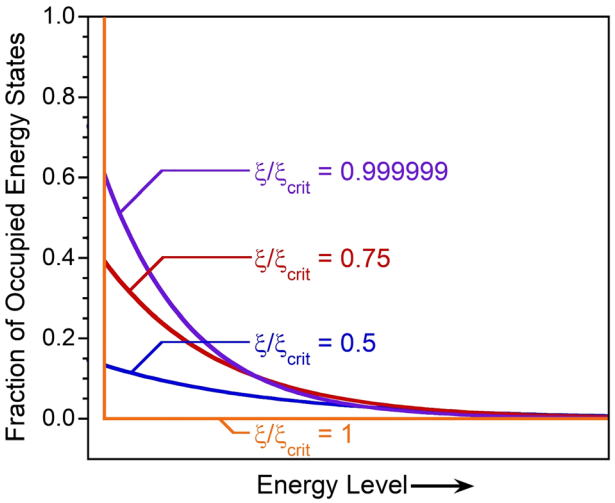

FIGURE 2 Distribution of counter-ion energy state occupation for a polyelectrolyte as it approaches the charge density threshold for condensation. As ξ/ξ_{crit} approaches the threshold for condensation, the counter-ions' occupations of energy levels shift to increasingly favor positions with low free energy, adjacent to the attractive and oppositely-charged fixed charge groups. In the limit of $\xi/\xi_{crit} \to 1$, exclusively low-energy states along the polymer backbone get occupied: A delta function at the minimum energy level. This singular occupation must continue until enough counter-ions condense to reach the condition $(\xi/\xi_{crit})_{effective} < 1$. This figure was generated by plotting Equations (4) and (5) from Manning's original manuscript[23] as Boltzmann distributions

the total number of condensed counter-ions is independent of the amount of added salt. Any additional counter-ions introduced by added salts merely dilute the fraction of counter-ions which are condensed. In real systems of polyelectrolytes, Manning notes that this behavior has proven reasonable up to moderate concentrations of ~0.1 M, although the number of condensed counter-ions is only independent of added salts in the dilute limit.[43]

Condensation describes the overall neutralization of the excess charge density of a polyelectrolyte. This includes all "site" bound ion pairing between the counter-ions and single fixed charge groups along the backbone (akin to traditional ion pairing), but also extends to "territorially" bound counter-ions which exist at intermediate points along the polymer backbone yet near no single fixed charge.[26] While it is reported that condensed divalent counter-ions exhibit a near-even split between these populations, condensed monovalent counter-ions heavily favor the territorial state over the site-bound one.[44] It has been observed that even some weakly charged polymers, below the threshold for condensation, still form site-bound ion pairs with some counter-ions.[45] Rather than contradicting condensation, this observation highlights how the two phenomena are complementary. That is, if a system favors site-bound ion

pairing, this neutralization still serves to reduce the charge density. Then, if ion-pairing equilibria still leave the polyelectrolyte beyond the dimensionless charge density (ξ/ξ_{crit}) of 1, further territorial condensation completes the process. In a pairing-dominated system, condensation does not play an additional role. In a condensation-dominated system, ion-pairing describes the distribution between site-bound and territorially bound counter-ions. Because we lack a way to quantitatively predict ion-pairing in general, Manning's condensation theory also lacks the means to describe distributions of territorial and site-bound condensed counter-ions.[26] As such, an implicit assumption in Manning's model is that ion pairing is not strong enough for the system to leave the condensation-dominated regime.

There is one primary difference between ion-pairing phenomena and condensation phenomena which may be observed through measurable polyelectrolyte solution properties. Ion pairing (or, when a fixed charge group is involved, ion adsorption) kinetics are expected to obey the law of mass action. Thus, the extent of ion-pairing would increase with increasing concentrations of mobile salts, which is consistent with the monotonic decrease in solution-phase electrolyte activity coefficients.[40,46] On the other hand, condensation is proposed to be driven by electrostatic effects which would not follow the law of mass action.[26] Electrostatic effects become shielded and weakened as salt concentrations increase, which yields an increase in mobile salt activity coefficients. This latter scenario is experimentally observed for IEMs and dilute polyelectrolyte solutions,[22,25,47–50] indicating that any framework for ion activity coefficients must derive from electrostatics or another driving force with similar concentration dependence.

The molecular difference between these two types of condensation rests in the inner hydration of the ions: the inner hydration of site-bound counter-ions is perturbed, while that of the territorially bound counter-ions remains intact.[26,44] This is perhaps best explained in terms of three populations, as connected by Fong et al.[51]: ions are either free (uncondensed), in a solvent-separated ion pair (territorially condensed), or in a contact ion pair (site-wise condensed). We also add that, as discussed by Manning,[39] not every counter-ion in close proximity to the polyelectrolyte should be considered condensed. Uncondensed counter-ions and co-ions still diffuse about in the surrounding solution, and may still approach the polymer chain, so long as they do so in a charge-neutral (coupled) manner. This behavior might even be expected, considering that the net charge on the polymer still opposes the counter-ions. Because the distance of approach does not distinguish the uncondensed and territorially condensed counter-ions, a more reliable distinction might be the ion's ability to diffuse freely away from the polymer or to exert osmotic pressure.

After accounting for condensation, the remainder of Manning's theory details the residual long-range point-to-line electrostatic forces, which Manning treated analogously to Debye and Hückel.[23] The assumptions and development follow the Debye-Hückel theory, but in a cylindrical geometry. This review details the ion activity coefficients obtained in this manner due to their relevance in discussing IEM properties (Section 2.1.2). For the more expansive set of polyelectrolyte solution colligative properties predicted by Manning, the reader is referred to the original publication.[23] Manning derived the point-to-line contributions toward a counter- or co-ion activity coefficient (γ_i) in a system without condensation as:

$$\ln\gamma_i = -\frac{1}{2} * \frac{\frac{\xi}{\xi_{crit}} X \left(\frac{z_i}{z_g}\right)^2}{X + \left|\frac{z_c}{z_A}\right| (\nu_g + \nu_c)} \text{ for } \xi \le \xi_{crit}, i = g; c \qquad (10)$$

In this equation, ν_c represents the number of co-ions per salt molecule. This equation was then modified for the case when counter-ion condensation occurs. With condensation, ξ is fixed to its effective value, ξ_{crit}. Then, X is replaced with its effective value, $X\xi_{crit}/\xi$, which is consistent with Equation (8). These substitutions have already been made in Equations (11) and (12), so ξ must be left as the true value in the equations that follow.

$$\ln\gamma_g = \ln f_u - \frac{1}{2} * \frac{X}{X + \frac{\xi}{\xi_{crit}} \left|\frac{z_c}{z_A}\right| (\nu_g + \nu_c)} \text{ for } \xi \ge \xi_{crit} \qquad (11)$$

$$\ln\gamma_c = -\frac{1}{2} * \frac{X \left(\frac{z_c}{z_g}\right)^2}{X + \frac{\xi}{\xi_{crit}} \left|\frac{z_c}{z_A}\right| (\nu_g + \nu_c)} \text{ for } \xi \ge \xi_{crit} \qquad (12)$$

The direct effects of condensation even in the calculation of these point-to-line effects highlight that condensation is not merely an effective decrease in concentration, like many other activity coefficient contributions. Rather, condensation entails a physical decrease in concentration as the condensed counter-ions leave the aqueous solution in favor of the polymer phase. For most purposes, this effect can be treated as part of the activity coefficient, as demonstrated in Equation (11). However, in the discussion of ion transport (Section 3.2) we discuss how this distinction may be an important consideration. It should also be emphasized that these equations only account for condensation and residual long-range point-to-line electrostatics. The equations may not be able to describe the

behavior of systems where other effects, such as solvation, short-range electrostatics, or point-to-point long-range electrostatics, measurably contribute to the free energy of the system.

Manning's model for counter-ion condensation has generally been received well in the polyelectrolyte literature. In addition to Manning's continued contributions, support, and developments regarding this theory,[27,28,39,52,53] researchers in this area still employ his model to describe polyelectrolyte behavior[42,54–57]—tracing the origin directly back to his mathematical derivation alongside contributions from Onsager[23,55] and Oosawa.[23,49,54] The theory is not universally accepted, but it does describe the behavior of an overwhelming number of polyelectrolyte systems.

2.1.2 | Manning's theory applied to IEMs

The possibility of counter-ion condensation has been invoked by several researchers to explain phenomena in IEMs.[29–37] To the best of our knowledge, the first quantitative application of Manning's model to describe ion activity coefficients in IEMs was by Kamcev, Paul, and Freeman.[38] The key connection between these two research areas is that IEMs are essentially polyelectrolytes constrained into a membrane geometry. Thus, the reasoning stood that the long-range Coulombic forces which govern the behavior of polyelectrolyte solutions could also play an important role in dictating the thermodynamics of IEMs.[22,38] While there are many similarities between polyelectrolyte solutions and IEMs, there are also several important differences that could complicate the direct application of Manning's model. Specifically, the calculation of ξ requires two values which may not be clearly known or directly measured for IEMs: b and ε.

The average distance between fixed charge groups, b, which is quite well defined for a polyelectrolyte homopolymer, is difficult to measure directly for an IEM. For a two-component copolymer (e.g., cross-linked IEM), b can be calculated from the theoretical or experimental IEC and knowledge of the membrane's molecular architecture.[38] Commonly, there are two monomer species which form a cross-linked IEM: a charged monomer and a bifunctional neutral cross-linker. For vinyl polymers, the projection length of a repeat unit is 2.5 Å, so the following equation has been used with reasonable success, neglecting any cross-linker geometry or functionality[58]:

$$b = 2.5\,\text{Å} * \left(1 + \frac{n_{xl}}{n_{ch}}\right) \tag{13}$$

Here, n_{xl} refers to the mole fraction of neutral crosslinker and n_{ch} refers to the mole fraction of charged monomer. Equation (13) assumes that the fixed charges are evenly distributed on the polymer backbone, so it should be appropriate for use in homogeneous IEMs. Some researchers have deviated from the definition given in Equation (13), so alternative approaches to calculating b are described in Section 2.2.1 alongside the accompanying results. Although there is currently no proven method of estimation, advanced structural characterization techniques may eventually enable precise experimental determination of b.

The mathematical treatment of ε is more complicated. The derivation of Manning's theory exclusively refers to long-range electrostatic forces, so the medium's average dielectric constant was originally used in Manning's development, which is consistent with a mean-field approximation.[23] The polyelectrolyte solutions considered by Manning were dilute, making the average dielectric constant simply that of water; this is not the case for IEMs, in which the polymer can occupy more than half of the total membrane volume. Even before discussing an appropriate value for ε, the concept of using the average ε for IEMs has been the subject of debate. Some researchers dispute the mean-field approximation, asserting that one or two molecules of water between ions does not merit invoking an average dielectric constant. The average dielectric constant is instead replaced with that of just the polymer.[45] However, the majority of researchers who have applied Manning's theory to predict the behavior of IEMs retain the use of an average dielectric constant. Because Manning's derivation considers exclusively long-range electrostatic forces ($\lambda_B = 7.14$ Å for the polyelectrolytes studied by Manning,[23] and is greater for membranes, for example, 13.4 Å in commercial membrane CR61[38]), but entirely neglects forces at play on length scales on the order of one or two water molecules (~3 Å), the continued use of the average dielectric constant seems to be appropriate.

Recently, average dielectric constants in charged and neutral polymer membranes have been experimentally determined by Geise et al. via broadband microwave dielectric relaxation spectrometry (Figure 3).[59–62] The results suggest that some membranes exhibit a co-continuous behavior, while other membranes behave as though they contain isolated water domains.[59,61] A cross-linked polymer network is continuous by definition, so for a membrane which swells with water, there should exist a singular transition from dispersed to co-continuous water phases as the water content in the membrane increases. IEMs typically contain higher water content (>30 vol%) than the materials discussed by Chang and Geise[61] (Figure 3), so it should be reasonable to use the co-continuous model for most cases in which direct measurements are unavailable[22]:

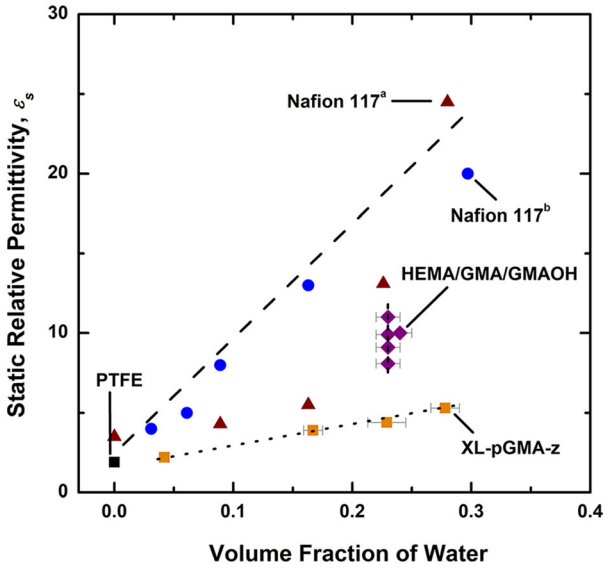

FIGURE 3 The dielectric constant (static relative permittivity) of various membranes plotted against the membrane water volume fraction.[61] The large dashed line represents the co-continuous model (Equation (14)). The small dashed line represents the Maxwell Garnett model for a dispersed water phase (Equation (15)). The full extent of the reported dielectric constant data fall on or between these two extreme cases. *Source*: Adapted with permission from Reference 61, 2020, American Chemical Society

$$\varepsilon = \varepsilon_p(1-\phi_w) + \varepsilon_w\phi_w \tag{14}$$

Here, ϕ_w is the membrane water volume fraction, while ε_p and ε_w are the polymer and water dielectric constants, respectively. In previous studies, ε_p has been given the approximate value of 6, while ε_w has been assigned the known value for pure water at 25 °C, 78.[38] It is worth noting that the membrane dielectric constant does not strongly depend upon the exact value used for the polymer dielectric constant at typical IEM water contents, due to the order-of-magnitude difference between reasonable values of ε_p and the known value of ε_w.[38] For membranes of exceptionally low water content or when water domains are dispersed, Chang et al. make use of the Maxwell Garnett model for a continuous polymer phase.[59] This model is presented below, though it has not yet been utilized in conjunction with Manning's equations.

$$\frac{\varepsilon-\varepsilon_p}{\varepsilon+2\varepsilon_p} = \phi_W\frac{\varepsilon_w-\varepsilon_p}{\varepsilon_w+2\varepsilon_p} \tag{15}$$

Predicting the dielectric constant of water-swollen polymer membranes is a complex task. There may be effects from the polymer chemistry beyond what the structural models reported above can detail because not every material follows one of these equations (Figure 3). Research which unveils a method to broadly describe dielectric constants of polymer membranes would be a substantial contribution to the field of theoretical IEM models, and indeed to the greater field of membrane science.

With the definitions of b and ε altered to better describe the structure of IEMs, the equations in Section 2.1.1 were applied to IEMs directly. The final note to make is that the quantity X, which remains clearly defined for polyelectrolytes, specifically refers to the fixed charge and sorbed salt concentrations within the membrane under any given volume scale. Two concentration scales are relevant for IEMs: the concentration defined per the volume of water within the membrane, w, or per the total volume of the membrane, t. The former is typically related to thermodynamic processes, whereas the latter is typically related to transport processes. The two concentration scales are related by the water volume fraction $\phi_w = C_i^{m,t}/C_i^{m,w}$. Here, the volume scale does not matter so long as the same choice is made for both quantities ($X = C_A^{m,w}/C_s^{m,w} = C_A^{m,t}/C_s^{m,t}$).[50] Having adjusted b, ε, and X, Kamcev et al. demonstrated that the ion activity coefficients for some homogeneous commercial IEMs could be described by Manning's theory. This application of Manning's model yielded reasonable agreement with the ion activity coefficients extracted from experimental ion partitioning results via a Donnan equilibrium analysis, a framework more typically used to describe ion activity coefficients in IEMs.[38]

Of greater interest than the agreement between these two frameworks was the ability to combine them to yield a predictive equation of ion partitioning in IEMs. Thus, the expressions from Manning's theory for ion activity coefficients were inserted into the equation for nonideal Donnan equilibrium, given below[22]:

$$\left(a_g^s\right)^{\nu_g}\left(a_c^s\right)^{\nu_c} = \left(a_g^m\right)^{\nu_g}\left(a_c^m\right)^{\nu_c} \text{ or}$$
$$\frac{\left(C_g^{m,w}\right)^{\nu_g}\left(C_c^{m,w}\right)^{\nu_c}}{\nu_g^{\nu_g}\nu_c^{\nu_c}\left(C_s^s\right)^{(\nu_g+\nu_c)}} = \frac{\left(\gamma_\pm^s\right)^{(\nu_g+\nu_c)}}{\left(\gamma_g^m\right)^{\nu_g}\left(\gamma_c^m\right)^{\nu_c}} = \Gamma \tag{16}$$

In this definition, a_i^j represents the activity of the counter- or co-ion in the solution or membrane phase, C_s^s represents the salt concentration of the equilibrating solution, and $\gamma_\pm^s$ represents the mean activity coefficient of the salt in the external solution. Γ is an ideality ratio: setting it equal to 1 is to claim that ions within the membrane are exactly as nonideal as those in the contiguous solution. This assumption of $\Gamma = 1$ has led to very poor agreement between modeled and experimental sorbed salt concentrations in IEMs.[2,22,38,48,63–67] For a more informed value of Γ, the well-established Pitzer model was used for

solution-phase ion activity coefficients[68–70] alongside Manning's theory for membrane ion activity coefficients. Upon enforcing electroneutrality ($-z_g C_g^{m,w} = z_c C_c^{m,w} + z_A C_A^{m,w}$), Equation (16) implicitly defines the co-ion concentration in terms of the membrane properties and the external experimental conditions. Thus, the co-ion and counter-ion concentrations in an IEM equilibrated with an aqueous solution of a single electrolyte can be predicted through the Donnan-Manning model.

The discussion and equations to this point have remained generalized to any polyelectrolyte or membrane, any counter-ion, and any co-ion. For simplicity, the assumption of a 1:1 electrolyte and a membrane with monovalent fixed charge groups is introduced. Mathematically: $|z_A| = |z_g| = |z_c| = \nu_g = \nu_c = \xi_{crit} = 1$. This limiting case yields the following expressions as simplified versions of the equations from this section:

$$f_u = \frac{\frac{X}{\xi}+1}{X+1} \text{ for } \xi \geq 1 \tag{17}$$

$$\ln\gamma_i^m = -\frac{1}{2} * \frac{\xi X}{X+2} \text{ for } \xi \leq 1, i = g;c \tag{18}$$

$$\ln\gamma_g^m = \ln f_u - \frac{1}{2} * \frac{X}{X+2\xi} \text{ for } \xi \geq 1 \tag{19}$$

$$\ln\gamma_c^m = -\frac{1}{2} * \frac{X}{X+2\xi} \text{ for } \xi \geq 1 \tag{20}$$

$$\frac{C_c^{m,w}}{C_s^s} = \left(\left(\frac{C_A^{m,w}}{2C_s^s} \right)^2 + \frac{\gamma_\pm^{s\,2}}{\gamma_g^m \gamma_c^m} \right)^{\frac{1}{2}} - \frac{C_A^{m,w}}{2C_s^s} \tag{21}$$

In these more explicit forms, it is immediately apparent how Manning's theory may be used to predict the concentration of co-ions within an IEM. Once ξ has been calculated, the inputs of the model are: the fixed charge concentration, the external salt concentration, and the salt activity coefficient of the external solution ($C_A^{m,w}$, C_s^s, and $\gamma_\pm^s$). It should be noted that through the activity coefficient dependence on X, Equation 21 is still implicit in $C_c^{m,w}$ and must be solved numerically.

As will be discussed in Section 2.2, this framework has proven remarkably successful as a tool for predicting ion partitioning between an IEM and aqueous solution containing a single electrolyte. However, some researchers have had better success describing the data than predicting it. Collecting experimental ion partitioning data has allowed ξ to be fit from data. Once calibrated in this way, other experimental conditions may be successfully predicted based on the fitted value of ξ.[71] This is because the membrane's fixed charge spacing, b, does not vary as the external salt concentrations, counter-ion forms, and membrane water contents change. Thus, even when the a priori predictions are inadequate, the functional form of the Donnan-Manning model may still be useful.

2.2 | Experimental ion partitioning studies

As it has been defined in Section 2.1, or with minimal modification, the Donnan-Manning model has been used to describe ion partitioning in a wide variety of IEMs. Electrolytes have been varied as well to exemplify the ability of the framework to accommodate counter- and co-ion valence and identity. Below, we discuss these sets of data organized primarily by the type of membrane: commercial membranes are discussed Section 2.2.1, followed by laboratory prepared membranes of exactly known monomer composition in Section 2.2.2. Membranes with characterized heterogeneity are discussed in Section 2.2.3. The Donnan-Manning model uses average fixed charge spacing values (b) and a mean-field approximation, so the framework is expected to capture the behavior of homogeneous materials more accurately than heterogeneous materials. The studies in Section 2.2.3 discuss the extents of phase separation and the length-scales at which ordered structures seem to be relevant, as well as what modifications can be made to account for the heterogeneities and improve agreement between the model and experimental results.

Researchers have compared the predicted and experimental values of either ion activity coefficients, calculated from the nonideal Donnan equilibrium framework, or ion concentrations in the membranes. In some cases, the salt partition coefficients, which are ion concentrations in the membrane normalized by ion concentrations in the external solution, are also discussed. When comparing between data sets, it is important to remember the distinction between these modes of presentation. Most importantly, errors of over 100% in activity coefficients may still lead to accurately predicted ion concentrations in IEMs at low external solution salt concentrations. Agreement between predicted and experimental membrane ion activity coefficients indicates agreement between predicted and experimental membrane ion concentrations as a rule. However, the inverse is not always true. A good example of this effect may be found in the CR61 data set discussed below (Figure 4A,B).[22,38]

2.2.1 | Ion partitioning in commercial membranes

The original introduction of the Donnan-Manning model by Kamcev et al. focused on three composite membranes

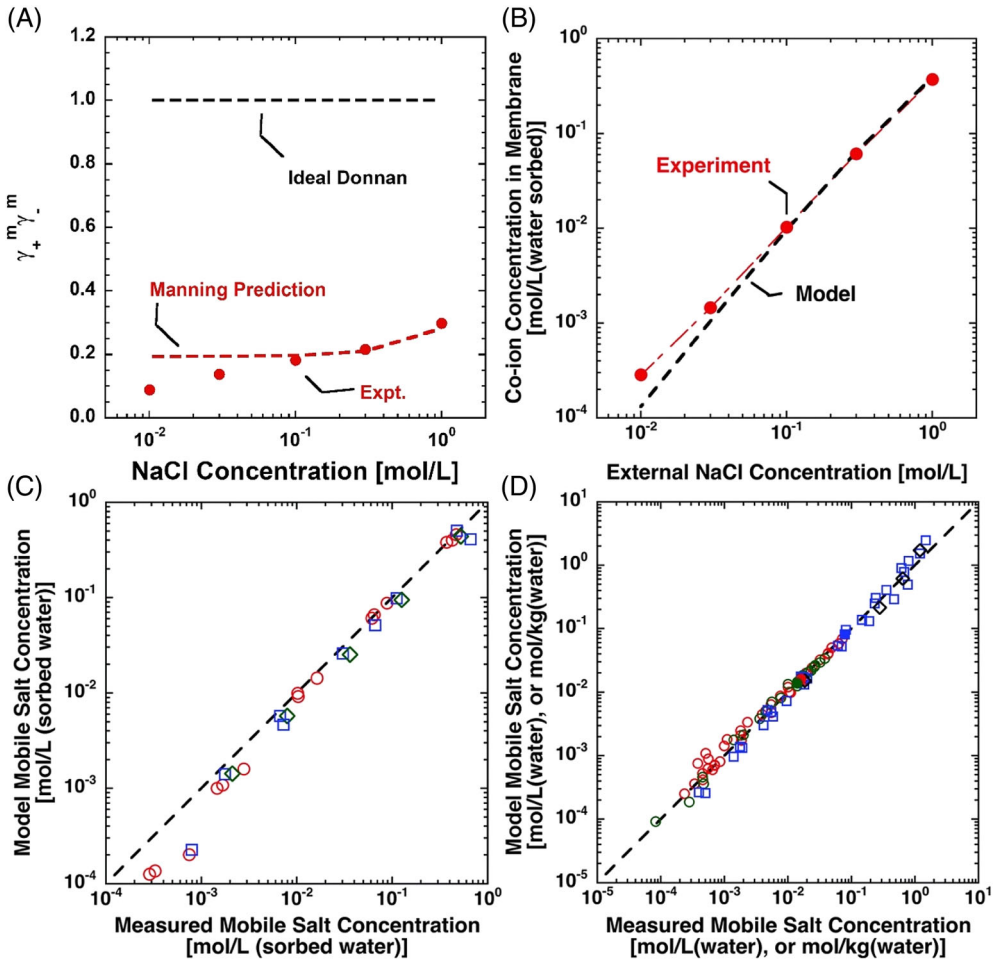

FIGURE 4 Comparison between predicted and experimental ion partitioning data for commercial charged polymers (membranes and resins).[22,38] (A) NaCl activity coefficients in CR61 cation-exchange membrane versus external solution NaCl concentration. The symbols represent experimental ion partitioning data analyzed via the nonideal Donnan model. (B) Co-ion concentrations in CR61 versus external solution NaCl concentration. The red symbols and line represent the experimental data, while the black line represents the predictions of the Donnan-Manning model. (C) Parity plot of modeled mobile salt concentrations within IEMs versus the same value measured experimentally. The membranes are CR61, AR103, and AR204. NaCl data are depicted in red, $MgCl_2$ in blue, and $CaCl_2$ in green. D) Parity plot of modeled mobile salt concentrations in charged polymers, produced semi-predictively with the Donnan-Manning model, against the reported experimental values. The filled symbols represent data points used to fit ξ, and the empty symbols represent data predicted using the fitted value of ξ. A) *Source*: Adapted with permission from Reference 38, 2015, American Chemical Society. B, C, D) Adapted with permission from Reference 22, 2016, Royal Society of Chemistry

(styrenic CR61, styrenic AR103, and methacrylic AR204) equilibrated with 0.01 to 1 M NaCl, $MgCl_2$, and $CaCl_2$ solutions.[22] The ion-exchange phase of these IEMs is presumed to be reasonably homogeneous. Excellent agreement was observed between the predicted and measured co-ion concentrations in IEMs equilibrated with relatively highly concentrated salt solution (Figure 4). At lower salt concentrations, the agreement worsened, but was still reasonable and significantly improved over model predictions with the assumption $\Gamma = 1$. Partitioning experiments at such low concentrations present additional difficulties, because a minute concentration is being measured. This phenomenon has been well documented in older ion exchange resin studies, where incomplete separation of the resin and aqueous solution or contamination have led to an underrepresentation of experimental ion exchange resin ion activity coefficients.[72–75] When more precise experimental techniques were utilized, experimental data analyzed with the Donnan model exhibited a plateau in ion activity coefficients below 0.1 M, similarly to that predicted by the Manning model. Thus, it is critical that researchers perform these experiments with great attention to detail when dealing with dilute salt solutions.

This collection of data supported the assumptions that the membrane dielectric constant was well approximated

by the volume-weighted co-continuous model (Equation 14) and that the fixed charge groups were evenly dispersed within the membrane's ion exchange phase. The model was also tested against two sets of ion partitioning results for various resins and membranes reported in the open literature. Incomplete characterization of these materials necessitated using ξ as a fitting parameter. Kamcev et al. applied the Donnan-Manning model semi-predictively, wherein ξ was fit from a single (in this case, randomly selected) data point and then used to predict the remaining partitioning data, as illustrated in Figure 4D. Thus, the Donnan-Manning model was used to (semi-) predictively describe ion partitioning in many densely-packed and densely-charged polymeric materials.

The Freeman and Paul groups have continued their studies on these commercial membranes by collecting a more extensive set of ion partitioning data for the CEM, CR61.[47,76,77] Galizia et al. investigated ion partitioning in CR61 equilibrated with LiCl, NaCl, KCl, $MgCl_2$, and $CaCl_2$ solutions with concentrations ranging from 0.01 to 1 M.[77] The agreement between predicted and experimental membrane co-ion concentrations for NaCl and KCl was quantitative at higher salt concentrations (0.1–1 M), but poorer at salt concentrations lower than 0.1 M. The reverse was true for LiCl, where the greatest deviation between model and experiment was at 1 M. The agreement between modeled and experimental data for $MgCl_2$ and $CaCl_2$ was reasonable over the entire salt concentration range considered. In a separate study, Galizia et al. also investigated the effect of co-ions on the sorption of sodium halide salts (NaCl, NaF, and NaI).[76] This study demonstrated that the co-ion identity had little effect on co-ion partitioning in CR61, as predicted by the Donnan-Manning model. The collection of results reported by Galizia et al. for these varied counter-ions and co-ions are reproduced in Figure 5.

Galizia et al. also studied NaCl and $CaCl_2$ sorption in CR61 at concentrations considerably higher than 1 M, which are relevant for applications involving brines.[47] Because Manning observed that his polyelectrolyte model functioned well up to 0.1 M of added salt,[43] the Donnan-Manning model would also be expected to lose its accuracy under concentrated conditions where the salt concentration in the membrane exceeds 0.1 M. The Donnan-Manning model provided an excellent prediction of the membrane co-ion concentrations for concentrated NaCl brines up to 5 M of external salt, but greatly over-predicted sorption of $CaCl_2$ brines between 1 and 6 M (Figure 6). The discrepancy between modeled and experimental data persisted despite accounting for corrections to ξ based on the significant osmotic de-swelling of the IEM at high salt concentrations, which altered the predicted dielectric constant of the membrane. The authors suggested that effects beyond the electrostatic interactions present in the Manning model may be responsible for the worsened model-experiment agreement in the $CaCl_2$ data. Point-to-point electrostatics between mobile ions (including ion pairing) are neglected in Manning's framework, but could be significant, especially for divalent ions. This is consistent with the expansive model-experiment agreement for NaCl but not $CaCl_2$, meaning that Figure 6A is encouraging for applications of the Donnan-Manning model to concentrated electrolytes containing monovalent species.

The Donnan-Manning model has also been utilized by other researchers to describe ion partitioning in IEMs. Although predicted values of ξ were not included, Kingsbury et al. employed the Donnan-Manning model across a broad library of 20 commercial IEMs equilibrated with 0.5 M NaCl.[78] They sought to semi-predictively model the partitioning behavior of these IEMs at 4 M, although these predictions were not experimentally verified. This survey includes many common commercial IEMs and significantly widens the scope of membranes studied through the Donnan-Manning model. Many highly-charged, low-water-content membranes were involved in this study, representing IEMs for which some of the assumptions going into the Donnan-Manning model are invalid. Nevertheless, the one-point fit at 0.5 M succeeded in describing the sorption data of each membrane. The values of ξ for the IEMs studied by Kingsbury et al. were generally greater than 1, so the overwhelming majority of these commercial IEMs are expected to exhibit counter-ion condensation. From these results, the reported average value of $\xi \approx 2$ may be taken as a rough first-approximation for commercial IEMs when theoretical calculations of ξ are not possible. Indeed, this one-size-fits-all approximation of $\xi = 2$ has been used in another application of the Donnan-Manning framework: Hassanvand et al. accurately predicted the performance of a membrane capacitive deionization unit equipped with IEMs CMX and AMX based on this approximation.[79]

Another study by the Coronell group expanded the scope of the Donnan-Manning model in both membrane and electrolyte identity.[80] Wang et al. applied the framework predictively to the active layer of SWC4+, a commercial reverse osmosis (RO) membrane. RO membranes are generally less ionizable and more complexly structured than IEMs.[81] To account for the unknown membrane structure, the authors utilized the fixed charge concentration ($C_A^{m,w}$) rather than the monomer geometry to estimate b (and subsequently ξ). This calculated value of ξ was utilized to predict salt partition coefficients in SWC4+ membranes equilibrated with LiCl, NaCl, KCl, RbCl, and CsCl solutions over the concentration range of 0.1 to 1 M. The predictions of the Donnan-Manning model did not agree with the experimental values for all

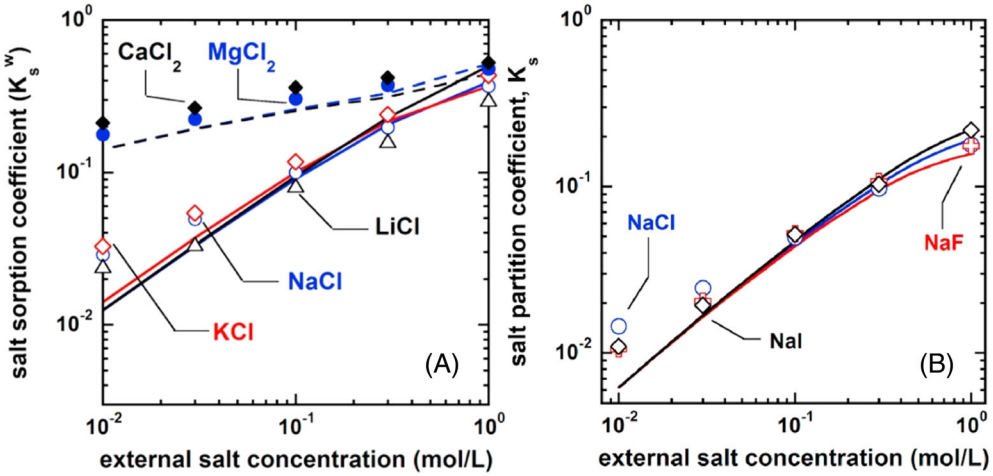

FIGURE 5 The salt sorption/partition coefficients of various salts in CR61 as a function of external salt concentration, as reported by Galizia et al.[76,77] The symbols represent experimental data, while the lines represent predictions by the Donnan-Manning model. *Source*: Adapted with permission from References 76,77, 2017 and 2020, Elsevier

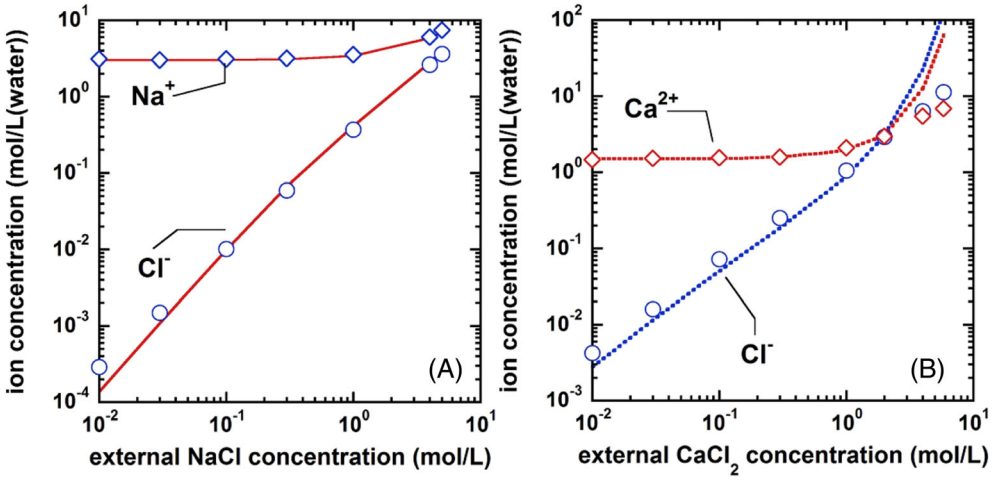

FIGURE 6 Equilibrium ion concentrations in CR61 versus external solution concentrations of (A) NaCl and (B) $CaCl_2$. The symbols represent the experimental results and the lines represent predictions of the Donnan-Manning.[47] *Source*: Adapted with permission from Reference 47, 2019, Elsevier

of these alkali salts (Figure 7). The model predictions were accurate for NaCl and, to an extent, for KCl, but were far less accurate for LiCl, RbCl, and CsCl. Though different in the magnitude of agreement, these data from Wang et al.[80] agree with that previously discussed by Galizia et al.[77] in that LiCl behaves differently from NaCl and KCl. Considering that RO membranes are significantly different from both polyelectrolytes and IEMs, it is remarkable that some salt partitioning behavior was predicted so well.

The Kentish group has investigated the partitioning of various electrolytes in a small host of commercial IEMs: Neosepta membranes CMX, CSE, AMX, and ASE (Figure 8).[82] This is another set of highly-charged, low-water-content IEMs, so the applicability of the Donnan-Manning model for these materials is of great interest. Chen et al. examined two monovalent and one divalent counter-ion for each membrane, holding the co-ion constant (NaCl, KCl, and $CaCl_2$ for the CEMs and NaCl, $NaNO_3$, and Na_2SO_4 for the AEMs). The experiments were performed over an external concentration range of 0.1–1 M. ξ was treated as an adjustable parameter, but the electrolyte

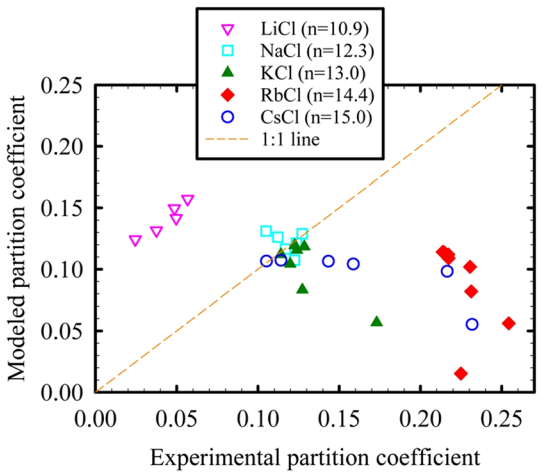

FIGURE 7 Parity plot of the partition coefficients predicted by the Donnan-Manning model and the experimentally measured values for salts equilibrated with SWC4+ reverse osmosis membrane.[80] The legend lists salt hydration numbers used for quantifying ion sorption in the membrane via the gravimetric method employed by the authors. *Source*: Adapted with permission from Reference 80, 2017, American Chemical Society

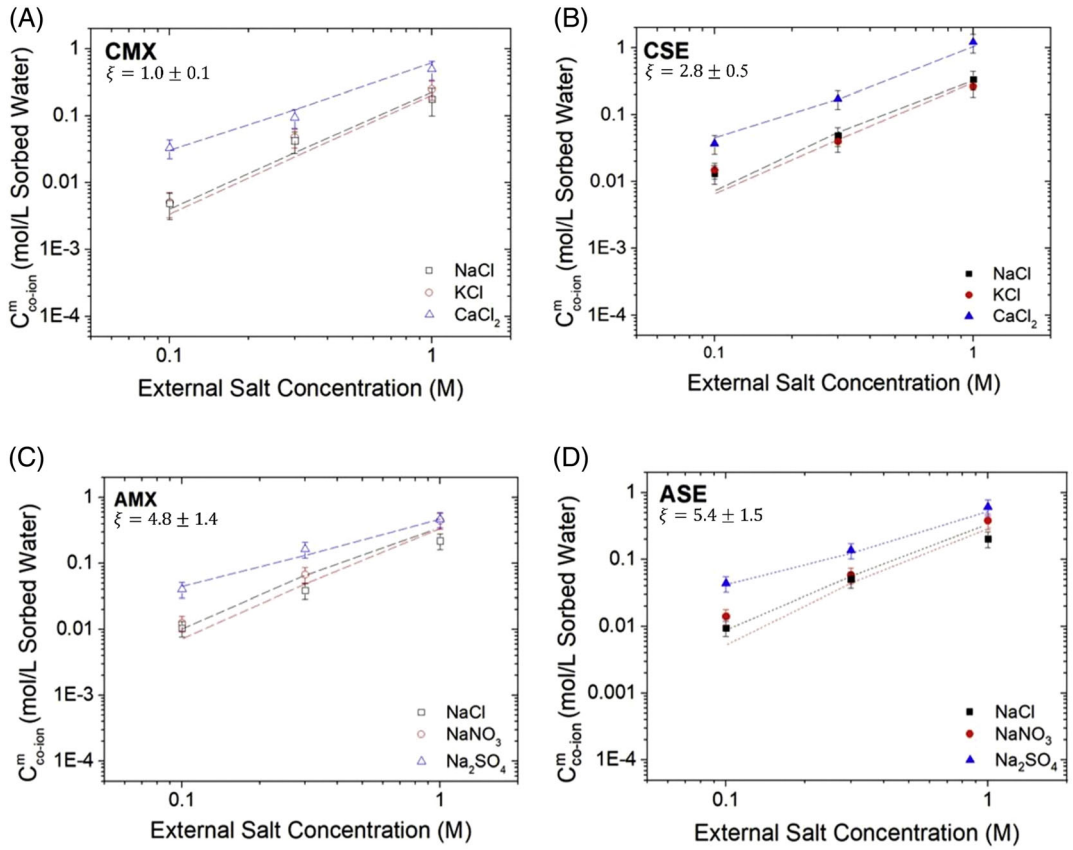

FIGURE 8 Equilibrium co-ion concentrations in Neosepta membranes versus external solution salt concentration.[82] (A) CMX and (B) CSE were characterized with NaCl, KCl, and $CaCl_2$ solutions. (C) AMX and (D) ASE were characterized with NaCl, $NaNO_3$, and Na_2SO_4 solutions. The symbols represent experimental results while the lines represent predictions from the Donnan-Manning model. All nine data points for each membrane were optimized simultaneously to produce the reported model results. *Source*: Adapted with permission from Reference 82, 2020, Elsevier

data were taken together such that a single value was used for each membrane's three data sets. This optimization led to reasonable agreement for all nine data points for each membrane. These results demonstrated that ion partitioning in each of these four membranes could be accurately described by a single ξ value. In review, we add that the fitted ξ values for CMX and AMX was similar to the values reported by Kingsbury et al.[78] Chen et al. also noted that the ξ values are larger for the next-generation Neosepta membranes (CSE and ASE) than the previous generation IEMs (CMX and AMX), suggesting that counter-ion condensation may play a larger role in these more recently developed membranes.

The Kentish group has also studied the partitioning of organic acid salts into commercial AEMs, AR103, and AR204. Sodium acetate (NaAc) and sodium lactate (NaLa) partitioning data were produced by Wang et al. over an external concentration range of 0.1–1 M with the intention of testing the Donnan-Manning model's applicability to ions common for food processing applications (Figure 9).[83] The NaLa data were well predicted by the Donnan-Manning model using the theoretical values of ξ, with a small improvement possible by treating ξ as an adjustable parameter. Meanwhile, the NaAc data were significantly overestimated by the predictions of the Donnan-Manning model. However, a fitted value of ξ, which was below ξ_{crit}, described the NaAc data well. The authors suggested that the failure of the model to predict partitioning in the presence of Ac^- may be a result of specific interactions between the ions which are unaccounted for in Manning's model, such as Ac^- dimer formation. In general, the behavior of many complex ions are subject to additional interactions and reactions, so the inability of the purely electrostatic Donnan-Manning model to predict such results is not surprising.

2.2.2 | Ion partitioning in laboratory prepared membranes

The Donnan-Manning model has also been tested with membranes of known monomer composition and no fabric backing, both of which simplify the calculation of

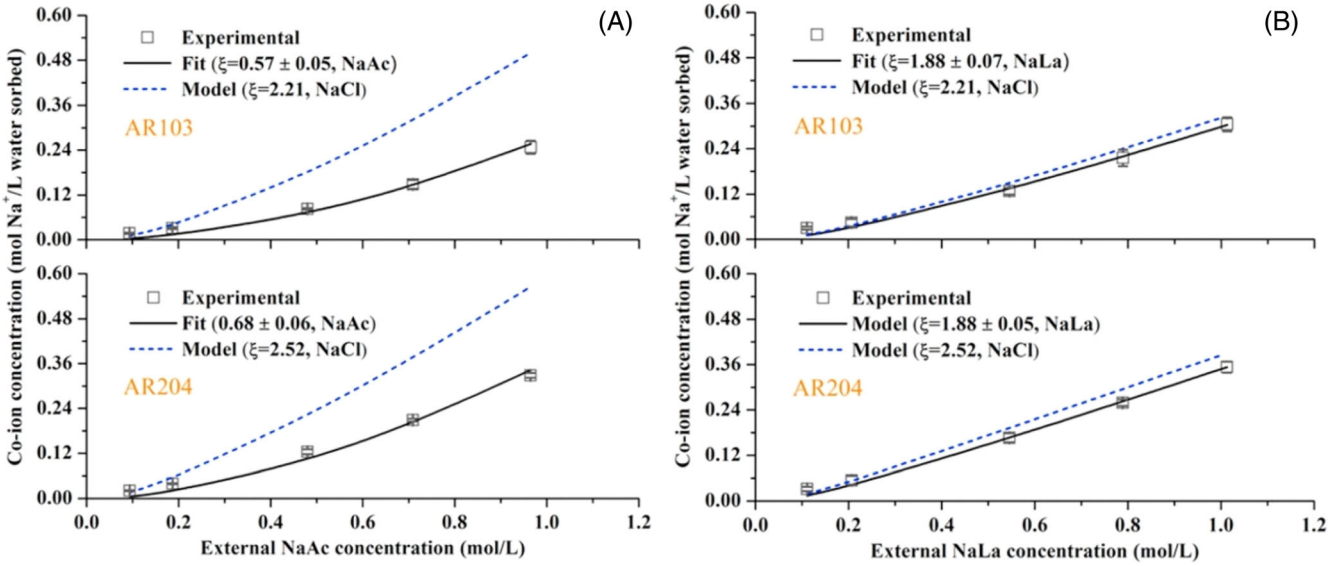

FIGURE 9 Equilibrium co-ion concentration versus external solution salt concentration for anion-exchange membranes, AR103 and AR204, equilibrated with (A) sodium acetate (NaAc) and (B) sodium lactate (NaLa) solutions.[83] The symbols represent experimental data, the dashed lines represent the co-ion concentrations predicted by the Donnan-Manning model, and the solid lines represent the co-ion concentrations calculated from the Donnan-Manning model with ξ as a fitting parameter. *Source*: Adapted with permission from Reference 83, 2020, Elsevier

parameters such as ε and b. Yu et al.[84] applied the Donnan-Manning model to NaCl sorption data in the expansive set of 2-acrylamido-2-methylpropane sulfonic acid (AMPS) poly(ethylene glycol diacrylate) (PEGDA) crosslinked CEMs synthesized by Yan et al.[48] These membranes range from minimally charged (0 and 0.6 mol% charged monomer) to highly charged (65 mol % charged monomer) to allow for a systematic investigation of ion partitioning in IEMs with varied charge density. The authors demonstrated that the theoretical values for ξ, calculated from the polymer backbone compositions through Equation (13), yield poor prediction of ion partitioning in all of the IEMs. Fitting the data for their most charged membrane to the model yielded good agreement, but produced a ξ value below the threshold of condensation, $\xi_{fit} = 0.327$, as opposed to the theoretical value of $\xi_{theor} = 2.52$. Yu et al. scaled their predicted ξ values for other membranes to the same extent (ξ_{fit}/ξ_{theor}) to semi-predictively model the remaining IEMs in the series. They report that this procedure did not yield accurate predictions of ion sorption in the lesser-charged IEMs (Figure 10). Yu et al. concluded that the Donnan-Manning model's failure to predict the data in membranes of such low charge density derives from not accounting for the nonideal effects most relevant to these systems. The authors corrected for additional nonideal effects by establishing the peNRTL model, which is discussed among the alternative models in Section 2.4.

The Geise group has also studied AMPS-PEGDA membranes to probe the effect of co-ion identity on ion partitioning in the IEMs. Ji et al. characterized ion partitioning in the membranes equilibrated with NaCl, NaBr, $NaNO_3$, and $NaClO_4$ at 0.1 and 0.5 M external solution concentrations.[85] These membranes contained 50 mol% of AMPS and PEGDA, making them comparable to the second-most densely-charged IEM studied by Yan et al.[48] The authors reported reasonable agreement between the Donnan-Manning model and the experimental partitioning data for NaCl, but the model increasingly under-predicted the experimental results as the size of the anion increased. This data set is unique because, among these four co-ions, the identity of the co-ion strongly affects the partitioning behavior, as opposed to the sodium halides (NaF, NaCl, and NaI) studied by Galizia et al.[76] The differences for NO_3^- and ClO_4^- may be due to their nature as large multi-atom anions, but Br^- would have been expected to be consistent with the other halide ions, suggesting that a more complex description may be necessary to understand co-ion identity effects. Any co-ion dependence of ion partitioning properties leads to an inherent error in the Donnan-Manning model: Manning's equations give no consideration to co-ion size, so they predict identical behavior for any co-ion of a given valence. With this study, it is important to note that the authors calculated the fixed charged group spacing using a different methodology from that presented in Section 2.1. Ji et al. considered the geometry of the cross-

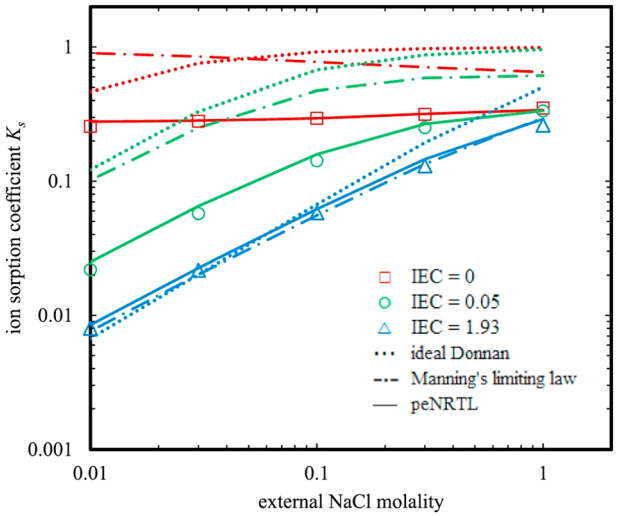

FIGURE 10 Ion sorption coefficients versus external solution NaCl concentration for three AMPS-PEGDA membranes that differ in IEC.[48,84] The symbols represent the experimental data. The dotted lines represent the ideal Donnan model, the dashed lines represent the Donnan-Manning model, and the solid lines represent the peNRTL model (discussed in Section 2.4). The ξ value for the membrane with IEC = 1.93 meq/g was fitted, while the ξ values for the other two membranes were scaled down for semi-predictive use. *Source*: Reproduced with permission from Reference 84, 2021, Elsevier

linker, in an attempt to give a more realistic estimation of b. AMPS and long-chain ($n = 10$ or $n = 13$) PEGDA possess very different sizes and contour lengths, so the relatively simple Equation (13) may not be appropriate for this set of monomers. This consideration is perhaps the reason that Ji et al.'s[85] AMPS-PEGDA sorption data was predicted much more accurately than Yu et al.'s,[84] who had used the standard, size-indifferent calculation method for b.

The Geise group brought a second major contribution toward assessing the utility of the Donnan-Manning model: direct measurement of the hydrated membrane dielectric constant (Figure 11). As was discussed in Section 2.1.2, studies by the Geise group suggested that Equation (13) is not universally applicable.[59,61] This conclusion was further illustrated by Chang et al.'s work with sulfonated polysulfone membranes.[60] The authors directly measured the dielectric constant of 6 different membranes with water volume fractions between 0.13 and 0.25, finding that the measured dielectric constants were ~ 3× smaller than values that would have been predicted by Equation (13). Similarly, the authors found very poor agreement between their experimental data and the Donnan-Manning model predictions made for 1 M NaCl partitioning using these true, experimentally measured dielectric constants. Predicted co-ion concentrations were an order of magnitude larger than those measured for the 1 M NaCl equilibrated sulfonated polysulfone membranes. Chang et al. cite the abnormally low water uptake as a potential reason for this failure to predict their sorption data accurately, raising concern that dispersed water domains may lead to heterogeneous distribution of charge groups and an invalidation of their estimated b value.

2.2.3 | Ion partitioning in heterogeneous membranes

This section discusses application of the Donnan-Manning model to predict ion partitioning in heterogeneous IEMs. The most widely studied of such membranes is Nafion 117, which features a phase separated morphology of hydrophilic and hydrophobic domains.[86] Kamcev et al. tested the predictions of the Donnan-Manning model on Nafion 117 HCl partitioning data taken from the literature[32] alongside the first predictive demonstration of the Donnan-Manning model.[22] Using an average value of b which does not account for the phase-separated morphology of Nafion 117 provided a poor prediction of the reported HCl partitioning results, but an amended b value for just the aqueous domains led to good agreement between the Donnan-Manning predictions and the literature data (Figure 12). This first example of modeling microscopically heterogeneous materials with the Donnan-Manning model illustrated that, with an accurate description of the phase separation behavior, ion partitioning in these complex materials could be predicted accurately.

The Donnan-Manning model has been applied to describe partitioning of a greater variety of acids in Nafion 117. Applications such as vanadium redox flow batteries rely heavily on proton transport in CEMs, so Peng and Zawodzinski studied the partitioning of HCl and HBr in Nafion 117 as well as H_2SO_4 in Nafion 117 and 3M825 perfluorinated ionomers.[87] The authors utilized the same value of b that was used by Kamcev et al.,[22] but performed the sorption experiments over an extremely broad concentration range (0.5–16 mol kg^{-1} for HCl, 0.5–6 mol kg^{-1} for HBr, and 0.5–12 mol kg^{-1} for H_2SO_4), pushing the upper concentration limit far beyond any previous study making use of the Donnan-Manning model. For the monoprotic acids at moderate concentrations, the membrane ion activity coefficients measured through the Donnan model were slightly above the Manning model's predicted values. At high concentrations, the model severely underpredicted the experimental membrane ion activity coefficients. The experimental and predicted high-concentration activity coefficient trends are fundamentally different: the data

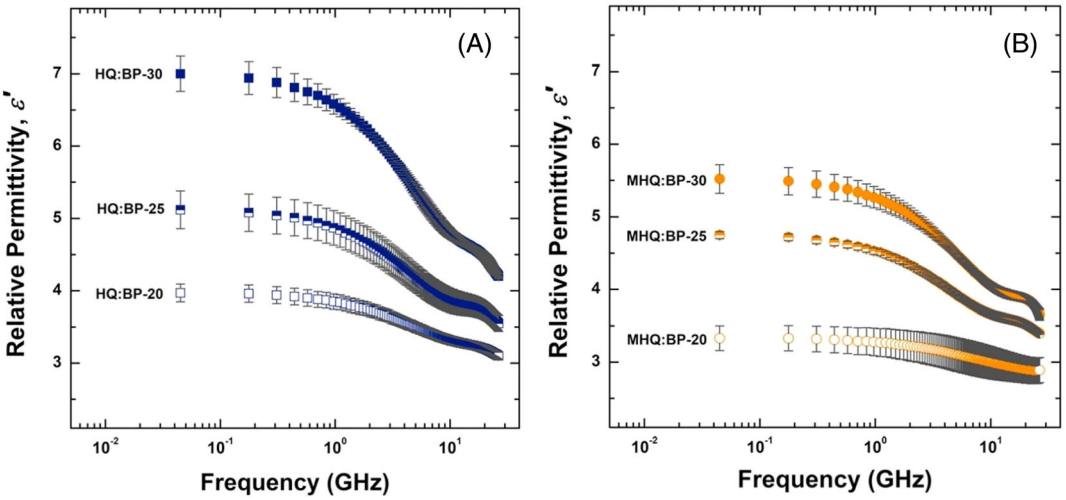

FIGURE 11 The relative permittivity of hydrated sulfonated polysulfone membranes with varied sulfonation extents versus frequency.[60] The plateau value at low frequencies represents the dielectric constant of each material. *Source*: Adapted with permission from Reference [60] 2021, Elsevier

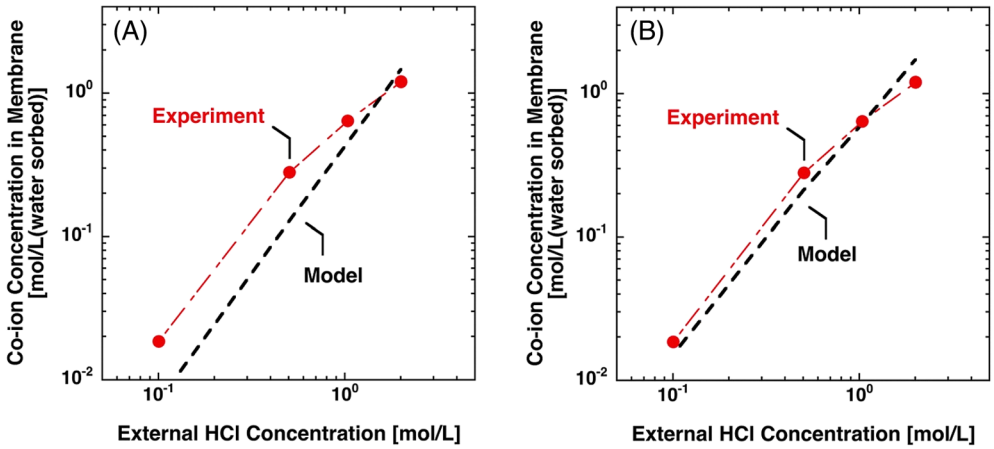

FIGURE 12 Equilibrium co-ion concentrations versus external solution HCl concentration for Nafion 117 equilibrated with HCl.[22] The symbols represent the experimental data, and the dashed lines represent predictions by the Donnan-Manning model in which (A) the ξ value was calculated assuming a homogeneous membrane and (B) the ξ value was calculated by using a more realistic value for the average distance between fixed charges, thus accounting for the phase separated morphology. *Source*: Adapted with permission from Reference 22, 2016, Royal Society of Chemistry

suggests a monotonic increase in activity coefficients whereas the modeled values plateau for concentrations higher than 3 mol kg^{-1}. The continual increase in experimental activity coefficient data is similar to the trends observed by Galizia et al. for concentrated NaCl and $CaCl_2$ partitioning into CR61.[47] For the diprotic data, it was assumed that the H_2SO_4 dissociated just once, as would be the case in concentrated solutions. Despite this assumption, there were large discrepancies between the predicted and observed ion activity coefficients for H_2SO_4 in both membranes.

A more recent study by Sujanani et al. discussed ion partitioning in Nafion 117 equilibrated with salt solutions of NaCl, $MgCl_2$, and Na_2SO_4.[88] Over the range of 0.01–1 M, the NaCl and $MgCl_2$ experimental membrane ion activity coefficients were predicted well by the Donnan-Manning framework. However, the Na_2SO_4 predictions did not match the partitioning data at any of the concentrations explored. Sujanani et al. attributed this discrepancy to incomplete ion dissociation in the solution and membrane phases. In aqueous solutions, it is known that Na_2SO_4 does not dissociate completely, particularly when the electrolyte concentration is higher than 0.03 M.[88] Similarly to Peng and Zawodzinski treating H_2SO_4 as a monoprotic acid,[87] these authors explored the same assumption. Sujanani et al. reported that assuming

incomplete dissociation improved the ability of the Donnan-Manning model to predict the membrane ion activity coefficients. To compare the methods, they modeled both H_2SO_4 and Na_2SO_4 sorption in Nafion 117 for both the monovalent and divalent cases (Figure 13). Using their own Na_2SO_4 partitioning data and literature partitioning data for H_2SO_4 measured over the same range,[89] the authors demonstrated that both electrolytes behave as monovalent species at high concentrations, but that lower concentrations of equilibrating Na_2SO_4 led to experimental behavior inconsistent with either assumed valences. A fraction of dilute Na_2SO_4 salt molecules appear to dissociate fully, and another fraction dissociate once. Additional context may be gained by comparing the fourth and only remaining analysis of SO_4^{2-} via the Donnan-Manning model in the open literature: that by Chen et al. in Figure 8.[82] When SO_4^{2-} is a counter-ion for AMX and ASE, as opposed to the co-ion role it fulfills for Nafion 117, it is possible to treat the electrolytes as fully divalent in the membrane. SO_4^{2-} surrounded by an excess of H^+ or Na^+ (partitioned into CEMs) prefers to partially associate, but SO_4^{2-} in an environment with minimal Na^+ (partitioned into AEMs) presumably does not associate with the Na^+ that is present. Analyzing these studies on SO_4^{2-} jointly highlights the importance of accounting for effects like ion pairing when they are present.[82,87,88]

Beyond Nafion 117, additional membranes were utilized by the Freeman and Paul groups to test the predictive power of the Donnan-Manning model for heterogeneous materials. Cross-linked IEMs were synthesized in sets of three membranes each, wherein experimental ion partitioning data were collected for two sets of heterogeneous CEMs and one set of relatively-homogeneous AEMs.[58,71,90] NaCl, KCl, and $MgCl_2$ sorption data spanning 0.01 to 1 M for sets of AEMs and CEMs were first tested by Kamcev et al.[71,90] The authors observed that the AEMs were somewhat phase separated at the length scale of visible light, due to visible light scattering, but presumed that would not be significant enough to affect ion sorption. The CEMs were observed to diffract light to a much greater extent, and therefore were expected to be phase separated to a greater extent as well. This increased degree of heterogeneity was suspected to be extreme enough to affect ion partitioning. A later study supported this distinction through cryo-SEM characterization, wherein the authors detected heterogeneous surface morphologies in the CEMs but not the AEMs.[71] Continued support for this qualification lies with the modeled partitioning results: the predictions of the Donnan-Manning model using the theoretical values of b were in good agreement with the experimental AEM partitioning data, but did not agree with the CEM data under the same assumption. The experimental partitioning results for the CEM were described well by the Donnan-Manning model using a fitted value of ξ for each membrane in the series.[90] The semi-predictive nature of the Donnan-Manning model was demonstrated by using the ξ value fitted with the NaCl data to successfully predict KCl and $MgCl_2$ partitioning in these heterogeneous CEMs, as seen in Figure 14.

In a separate study, Jang et al. collected NaCl partitioning data over the same salt concentration range for the third series of heterogeneous CEMs.[58] For these CEMs, the appearance was clear and transparent, so the phase separation was not on the length-scale of visible

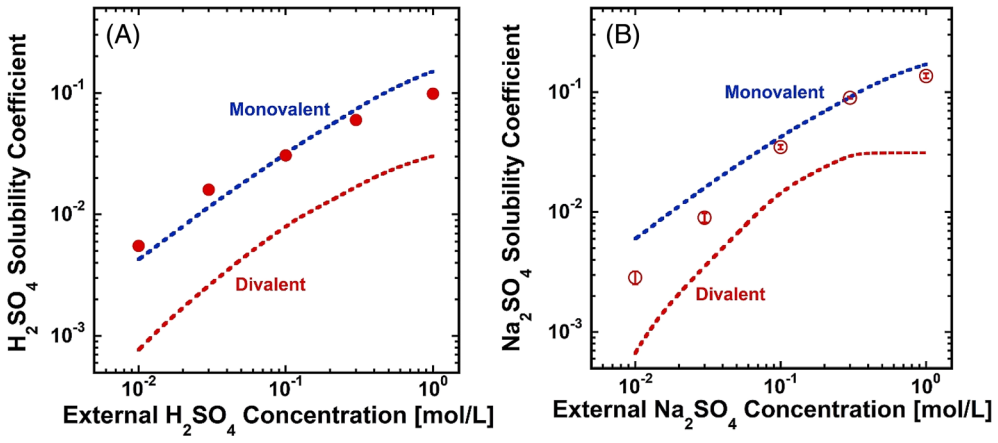

FIGURE 13 Solubility coefficients of SO_4^{2-} electrolytes in Nafion 117 versus the external solution concentration.[88] The lines on both plots represent predictions by the Donnan-Manning model. The red lines were generated by assuming full dissociation of the electrolytes (i.e., the co-ions were treated as SO_4^{2-}), while the blue lines were generated by assuming half dissociation of the electrolytes (i.e., the co-ions were treated as HSO_4^- or $NaSO_4^-$). (A) H_2SO_4 partitioning data collected by Verbrugge and Hill.[89] (B) Na_2SO_4 partitioning data collected by Sujanani et al. *Source*: Adapted with permission from Reference 88, 2021, Elsevier

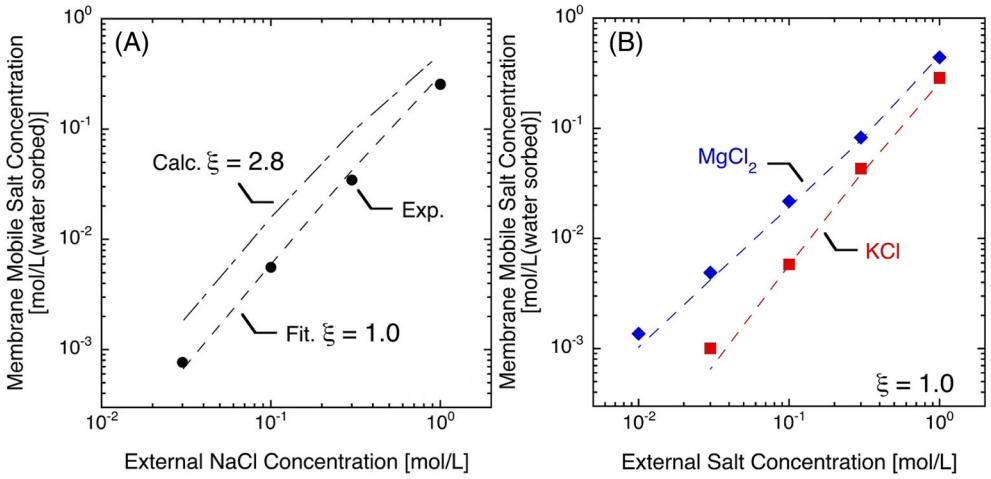

FIGURE 14 Salt partitioning data for laboratory prepared membrane CA267.[71,90] (A) NaCl concentrations in the membrane versus external solution NaCl concentration. The symbols represent the experimental results, and the dashed lines represent predictions by the Manning model. The $\xi = 2.8$ value was calculated by assuming a homogeneous membrane, and the $\xi = 1.0$ value was obtained by fitting the model to the experimental data. (B) KCl and $MgCl_2$ concentrations in the membrane versus external solution salt concentration. The symbols represent the experimental results, and the dashed lines represent predictions by the Manning model using the ξ value fitted via the NaCl data. *Source*: Adapted with permission from Reference 71, 2018, Elsevier

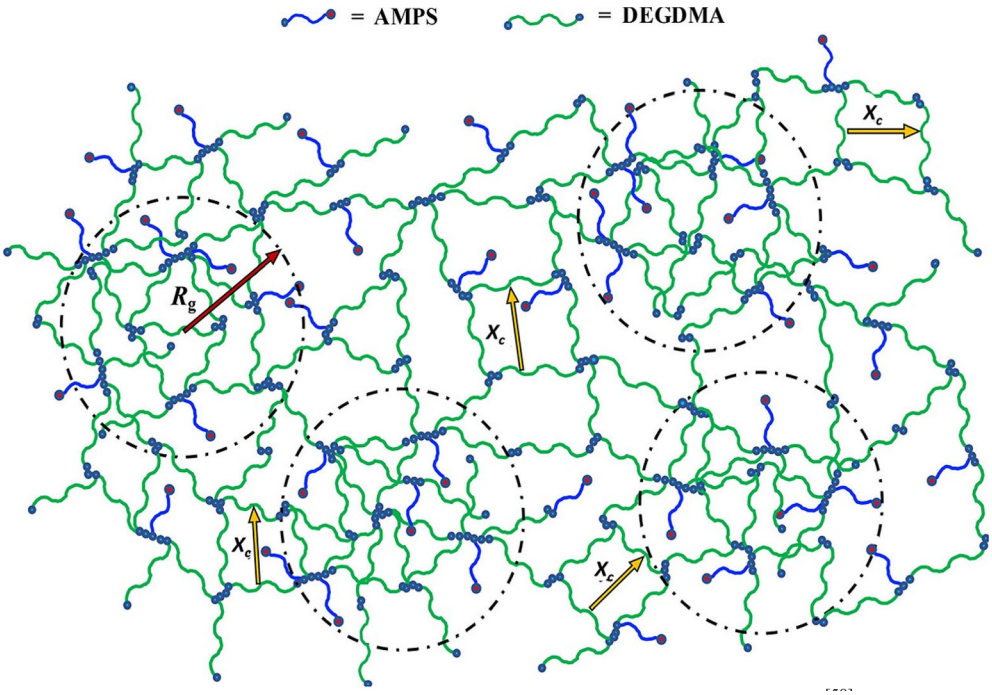

FIGURE 15 The proposed microstructure of the CEMs studied by Jang et al.[58] The authors illustrate areas of hydrophobic, densely cross-linked polymers which exist within a sphere of average radius R_g. Surrounding these domains is a matrix of hydrophilic, charged, and loosely cross-linked polymer of mesh size X_c. The depicted scales in this graphic were informed by SAXS data acquired by the authors. Such inhomogeneous morphologies can rationalize the discrepancy between the fitted and calculated values for b, in which the calculations assumed that fixed charge groups were distributed evenly throughout the membranes. *Source*: Reproduced with permission from Reference 58, 2019, American Society of Chemistry

light. Rather, the heterogeneity was quantified to be on the nano-scale through small angle X-ray scattering (SAXS). The predicted partitioning data, based on the assumption of a homogeneous membrane, did not agree with the experimental results. Like the other heterogeneous CEMs, Jang et al. report excellent agreement between modeled and experimental partitioning data after using a fitted value for ξ. This study proposed a

morphology for their IEMs, discussing the nature of two distinct domains which may form during polymerization (Figure 15). Continued analysis in this manner may allow the prediction of *b* from knowledge of the phase-separated domain sizes, in a similar manner to which an appropriate value of *b* was estimated through the extensively-characterized structure of Nafion 117.[22]

The Arges group studied ion partitioning into block copolymer electrolyte (BCE) phase-separated membranes, which are of interest because of their enhanced performance: the phase separation in block copolymer structures yields restricted swelling and improved mechanical properties.[91,92] The domain-based structure of these BCEs complicated predicting the electrolyte partitioning behavior. In a pair of manuscripts, Lei et al.[92] prepared a poly(styrene-*block*-vinyl pyridinium) BCE while Ramos-Garcés et al.[91] prepared the same system as a random copolymer to study the effect of macromolecular architecture on membrane transport properties. Specifically, the authors performed potassium iodide (KI) partitioning experiments with external solutions ranging from 0.01 to 1 M. Because the structure of the BCE was known, the authors predicted *b* based only on the charged half of the BCE structure. Accounting for the phase separation in calculating ξ yielded astounding agreement between predicted and measured ion activity coefficients in the BCE (Figure 16A). The results for the random copolymer membrane exhibited a qualitatively correct trend but did not reach the same quantitative agreement as the block copolymer system. Manning's model has generally performed poorly when applied to weakly-charged membranes (Section 2.2.4), so a better comparison might be made between a random/block copolymer pair which are both densely charged (BCE: $C_A^{m,w} = 1.8$ M, random copolymer: $C_A^{m,w} = 1.4$ M). Another unique aspect of this study relates to the calculation of the dielectric constant in their membranes. Whereas most studies employing the Donnan-Manning model attribute the dielectric constant of pure water to the aqueous phase in membranes, this study utilized a dielectric constant calculated for the salt concentration within the membrane.[92] Aqueous salt solutions exhibit a decrease in their dielectric constant as the salt concentration increases. It is therefore reasonable to suspect that the water-salt mixture imbibed by IEMs would exhibit lessened dielectric shielding as well. This modification led to a ~15% increase in ξ and may be a contributing reason to the Donnan-Manning predictions aligning so well with the experimental BCE partitioning data.

Lei et al.[92] also compared the fraction of condensed counter-ions obtained via Manning's model (Equation (9)) to values obtained via several experimental approaches (Figure 16B), including solution uptake experiments, ion sorption experiments analyzed via the Gibbs-Donnan equation, and environmental grazing incidence small-angle x-ray scattering (GI-SAXS). The utility of these experimental approaches for quantifying the fraction of condensed counter-ions in IEMs warrants further discussion. The approaches based on membrane osmotic de-swelling (measured via solution uptake and

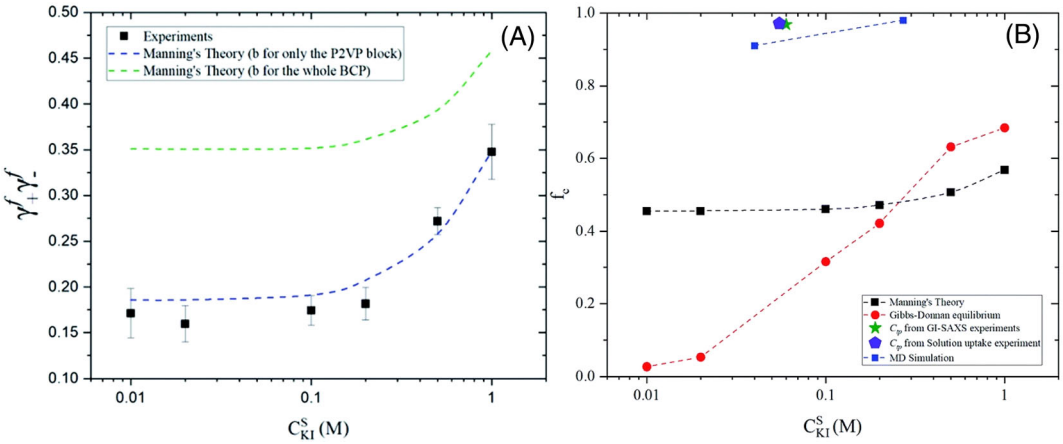

FIGURE 16 (A) Membrane ion activity coefficients in a block copolymer electrolyte (BCE) as a function of external KI concentration.[92] The symbols represent the experimental results. The green dashed line represents predictions from the Donnan-Manning model in which *b* was averaged over both blocks of the BCE, while the blue dashed line represents predictions from the Donnan-Manning model in which *b* was averaged over the charged block of the BCE. (B) The fraction of condensed counter-ions in the membrane as a function of external KI concentration. Various methods were used to quantify this fraction: The values from Manning's theory which predicted the data in Figure 16A are depicted as a black line. The values predicted by molecular dynamics (MD) simulation results, which are discussed in Section 2.3, are depicted as a blue line. The remaining experimental methods include: The Gibbs-Donnan equation (red line), GI-SAXS data (green star), and solution uptake experiments (blue pentagon). *Source*: Adapted with permission from Reference 92, 2020, Royal Society of Chemistry

GI-SAXS experiments) follow a procedure detailed by Beers et al.[32] This approach assumes that the external solution salt concentration at which one can first detect osmotic de-swelling is the effective membrane counter-ion concentration at all lower external salt concentrations. Comparing this effective counter-ion concentration to the stoichiometric counter-ion concentration yields the fraction of uncondensed counter-ions. Aside from the fact that osmotic de-swelling occurs even in uncharged membranes, this process assumes that all other contributions to ion activity beyond condensation are equivalent in the membrane and in the external solution (for the external and membrane ion activities would be equivalent, not their concentrations). It has been demonstrated that experimental ion activity coefficients in charged membranes[22,47,48] (and polyelectrolytes[23,49,50]) diverge from salt solution activity coefficients in dilute regimes, with the former trending toward zero and the latter toward unity. These differences in ideality raise questions about the rigor of this method for quantifying the extent of counter-ion condensation.

The other method for calculating the extent of counter-ion condensation, the Gibbs-Donnan equation used by Lei et al., is analogous to Equation (21) in this manuscript; the only difference is that the fixed charge group concentration, $C_A^{m,w}$, has been replaced with the concentration of uncondensed counter-ions, C_{up-}.[92] The authors first extracted ion activity coefficients in the membrane from the experimentally determined counter-ion and co-ion concentrations in the membrane through the equation for nonideal Donnan equilibrium (Equation (16)), where measuring both values allowed them to forgo a charge balance. Subsequently, the authors obtained C_{up-} from the Gibbs-Donnan equation, which is the same as the Donnan equilibrium equation coupled with a charge balance. Lei et al. used ion activity coefficients in the membrane obtained from the nonideal Donnan equation in this calculation. Because the Gibbs-Donnan equation is derived from the nonideal Donnan equilibrium equation for monovalent species in tandem with a charge balance across the membrane, this total approach amounts to using experimental ion sorption results to calculate $C_A^{m,w} = C_g^{m,w} - C_c^{m,w}$. The authors refer to this value as C_{up-}. To relate C_{up-} to fractional condensation, f_c, Lei et al. normalize C_{up-} by the fixed charge group concentration of a membrane equilibrated with pure water. From the discussion above, this approach likely does not give information on the distribution of condensed and uncondensed counter-ions in a membrane—it is simply performing a charge balance in the membrane from experimental ion sorption data. This can be demonstrated by inserting Equation (21) into Equation (16) (their Equation (7) into their Equation (6)[92]) and rearranging to obtain the equation for electroneutrality. The discussion in these two paragraphs could explain the differences in the extents of counter-ion condensation reported by Lei et al. in Figure 16B. Accurate experimental determination of the extent of counter-ion condensation in IEMs should be a priority for the field moving forward, potentially by employing newer methods not typically utilized with IEMs, such as anomalous SAXS.[93]

2.2.4 | Overall trends

Beyond considering the individual reports in these studies, we also hope to define the general trends that they inform when taken together. For ease of discussion, we have collected Donnan-Manning model predictions of co-ion partitioning from all the studies discussed above but compressed the varied concentrations into a single error term, representative of a given salt and membrane. To enable discussions of agreement across such discrepant concentration ranges, we define for each salt/membrane pair the Root-Mean-Square (RMS) Log Error averaged over each experimentally tested external salt solution concentration:

$$RMS\,Log\,Error = \sqrt{\frac{1}{n}\sum_{C_{s,i}^s}^{C_{s,n}^s}\left(\log\left(\frac{C_{s,experimental}^m}{C_{s,predicted}^m}\right)\right)^2} \quad (22)$$

This choice of metric for error is intuitively linked to the visual agreement seen in log–log ion partitioning plots: a given value for the RMS Log Error on a logarithmically scaled graph appears identical to the same value of a RMS Linear Error on a linearly scaled graph. The selection of a useful error metric is important because linear errors behave counter-intuitively on logarithmic scales. We provide two examples to illustrate this point: A point with an RMS Log Error of 0.2 is either over-predicted by ~50% of the true value or under-predicted by ~33% of the true value when considered on a linear scale. Comparatively, a point with an RMS Log Error of 1.0 is either over-predicted by ~900% of the true value or under-predicted by ~90% of the true value when considered on a linear scale. Because partitioning data spans many orders of magnitude, the RMS Log Error is a fair metric to assess a model's performance at all of the experimental conditions.

When predictive data was implicit (ξ_{theory} values were reported, but due to high predictive error, only fitted results were included), we performed the predictions ourselves using the reported model inputs. When available, the explicitly reported concentration predictions were

considered. Because these implicit predictions are included below, the following analysis does not discount data sets with very poor predictive model agreement.

First, we present a collection of the membranes tested with at least four equilibrating salts (Figure 17). The variety of membranes (one commercial CEM, one commercial AEM, one commercial RO membrane, and one noncommercial laboratory prepared CEM) which were analyzed helps to extend these trends broadly. The RMS Log Error for NaCl predictions in each membrane is reasonable, though greater in the commercial IEMs than the RO and noncommercial IEM. Studies which employed CR61 and AR103 examined the effect of both their counter- and co-ions, and neither membrane exhibited great variability in the error of the model predictions. This data suggests that the Manning model's indifference toward ion size or identity is reasonable. The SWC4+ and AMPS-PEGDA plots indicate the opposite. The error changed drastically for the different counter-ions in the SWC4+ study and the different co-ions in the AMPS-PEGDA study. The data available at present does not conclusively indicate whether the counter- and co-ion identities are significant for ion partitioning behavior, but they do suggest that Manning's model captures the near-full extent of NaCl interactions in IEMs.

Second, we examine the effects of membrane properties on the predictions of the Donnan-Manning model, highlighting the charge density, $C_A^{m,t}$, and water content, ϕ_w (Figure 18). In the preceding analysis, we observed that the RMS Log Error of NaCl for each membrane was relatively low. This informed the discussion below, where we now only discuss NaCl data, to more directly compare the effects of the membrane properties. In a multifaceted graph, we plot the RMS Log Error against both the total membrane charge density and the water content. There is a reasonable distribution of data across the full range of charge densities, but there are more data points for high-water-content membranes than for low-water-content membranes. As a general trend, partitioning into densely charged membranes with high water volume fractions, with cutoffs at about $C_A^{m,t} > 1.0$ M and $\phi_w > 0.4$, is predicted well by the Donnan-Manning model.

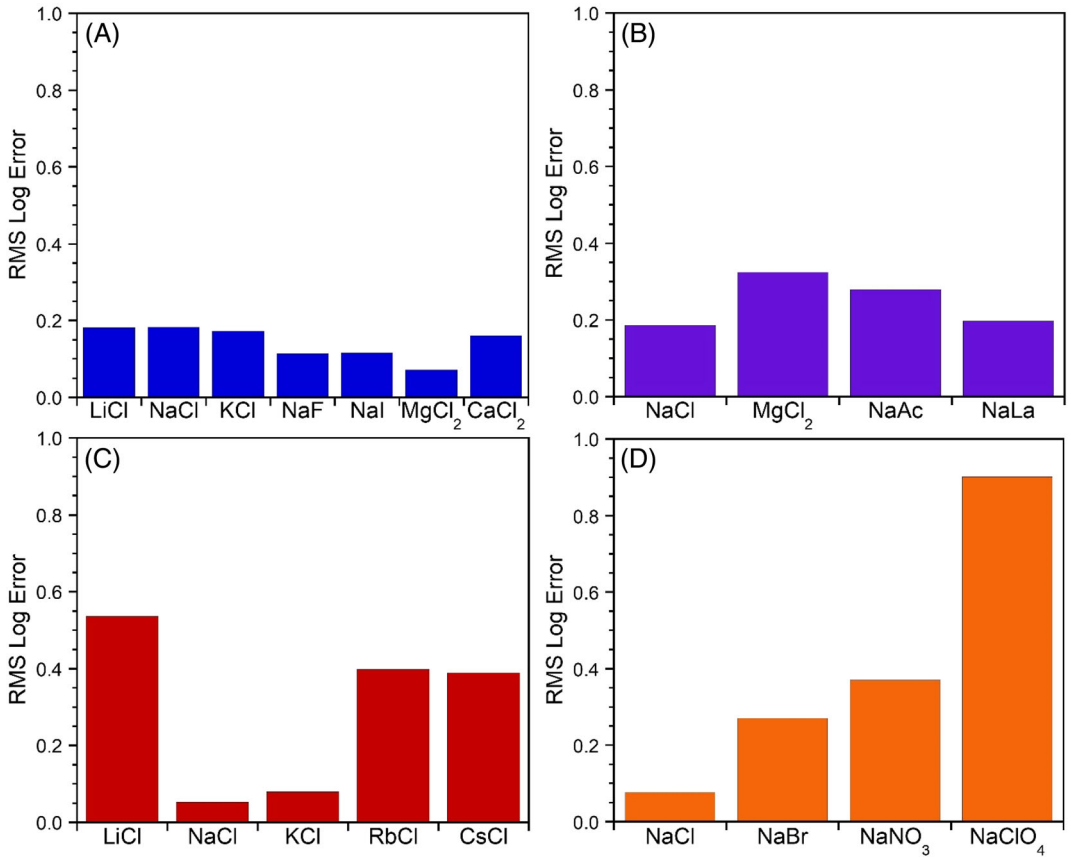

FIGURE 17 Collections of data for single membranes but various salts, presented as the RMS log error of the Donnan-Manning model prediction and experimental data averaged across the various concentrations tested. (A) Salt partitioning into CR61 as tested by Galizia et al. the plot includes only the data up to 1 M for NaCl and $CaCl_2$.[76,77] (B) Salt partitioning into AR103 as tested by Kamcev et al. and Wang et al.[22,83] (C) Salt partitioning into SWC4+ as tested by Wang et al.[80] (D) Salt partitioning into an AMPS-PEGDA membrane as tested by Ji et al.[85] The data used to generate these plots is available in the Data S1

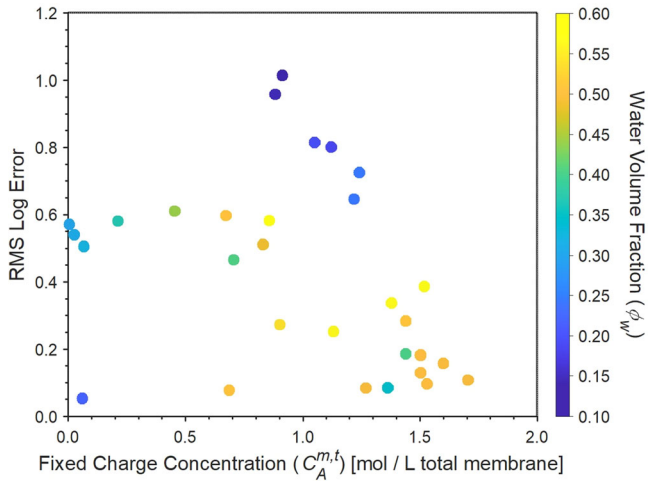

FIGURE 18 The RMS Log Error for predictions made by the Donnan-Manning model for NaCl partitioning in various IEMs with broad sets of properties.[22,58,60,76,77,80,84,85,88,90] The abscissa is the fixed charge concentration, $C_A^{m,t}$, as reported for membranes equilibrated with DI water or the most dilute NaCl solution used in the study. The color of each data point indicates the water volume fraction, ϕ_w, when measured under the same conditions. Warm-colored data points at the right of the graph display lower error, indicating that the Donnan-Manning model provides reasonably accurate predictions for NaCl partitioning in highly-charged, high-water-content membranes. The data used to generate this plot is available in the Data S1

Meanwhile, having a smaller value of either property tends to increase the RMS Log Error. This trend is reasonable: the high water content prevents uncompensated effects such as ion pairing from becoming relevant, while high charge densities ensure that the compensated point-to-line electrostatics are very relevant. Next-generation IEMs are frequently lower in water content, but most commercial membranes are highly charged. With this in mind, these conglomerated results suggest that the partitioning of simple electrolytes (e.g., NaCl) into high-water-content IEMs should be described well by the Donnan-Manning model.

2.3 | Computational ion sorption studies

Much can be learned about the phenomenon of counter-ion condensation in IEMs when studied via molecular dynamics (MD) simulations. Most of the MD studies discussed below do not directly quantify ion partitioning in IEMs contacted by an aqueous salt solution, but rather attempt to describe the distribution of counter-ions in various states (e.g., condensed and uncondensed). As discussed in Section 2.1, these populations directly affect the membrane ion activity coefficients and therefore ion partitioning between a membrane and aqueous salt solution. In this section, we discuss key discoveries in computational studies of counter-ion condensation in IEMs. Instead of centering the discussion around fixed charge concentrations or water volume fractions, as is done in experimental studies of ion partitioning in IEMs, researchers employing simulations typically report and discuss λ:

$$\lambda \equiv \frac{\text{water molecules}}{\text{fixed charge groups}} = \left(\overline{V}_{H_2O} C_A^{m,w}\right)^{-1} \tag{23}$$

Thus, λ represents the ratio of water molecules per fixed charge group. Equation (23) describes how λ can be related to the fixed charge concentration, $C_A^{m,w}$, through the molar volume of water, $\overline{V}_{H_2O}$. As a point of context, a nominal IEM value of $C_A^{m,w} = 3.0$ M corresponds to $\lambda = 18.5$, assuming $\overline{V}_{H_2O} = 18\,\text{cm}^3/\text{mol}$. This λ should not be confused with λ_B (the Bjerrum length) introduced in Section 2.1.

One powerful feature of MD simulations is the ability to describe the in situ positions of species relative to one another, expressed as radial distribution functions. Thus, it is vital to consider the expected location of condensed and uncondensed counter-ions within a membrane. IEMs are dense, so unlike the dilute solutions considered by Manning's limiting law for polyelectrolytes, the spatial region attributed to condensed counter-ions may represent a significant portion of the system volume. This region of condensation increases in radius with λ_B, and so to some extent, with ξ. By predicting both the number of condensed counter-ions and the volume attributed to them, Manning has calculated their expected effective concentration.[43,44] One may also calculate the Debye length (κ^{-1}) of the system,[39] which represents the length over which the electrostatic potential decreases by $1/e$. These values can help to set expectations for the location of condensed counter-ions in IEMs.

When κ^{-1} is much less than λ_B, it is expected that even uncondensed counter-ions would enter the layer of condensed counter-ions within the membrane. This can be rationalized because electroneutrality would be maintained even at relatively small length scales, and the polymer with its condensation layer still bears a net charge. To minimize ambiguity, in the polyelectrolyte literature, derived properties of the solution are heeded alongside simulated radial distribution functions, because the mere positioning of counter-ions does not uniquely determine their state as condensed or uncondensed.[27] Additionally, one may consider the stabilizing effects of adjacent polymer chains on the free energy of condensed counter-ions (a special case for dilute polyelectrolytes, but presumably the standard case for dense IEMs).

Manning demonstrated that the volume for condensed counter-ions between two nearby polyelectrolytes should expand to better span the distance separating them, lessening the entropic deficit inherent to condensation and allowing the condensed counter-ions to stray further than normal from either given polymer backbone.[39,94] Because IEMs are densely packed, it is reasonable to expect that the region of space containing condensed counter-ions is permanently expanded within IEMs. Thus, there is more volume for uncondensed counter-ions to intermix with territorially condensed counter-ions. With these considerations in mind, care must be taken when assigning the condensation state of counter-ions within IEMs based upon their position.

Lei et al. performed MD simulations to complement their experimental ion partitioning results discussed in Section 2.2.3.[92] To parallel their physical system, the authors simulated a poly(styrene-*block*-pyridinium) BCE populated with KI at concentrations informed by the experimental results. However, the simulations utilized a water content of $\lambda = 6$, significantly lower than that of the experimental system ($\lambda \sim 30$). The authors report an extremely high simulated extent of counter-ion condensation, in excess of 90% (Figure 16B), which is somewhat consistent with values extracted from osmotic deswelling experiments performed with the physical membrane analogue[92]—a discussion on these experimental approaches for quantifying counter-ion condensation is presented in Section 2.2.3. Lei et al. determined the state of counter-ions based on their distance from a reference fixed charge group: if a counter-ion breached a fixed charge's primary hydration shell, it was considered to be condensed. This choice of definition neglects territorially bound counter-ions, since such counter-ions do not penetrate the hydration layer of a fixed charge group, suggesting that the simulated amount of condensation may have been undercounted. The unusually high extent of condensation predicted by these MD simulations is potentially an indication of site-bound ion pairing dominating any amount of territorially condensed counter-ions, which may be related to the extremely low water content used for the simulation. Lei et al. investigated the effect of water content on their simulations by testing the BCE with $\lambda = 650$. Under these conditions, they observed condensation which neutralized only 40% of the fixed charge groups. This value is much more consistent with the predictions of Manning's model (45%–55% from Equation (9)), though it goes unstated whether simulations at the experimental conditions of $\lambda = 30$ would yield quantitative agreement.

Aryal and Ganesan considered both the fixed charge to counter-ion and the co-ion to counter-ion distribution functions in their MD simulations.[95–97] The authors simulated 30% sulfonated poly(styrene-*co*-divinylbenzene) membranes with $\lambda = 10$ in the presence of $C_s^{m,w} = 0.005 - 0.125$ M sorbed NaCl (which they note to be consistent with 0.04–1 M external NaCl). Although a cut-off distance was used as qualification for counter-ion condensation, they quantify several populations of counter-ions: free (uncondensed) counter-ions, counter-ions with a fixed charge group as a nearest-neighbor (condensed), counter-ions with a co-ion as a nearest-neighbor, and condensed counter-ions which function as the nearest-neighbor to a co-ion. This study reports high levels of counter-ion condensation, with a fraction of condensed counter-ions approaching 95% at low salt concentrations and dropping to 70% under more concentrated conditions (Figure 19). This extent of condensation is greater than that typically reported for polyelectrolyte systems. Interestingly, Aryal and Ganesan's approach of classifying co-ions (which is unique to this study) enables additional analysis by demonstrating a concept predicted by Manning. Manning detailed how uncondensed counter-ions and co-ions may enter the region of condensation, if they do so in an electroneutral manner.[39] Aryal and Ganesan considered such counter-ions condensed, but their documentation of the adjacent co-ions gives insight into the ionic equilibrium between condensed and uncondensed regions within IEMs. Aryal and Ganesan report that the majority, some 60%–80%, of the simulated co-ions are nearest-neighbors with a condensed counter-ion. If these identified counter-ions are thought of as uncondensed and simply within the region of condensation (per Manning), the fraction of condensed counter-ions would be lower, especially at higher Cl^- concentrations. A more detailed study on this matter would be helpful in better understanding counter-ion condensation and the distribution of mobile ions in IEMs.

Aryal and Ganesan also discussed systems of mixed ions, focusing on K^+ and Mg^{2+} counter-ions mixed with Na^+.[95] The membrane system remained the same throughout these studies, but later simulations used 1:1 molar ratios of KCl/NaCl and $MgCl_2$/NaCl. The extent of condensation reported for these mixed ion simulations also exceeded 70% under all conditions. In mixtures of salts, Manning's studies found that two monovalent salts may both condense, but a divalent salt would be expected to condense fully before any monovalent salt.[41] Aryal and Ganesan report that Na^+ entered the condensation layer more readily than K^+ at all concentrations. This result is somewhat unexpected, because the ions with larger bare radius are typically thought to be the preferred species within an IEM.[2,3] The authors also reported that Na^+ enters the condensation layer more readily than Mg^{2+} under dilute conditions, but that Mg^{2+} condensation

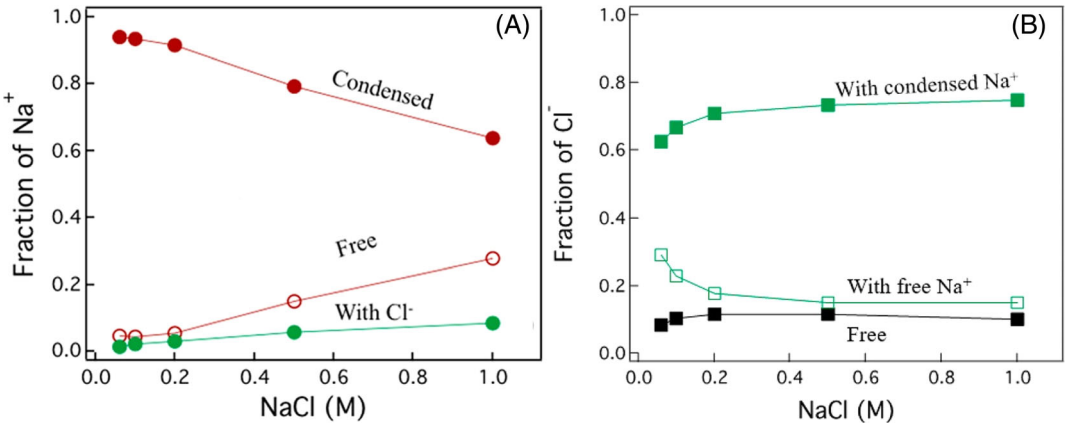

FIGURE 19 The states of ions in a simulated sulfonated polystyrene membrane.[96] (A) The fraction of counter-ions which are condensed, free, and free but adjacent to a co-ion. Condensed counter-ions which coordinate only fixed charge groups and those which coordinate both a fixed charge group and a co-ion are both labeled as condensed. These two populations of condensed counter-ions can be distinguished when taken in conjunction with Figure 19B. (B) The fraction of co-ions which are free, adjacent to a free counter-ion, and adjacent to a condensed counter-ion. Most co-ions in the membrane are found within the region of condensed counter-ions. *Source*: Adapted with permission from Reference 96, 2018, American Chemical Society

levels exceed those of Na^+ at moderate and high concentrations. This reversal of preference is very interesting because Manning reports that the counter-ion condensation theory is generally considered fully predictive until a breakdown point at 0.1 M—the same concentration at which this crossover occurs in the study by Aryal and Ganesan.

Vondrasek et al. used a different approach for discerning which counter-ions are condensed.[98] For their MD study, the authors simulated 50% sulfonated polysulfone membranes in the Na^+-form with no added salt and multiple water contents between $\lambda = 3 - 14$. The authors defined coordination between a counter-ion and a fixed charge group by a cut-off distance but noted that some counter-ions were coordinating multiple fixed charges and vice versa. This double-coordination is consistent with the territorially condensed state, and because they simulated monovalent Na^+ counter-ions, this coordination state is expected to describe the vast majority of condensed counter-ions in these systems (Section 2.1.1). Vondrasek et al. qualified condensation to only refer to this population of doubly-coordinated counter-ions. With this definition, their simulated fraction of condensed counter-ions was near 70% at $\lambda \sim 14$, but increased to 90% at $\lambda \sim 3$. This study adds further context to their results by comparing their simulated fractions of uncondensed counter-ions to those predicted by Manning's model for their system (Equation (8)), finding excellent agreement between the modeled and simulated values (Figure 20). The range of 70%–90% condensation is still higher than typically encountered in commercial IEMs, but the water contents were low for all conditions of study, even at $\lambda = 14$. The agreement between the MD simulations and Manning's model applied to the same materials is encouraging.

In another effort to distinguish between different states of counter-ions, Fong et al. evoked the nomenclature used in computational studies of battery separators.[51] The authors described free counter-ions, solvent separated ion pairs (SSIPs, territorially condensed counter-ions), and contact ion pairs (CIPs, site-wise condensed counter-ions). Their attention to the preservation of the counter-ion hydration shells coincides with the theoretical difference between site-wise and territorial condensation which we discussed in Section 2.1.1. Fong et al. applied these definitions to MD simulations of a polyelectrolyte solution containing poly(allyl glycidyl ether-sulfonate) with Li^+ counter-ions and no added salt. Targeting non-aqueous battery applications, the authors chose dimethyl sulfoxide (DMSO) as the solvent, and varied the fixed charge concentration from 0.05 to 1 M. Because these simulations utilized DMSO, the results may not completely translate to aqueous systems. However, the dielectric constant of DMSO is similar to those predicted by Equation (14) for IEMs of $\phi_w \sim 0.45$, so these MD studies could provide insight relevant for aqueous IEMs. Fong et al. found that it is much more common for Li^+ to undergo territorial condensation than site-wise condensation at all solvent contents (Figure 21). At 0.05 M, only ~25% of the counter-ions are condensed, which is consistent with the ranges typically ascribed to real polyelectrolyte systems. When the fixed charge

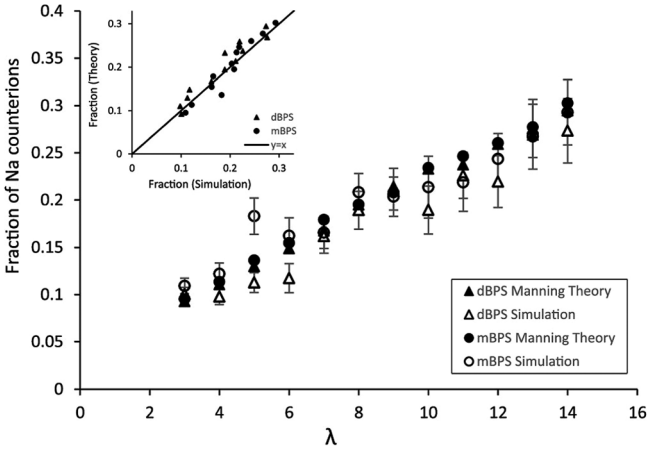

FIGURE 20 Counter-ion condensation predicted in polysulfone membranes for monosulfonated and disulfonated repeat units (mBPS and dBPS, respectively).[98] The main figure illustrates the fraction of uncondensed counter-ions versus the water content for both systems. The fraction of uncondensed counter-ions were predicted via Manning's model and via MD simulations. The inset reports the same data set as a parity plot between Manning's model and the simulations. *Source*: Reproduced with permission from Reference 98, 2021, American Chemical Society

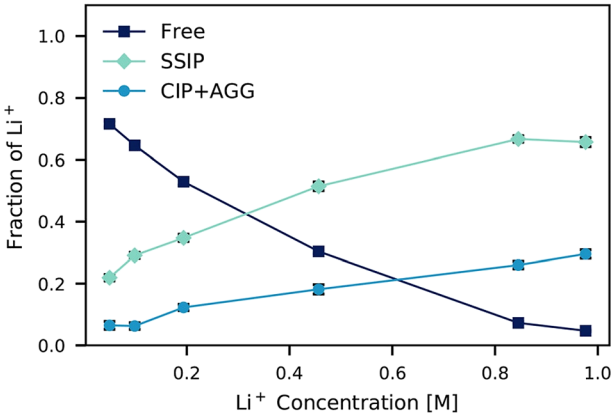

FIGURE 21 Distribution of Li^+ counter-ions in MD simulations of poly(allyl glycidyl ether-sulfonate) with Li^+ counter-ions and no added salt dissolved in DMSO.[51] Ions which are free, in a solvent separated ion pair (SSIP, territorially condensed), and either in a contact ion pair (CIP, site-wise condensed) or ion aggregate group (AGG) are depicted as a function of Li^+ concentration (equal to fixed charge concentration). *Source*: Reproduced with permission from Reference 51, 2019, American Chemical Society

concentration is increased to 1 M, the number of condensed counter-ions increases to >95%. Removal of solvent quickly causes condensation for these simulated polyelectrolytes, illustrating that condensation and ion pairing become common at much higher solvent contents for non-aqueous, low-dielectric systems. Application of Manning's model to describe the behavior of non-aqueous systems is uncommon, but this study illustrates the extent of information extractable by considering condensation in non-aqueous polyelectrolyte solutions and non-aqueous membranes.

Considering these highlighted MD studies in concert, we summarize this discussion with three statements on condensation in simulated charged polymers: First, water contents in the MD simulations are kept low, even beyond those of the IEMs discussed in Section 2.2. For example, the lowest value for λ in Figure 18 is $\lambda = 8.4$. Section 2.2.4 discusses the deviation of partitioning results for low water content membranes from Manning's predictions, so quantitative comparisons between MD simulations, Manning's theory, and a real system may be difficult to achieve. Second, when given the ability to atomistically describe the location of each counter-ion, there is no agreed-upon method to qualify condensation. From these examples, it can be seen that more complex definitions, which consider multiple types of coordination, tend to yield results that are more agreeable with Manning's model. Finally, there is significant benefit to be gained from MD simulations due to their ability to systematically vary system properties (e.g., chemistry, water content, charge density, etc.), which is difficult to do in experimental systems. As the utilization of MD simulations within the field of IEMs grows, a consensus on the optimal way to qualify condensation in these simulations may be reached, which would ultimately yield a better fundamental understanding of ion behavior in complex environments.

2.4 | Alternative models for quantifying ion sorption in IEMs

Beyond the adaptation of Manning's counter-ion condensation theory, there are numerous other frameworks for quantifying ion activity coefficients or partitioning in IEMs. Indeed, some of these frameworks are applied in concert with Manning's model to describe situations in which the Manning model alone fails to predict the experimental results. There are generally two approaches for model development: membrane-exclusive treatments and solution-adapted treatments. The primary focus of this section will be on the latter, because the relatively simpler environment of an ionic solution has allowed more quantitative developments, and these models tend to be more predictive than models with no solution-based analogue. However, we will first highlight progress within the former category.

2.4.1 | Membrane-exclusive models

Many researchers have approached the task of predicting ion partitioning in parallel with the prediction of water partitioning in charged polymers. A prominent study in this field which still influences research today, that by Katchalsky and Michaeli,[99] separated membrane ion activity coefficients into two components: a point-to-line Debye-Hückel term and an elastic compressive term. The Debye-Hückel consideration is analogous to the treatment discussed by Manning, whereas the elastic term effectively replaces the contributions of counter-ion condensation. In a similar fashion to the ideal Donnan model, this framework has not been broadly successful in predicting experimental data but is nevertheless thought to account for major contributions to the phenomenon of interest—in this case, membrane-solvent equilibrium. As such, these ideas have remained influential in the IEM literature, with more recent studies[100,101] still relating ion sorption to membrane water activity using relations which refer to Katchalsky and Michaeli (through theories by Flory-Rehner,[102] Bray-Merrill,[103] and Brannon-Peppas[63]). Although the agreement between model and experiment has improved as these theories have been refined, a major shortcoming of this framework when applied to IEMs is the inability to predict the experimental results a priori. The Flory-Huggins χ parameters are not well defined for essentially any crosslinked IEM, nor is the effective crosslinking density. Recent studies have made developments toward predicting both quantities for complex real systems,[104–106] but no method is generally accepted.

The water content has been related to ion activity coefficients in IEMs in a second manner: instead of considering the total water content in a membrane, some researchers have suggested that only the "free" or "bulk" water in the membrane is important for thermodynamic analysis.[45,107] IEMs, which generally have limited water content and a large internal polymer-water interface, can draw water into a strongly- or weakly- associated state similarly to concentrated ion solutions, limiting the amount of water in the membrane which is available to act as a solvent. Experimental techniques that quantify the amount of free water present in membranes rely on interactions between water molecules: hydrogen bonding or freezing. Namely, two of the more common experimental methods which probe the different states of water in IEMs are Fourier transform infrared spectroscopy (FTIR) and differential scanning calorimetry (DSC).[107,108] If these methods respectively detect water hydrogen bonding or freezing in a membrane similarly to bulk solutions, then that water is considered free and thermodynamically active.

Several studies have demonstrated improved agreement between the ideal Donnan model (i.e., $\Gamma = 1$ in Equation (16)) and experimental co-ion sorption results by expressing membrane concentrations in terms of the amount of freezable water, instead of total water, in the membrane. Münchinger & Kreuer[45] use an estimated value for the hydration number of Li^+ (assuming it to be equivalent to the value in aqueous solution) to achieve predictive agreement with 1–5 M LiCl sorption data in Nafion 117 (Figure 22A). The authors did not detail whether the approach is valid for lower concentrations of external salt, where there would be fewer electrolytes interacting with water in the membrane. Rather than approximate the water availability, Tran et al.[107] utilized DSC to experimentally measure the freezable water fraction for a wide variety of membranes, finding excellent to fair agreement between the predicted and experimental 0.5 M NaCl sorption results (Figure 23). However, we note that there is an untested assumption pertaining to Tran et al.'s freezable water content calculation: the method assumes a constant enthalpy of melting for all water molecules in the membrane, including free water, weakly bound water, and strongly bound water.[107] This method is also limited in its semi-predictive application, because multiple experimental parameters (e.g., membrane structure, external salt concentration, and salt identity) affect the freezable fraction of water in a membrane. Therefore, a single condition cannot calibrate a fitting parameter for other experimental conditions, as was the case with ξ in the Donnan-Manning model. Further study and additional examples are needed to make this approach for quantifying ion sorption in IEMs fully predictive.

The final membrane-exclusive consideration is related to the effects of the fixed charge groups. Some researchers have modeled nonideal ion behavior in membranes as adsorption (exclusively site-bound condensation or ion pairing) on the polymer backbone.[45,109] Through competitive ion sorption experiments or through pulse field gradient nuclear magnetic resonance spectroscopy (PFG NMR), researchers have measured counter-ion binding constants in an independent experiment and subsequently predicted ion partitioning in the membrane. In this context, the binding constant refers to the equilibrium constant for the reversible reaction between speciated and ion-paired counter-ions and fixed charge groups. Münchinger and Kreuer[45] specified that the charge densities of the membranes in their study were below the threshold for condensation, so they did not consider the counter-ions to be condensed. Instead, they estimated a Cs^+ binding constant in Nafion 117 via PFG NMR, then reduced the Cs^+ activity in the Donnan model accordingly to yield quantitative agreement with their experimental sorption data from 1 to 5 M

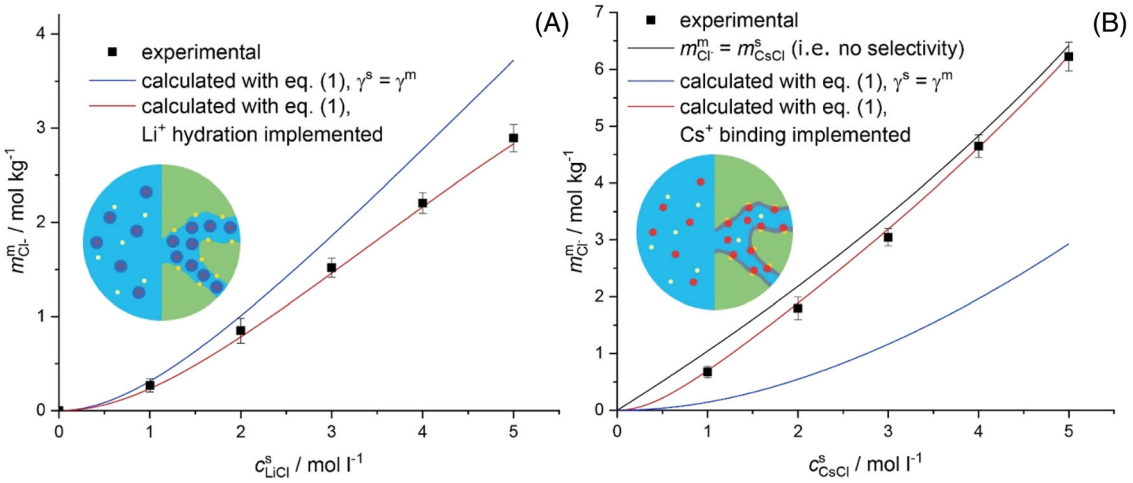

FIGURE 22 Co-ion concentrations in Nafion 117 as a function of external solution salt concentration.[45] (A) The symbols represent the experimental LiCl partitioning data. The blue line represents predictions by the ideal Donnan model. The red line represents predictions by the ideal Donnan model where the membrane concentration is expressed as moles per liter of free water. The amount of free water in the membrane was calculated by assuming a Li^+ hydration number of 3.4. (B) The symbols represent the experimental CsCl partitioning data. The blue line represents predictions by the ideal Donnan model with the assumption that all of the fixed charge groups are dissociated. The black line represents predictions by the ideal Donnan model with the assumption that none of the fixed charge groups are dissociated. The red line represents predictions by the ideal Donnan model for partial fixed charge dissociation, using a binding constant derived from PFG NMR data. *Source*: Adapted with permission from Reference 45, 2019, Elsevier

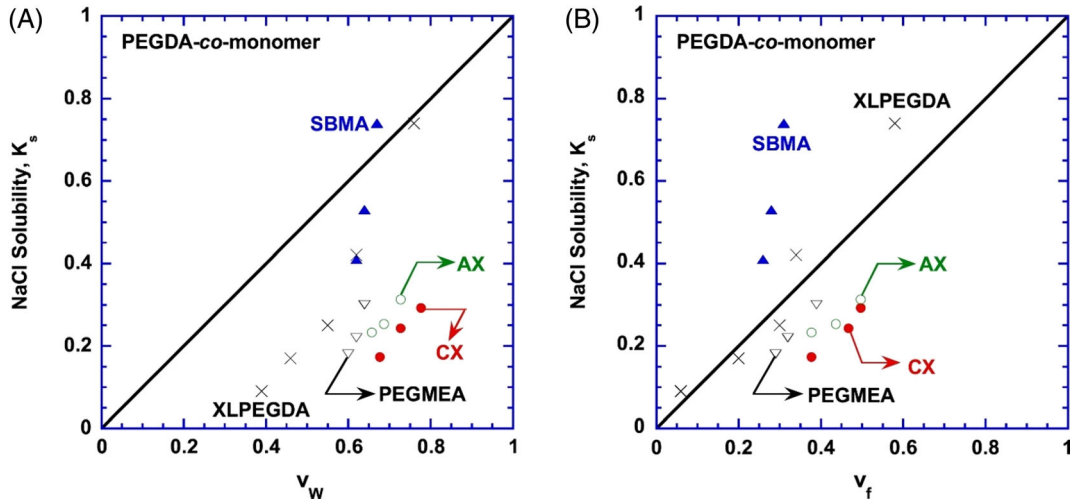

FIGURE 23 NaCl solubility coefficients for membranes equilibrated with 0.5 M NaCl solutions.[107] Results are presented for various membranes, including: linear neutral membranes PEGMEA made from poly(ethylene glycol) methyl ether acrylate, cross-linked neutral membranes XLPEGDA made from PEGMEA-*co*-PEGDA, cross-linked cationic membranes CX made from AMPS-PEGDA, cross-linked anionic membranes AX made from [2-(acryloyloxy)ethyl] trimethyl ammonium chloride (AETMAC)-PEGDA, and cross-linked zwitterionic membranes SBMA made from sulfobetaine methacrylate (SBMA)-PEGDA. The line in both graphs represent parity lines between salt solubility and water volume fraction. (A) The parity line was generated by calculating the water volume fraction using the total volume of sorbed water. (B) The parity line was generated by calculating water volume fraction using only the volume of freezable water in the membrane, informed by DSC data. *Source*: Adapted with permission from Reference 107, 2019, Elsevier

(Figure 22B). Through a separate approach, Breytus et al.[109] measured counter-ion binding constants with mixed salt sorption experiments for Cl^- and NO_3^- in commercial AMV, AMX, and FAB AEMs. The binding constants in this study allowed the author to describe ion partitioning in these membranes between 10 and 100 mM. Although it is very useful to predict ion sorption in IEMs using independent measurement of the membrane-binding constant, this process is still considerably more involved than describing the system from

quantities that are more readily determined such as the water content and fixed charge concentration. These binding models would have greater appeal if accompanied by facile techniques for predicting the binding constants. Additionally, most counter-ions do not bind with fixed charges as strongly as, for example, Cs^+ does.[3] Therefore, this approach may not yield a framework applicable to every counter-ion. Further, it has not been demonstrated that a large number of membranes of interest are within this ion pairing-dominated regime. Nevertheless, the successes described here demonstrate great promise for further development in these areas.

2.4.2 | Solution-adapted models

The second broad category of models for ion partitioning in IEMs is the solution-adapted models. Perhaps as the simplest way to introduce effects that are present in aqueous solutions, Galizia et al. assumed that all solution non-idealities are also present in the membrane, with the membrane adding additional contributions to the free energy of the system. These authors utilized the Modified Manning model[110] by incorporating all solution-phase non-idealities to the framework.[47] This was motivated by their experimental observations with $CaCl_2$ partitioning in CR61 at concentrations up to 6 M. Though this modification worsened agreement between the updated model and experimental data at moderate external concentrations (0.3–2 M), the accuracy of the framework for extreme external salt concentrations (0.01–0.03 M and 3–6 M) was significantly improved (Figure 24).[47,87] The advantage of this approach is that the solution activity coefficients are already involved in the nonideal Donnan model, so no new information is needed for this Modified Manning model. This ease of use comes at the cost of ignoring known differences between the membrane and the external solution. For example, the membrane dielectric constant is already utilized in calculating the activity coefficient contributions from Manning's model, but the solution activity coefficients utilize the solution-phase dielectric constant.

The Born model, which can quantify the energy of solvation for mixed-solvent systems,[111–113] is another framework that has been utilized for predicting ion partitioning in IEMs. The Geise group has applied this model to IEMs,[59,61,62,85] treating the membrane as a polymer-water mixture. The Born model's inputs are the membrane dielectric constant and ion-specific Born radii, making its use extremely straightforward. It is subtle, but the Born model adjusts the reference state of another activity model.[50] The implications are that another model must be applied in conjunction with the Born model. Thus, to apply the Born model alone is to claim that ion interactions are ideal within the membrane—only the state of infinite dilution is different. This is the way in which Chang et al.[59,61] applied the Born model. Ji et al.[85] relaxed this assumption by defining polarizability parameters to describe the London dispersion force-type interactions within the membrane as well.

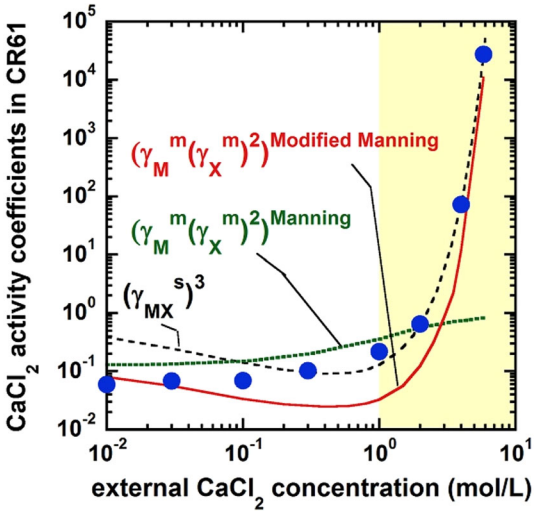

FIGURE 24 $CaCl_2$ activity coefficients in CR61 as a function of external solution salt concentration.[47] The symbols represent activity coefficients obtained from experimental ion partitioning data. The green dashed line represents predictions by the Manning model, the red solid line represents predictions by the modified Manning model, and the black dashed line represents predictions by the Pitzer model. *Source*: Adapted with permission from Reference 47, 2019, Elsevier

To test both the ideal-interaction and polarizability Born frameworks, Ji et al. reported partitioning data for the AMPS-PEGDA membrane equilibrated with 0.1 and 0.5 M NaCl, NaBr, $NaNO_3$, and $NaClO_4$. The authors observed poor agreement between sorption experiments and predictions by the ideal and dispersion-modified Born models, presented in Figure 25. Neither version of the Born model yielded predictions within an order of magnitude of the experimental data. Treating the membrane dielectric constant as an adjustable parameter allowed these models to fit the data reasonably well, on par with predictions from Manning's model for the NaCl data.[85] One notable advantage of the Born model is the allowance for ion-specific effects, which is important for the membrane in this study because the partitioning results demonstrate a strong dependence on the co-ion identity. Manning's model does not incorporate ion-specific effects, treating all ions simply as point-charges, so the Donnan-Manning model cannot explain co-ion specific effects.

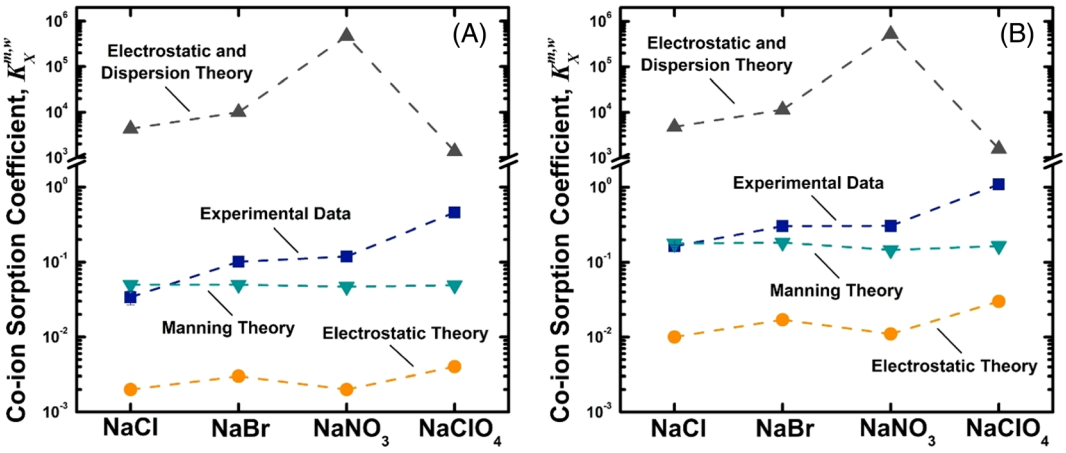

FIGURE 25 Co-ion sorption coefficients for AMPS-PEGDA membranes as a function of salt identity for (A) 0.1 M and (B) 0.5 M external solution concentrations. The blue squares represent the experimental data. The teal inverted triangles represent predictions by the Donnan-Manning model, the orange circles represent predictions by the ideal Born model, and the gray triangles represent predictions by the dispersion-modified Born model. *Source*: Adapted with permission from Reference 85, 2018, Elsevier

One of the most extensive developments among the solution-adapted approaches for modeling ion sorption in IEMs was performed by Yu et al.[84] The authors developed an all-encompassing approach: counter-ion condensation effects were incorporated through Manning's framework, reference state effects were incorporated through the Born model, and the solution-phase activity coefficients under the real conditions of the membrane were re-calculated. For long-range electrostatic effects between mobile ions within the IEM, the authors employed the Pitzer-Debye-Hückel model (PDH, an abbreviated and predictive version of the Pitzer model used for aqueous solution activity coefficients).[70] Then, for short-range forces in the sorbed solution and at the sorbed solution-polymer interface, they used the non-random two-liquid (NRTL) model.[114] As a combination of these four frameworks, Yu et al. proposed the polyelectrolyte NRTL (peNRTL) model for ion activity coefficients in the solutions of polyelectrolytes (Figure 26). With two manuscripts, the authors tested the utility of the peNRTL model first on polyelectrolytes,[50] then on IEMs.[84]

The peNRTL model requires multiple adjustable parameters, but it has the advantage of using the values broadly (e.g., all AMPS-based IEMs should be able to utilize the reported AMPS interaction parameters). The NRTL contributions to this model required binary interaction parameters between water and each monomer component of the membrane, as well as water and the sorbed salt. The water-salt parameters were available in the literature, but the water-monomer interaction parameters had to be fit from Yan et al.'s AMPS-PEGDA NaCl partitioning data.[48] Yu et al. also used ξ as an adjustable parameter, amounting to five values that were fit from the studied data set. With this in mind, Yu et al. report that their peNRTL model accurately described experimental ion activity coefficients

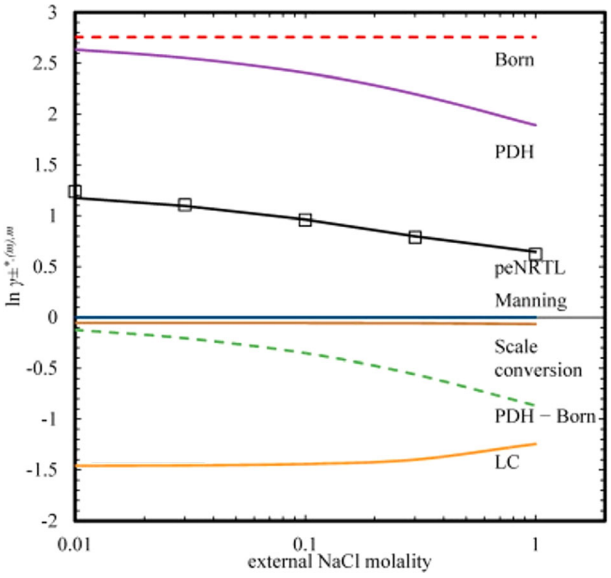

FIGURE 26 Contributions of the various factors to the peNRTL model predictions for NaCl ion activity coefficients in an uncharged PEGDA membrane. The symbols represent the experimental data. Highlighted contributions include the Born model, the Born-modified PDH model, the Manning model, a mole fraction-to-molarity correction, the PDH model without the Born model's correction, and local contributions (LC) as handled by the NRTL theory. *Source*: Adapted with permission from Reference 84, 2021, Elsevier

within the entirety of their membrane series from 0 to 65 mol% charged monomer.[84] The authors observed excellent agreement between the modeled and experimental ion activity coefficients in weakly charged membranes at external NaCl concentrations ranging from 0.01 to 1 M. For highly charged membranes, the modeled activity

coefficients described the partitioning data at high and low concentrations but the model predictions deviated slightly for the moderate concentrations. The excess of adjustable parameters limits the peNRTL model to being semi-predictive. However, the utility of this model could increase once more generalized interaction parameters are reported. The broad applicability of Yu et al.'s demonstration, ranging from uncharged to highly charged membranes, makes the peNRTL model compelling.

To summarize, although the Manning condensation framework for IEMs has some limitations, which many of the models discussed in this section attempt to improve upon, none of the models has reached the same level of expansiveness nor predictive power as the Donnan-Manning model. Despite these extensive efforts, a simple predictive model which applies to a broad range of materials, akin to the Debye-Hückel theory for electrolyte solutions, remains elusive.

3 | THE MANNING-MEARES MODEL FOR ION DIFFUSION IN IEMS

3.1 | Model development

Manning's original series of manuscripts on counter-ion condensation included a discussion of small ion diffusion in dilute polyelectrolyte solutions.[24] Analogously, Manning's model as adapted to IEMs contains a diffusive portion as well.[17] Three effects enter into this diffusion framework, referred to as the Manning-Meares model: counter-ion condensation and long-range electrostatic forces, which are treated with Manning's counter-ion condensation theory, are combined with membrane tortuosity considerations as handled by the Mackie and Meares model.[15,16] In addition to the previously discussed assumptions, this diffusion framework assumes that the polymer phase can be modeled as a cubic lattice of impermeable space, similarly to the classic treatments of Flory and Huggins.[102]

The most straightforward consideration in the Manning-Meares model is the tortuosity factor proposed by Mackie and Meares.[16] Although it has not been accurate in every study using the model, the Mackie and Meares model has been widely used because of its reasonable accuracy and completely predictive nature. In developing their model, Mackie and Meares considered an impermeable polymer phase with no sieving potential for the solutes of interest—the solution within the membrane permits ion diffusion similarly to an aqueous solution, but the phase is contorted around the polymer chains. For the timescales relevant to ion diffusion, the polymer chains were assumed to be stationary. Thus, this model exclusively accounts for tortuosity effects based on the random interweaving of solution domains and polymer chains across a cubic lattice. The resulting tortuosity factor is given by[16,17]:

$$\left(\frac{D_i^m}{D_i^s}\right)_{tort} = \left(\frac{\phi_w}{2-\phi_w}\right)^2 \text{ for } i = g,u;c \tag{24}$$

Here D_i^m refers to the diffusivity of species i in the membrane phase, D_i^s refers to the diffusivity of species i in the solution phase, and ϕ_w refers to the volume fraction of water in the membrane. When applying this model, Kamcev et al. reasoned that the tortuosity effects would be relevant for free ions which diffuse in the solution phase of a membrane, so the model applies just to the uncondensed counter-ions, along with the co-ions ($i = g,u;c$). This tortuosity factor contributes to a significant decrease in ion diffusivity in IEMs since water volume fractions are typically less than 0.6. Indeed, the Mackie and Meares model predicts nearly an order of magnitude decrease in ion diffusivity in conventional IEMs used for brackish water desalination (Figure 27).[17]

The fixed charges along the polymer backbone also affect the diffusivity of mobile ions. These pairwise interactions between ions were treated in accordance with Manning's counter-ion condensation theory. By assuming a lattice for ion movement about the polymer's electrostatic potential well and by employing the Einstein equation (which relates an ion's diffusivity to its mobility), Manning derived the following equations[24]:

$$\left(\frac{D_i^m}{D_i^s}\right)_{elec} = 1 - \frac{z_i^2}{3} * A \text{ for } i = g,u;c \tag{25}$$

$$A\left(\frac{\xi}{\xi_{crit}};X\right) = \sum_{m_1=-\infty}^{+\infty}\sum_{m_2=-\infty}^{+\infty}\frac{1}{z_g^2}\left(\frac{\pi\xi_{crit}}{\xi}\left(m_1^2+m_2^2\right)+1+\frac{\left|\frac{z_c}{z_A}\right|\left(\nu_g+\nu_c\right)}{X}\right)^{-2}$$
$$\text{for } \xi \le \xi_{crit} \text{ and } (m_1,m_2) \neq (0,0) \tag{26}$$

$$A\left(1;\frac{\xi_{crit}X}{\xi}\right) = \sum_{m_1=-\infty}^{+\infty}\sum_{m_2=-\infty}^{+\infty}\frac{1}{z_g^2}\left(\pi\left(m_1^2+m_2^2\right)+1+\frac{\xi\left|\frac{z_c}{z_A}\right|\left(\nu_g+\nu_c\right)}{\xi_{crit}X}\right)^{-2}$$
$$\text{for } \xi \ge \xi_{crit} \text{ and } (m_1,m_2) \neq (0,0) \tag{27}$$

Here, z_i refers to the valence of ion i, ξ is the reduced linear charge density, X is the ratio of fixed charge groups to sorbed salts, and ν_i refers to the number of ions i per salt molecule. Finally, there are two arbitrary summation indices m_i. The inputs of the function A are, for both

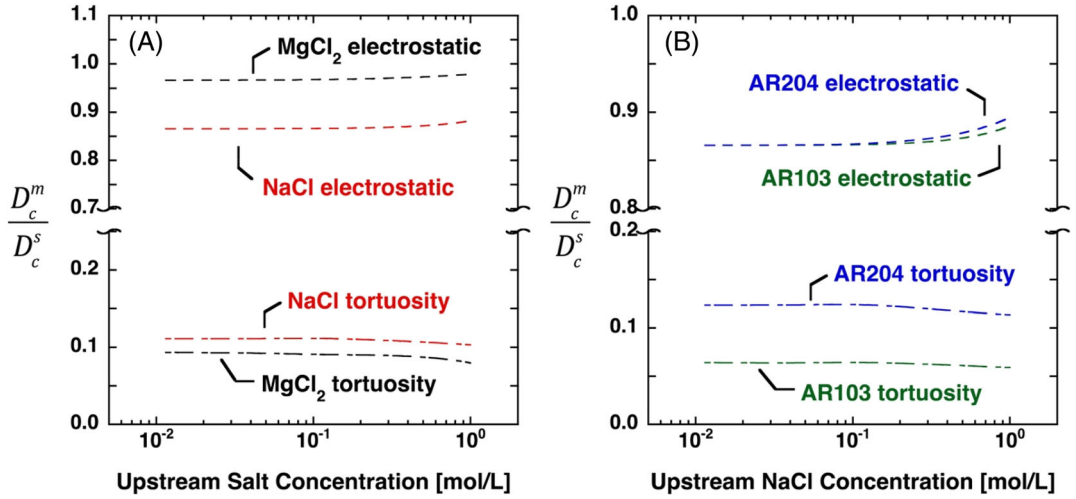

FIGURE 27 Contributions of the Mackie and Meares tortuosity model and the Manning electrostatic model to the predicted co-ion diffusivities of (A) NaCl and $MgCl_2$ in CEM CR61 and (B) NaCl in AEMs AR103 and AR204.[17] The plots present the diffusivity ratio of co-ions in the membrane to those in the external solution versus upstream salt concentration. *Source*: Adapted with permission from Reference 17, 2017, American Chemical Society

Equations (26) and (27), (1) the effective dimensionless charge density and (2) the ratio of the effective fixed charge group concentration to mobile salt concentration. The effective values are not equal to the true values in Equation (27) due to counter-ion condensation; these changes have already been made, so the true values for X and ξ/ξ_{crit} should be used in these equations. These electrostatic factors only contribute to the diffusivity of uncondensed counter-ions and co-ions, and will typically amount to just a moderate decrease in ionic diffusivity relative to an aqueous solution (Figure 27). It is interesting to note that uncondensed counter-ions and co-ions of equivalent valence are impacted identically in this electrostatic treatment.

As discussed previously, there are presumed to be two distinct populations of condensed counter-ions: site-bound and territorially bound. Territorially condensed counter-ions are almost assuredly mobile and contribute to ion transport.[15,24,53,115,116] Unfortunately, their mobility has not yet been understood on a fundamental level, and a framework to predict the sub-populations of territorially and site-wise condensed counter-ions has yet to be developed. For simplicity's sake, Manning did not attempt to predict the condensed counter-ion mobility, originally treating all condensed counter-ions as immobile.[24] In developing the diffusion model for IEMs, Kamcev et al. relaxed this assumption: they allowed for the condensed counter-ions to diffuse along the polymer backbone, and for their diffusivity to differ from that of the uncondensed counter-ions. The total counter-ion diffusivity was modeled as a weighted average of the uncondensed and condensed counter-ion diffusivities[15]:

$$D_g^m = f_u D_{g,u}^m + f_c D_{g,c}^m \tag{28}$$

$$\left(\frac{D_{g,c}^m}{D_g^s}\right)_{\text{condens}} = \frac{1}{3}\alpha \tag{29}$$

Here, f_u and f_c refer to the fraction of uncondensed and condensed counter-ions, respectively. In Equation (29), the factor of three is derived from measuring the transport in one dimension, while the polymer chains exist in three. The factor α, then, is left as an unknown adjustable parameter to capture various factors that might impact the mobility of condensed counter-ions, such as the molecular architecture of the nearby polymer or water. This parameter α should not be confused with the membrane selectivity, $\alpha_{i/j}$, which was defined in Equation (4).

Kamcev et al. rationalized the allowance of condensed counter-ion transport in IEMs by considering the continuity of polymer networks. A rather subtle difference between dilute polyelectrolytes and cross-linked IEMs is the total percolation of the polymer phase. That is to say, in a solution of dilute, finite polyelectrolytes, condensed counter-ions would not be able to travel great distances before reaching the end of a polymer chain.[115] In contrast, cross-linked IEMs contain a continuous, percolated polymer phase, which could allow a condensed counter-ion to cross from one end of the membrane to the other.[15] So, whereas potentially-mobile condensed counter-ions in polyelectrolyte systems would quickly become trapped in local energy minima, the same species would be free to transport continuously in percolated IEMs.

Combining the equations set forth in this section (Equations (24)–(29)) yields the Manning-Meares model for ion diffusion in IEMs. Returning to the assumption of monovalent species ($|z_A| = |z_g| = |z_c| = \nu_g = \nu_c = \xi_{crit} = 1$) and a highly-charged membrane ($\xi > \xi_{crit}$), the counter- and co-ion diffusivities are given below:

$$\frac{D_g^m}{D_g^s} = f_u\left(1 - \frac{1}{3}A\left(1;\frac{X}{\xi}\right)\right)\left(\frac{\phi_w}{2-\phi_w}\right)^2 + f_c\frac{\alpha}{3} \text{ for } \xi \geq 1 \quad (30)$$

$$\frac{D_c^m}{D_c^s} = \left(1 - \frac{1}{3}A\left(1;\frac{X}{\xi}\right)\right)\left(\frac{\phi_w}{2-\phi_w}\right)^2 \text{ for } \xi \geq 1 \quad (31)$$

Because α is an adjustable parameter, several researchers have found it more convenient to assume that condensed counter-ions do not transport, setting it to 0 (as discussed in the next section). This generally has led to poor agreement but may be a starting point for any predictive discussions.

The usefulness of modeling average diffusivities for both counter- and co-ions can be seen in any transport experiment. The application to electric field-driven ionic conductivity and concentration gradient-driven permeability are highlighted here. Both situations are special cases derived via the Nernst-Planck Equation as it is applied to membranes[15]:

$$J_i^m = -D_i^m\left(\frac{dC_i^{m,t}}{dx} + \frac{z_i F C_i^{m,t}}{RT}\frac{d\Psi}{dx}\right) \quad (32)$$

In this equation, J_i^m refers to the flux of species i across the membrane (assumed to be the x direction), $C_i^{m,t}$ refers to the concentration of species i in the total membrane volume, and Ψ refers to the electric potential across the membrane. F refers to the Faraday constant, R refers to the ideal gas constant, and T is the absolute temperature. For concentration gradient-driven membrane permeability experiments, the diffusion of ions is coupled through electroneutrality, so the electric potential term may not be wholly neglected. The coupled salt diffusion coefficient can be related to the ion diffusivities and concentrations of a single electrolyte as[15,17]:

$$D_s^m = \frac{D_g^m D_c^m\left(z_g^2 C_g^m + z_c^2 C_c^m\right)}{z_g^2 C_g^m D_g^m + z_c^2 C_c^m D_c^m} \quad (33)$$

$$D_s^m \approx D_c^m \text{ for } C_g^m \gg C_c^m \quad (34)$$

Here, the electrical potential term in the Nernst-Planck equation has been invoked as the electroneutral coupling which arises in the co-transport of counter- and co-ions. The concentration scale (w for sorbed water or t for total membrane) does not matter so long as the same volume scale is used for each concentration in Equation (33). From Equation (34), which is a more limited version of Equation (33) in the limit of many more counter-ions than co-ions, it can be immediately seen that the co-ions dominate the salt diffusion across IEMs. Per the solution-diffusion model,[117] the salt permeability of a membrane is related to the salt partition coefficient and the salt diffusivity of the membrane ($P_s = K_s D_s^m$), which then yields Equation (2).[17] Simultaneously applying Equations (16) and (33) with activity coefficients and diffusivities defined per Equations (11), (12), (30), and (31) yields a framework for predicting the salt permeability coefficients of highly charged IEMs contacted by single electrolyte solutions. In the limit of low co-ion sorption, the counter-ion diffusivity is weighted only minimally, so the adjustable parameter that quantifies condensed counter-ion transport may be safely excluded to the point where the Manning-Meares Model is entirely predictive for membrane permeability.[17]

To examine the ionic conductivity of IEMs, we assume that electroneutrality and concentration gradients will not influence the steady-state ion transport. In Equation (32), this leaves only the electric field driving force for the ionic flux, which yields a current density I.[15]

$$I = F\sum_i z_i J_i^m = -\frac{F^2}{RT}\sum_i z_i^2 C_i^{m,t} D_i^m \frac{d\Psi}{dx} \quad (35)$$

By assuming that there are only two species in the membrane, the counter- and co-ions, we arrive at the definition for conductivity given in Equation (1). Here the independent motion of ions yields an additive relationship of the current carried by counter- and co-ions. Therefore, the speed of condensed counter-ions cannot be downplayed by their overabundance, and the modeled membrane conductivity is not predictive due to the adjustable constant α. Fitting a single value of α, which remains independent of salt concentration and falls in the range $0.5 < \alpha < 1$, described conductivity data quite well in the introductory study by Kamcev et al.[15] This agreement between fit and experimental data suggests that Equation (30) and Equation (31) have the right functional form. The values of α fit in this study suggest that condensed counter-ion diffusivities may be around twice as high as those of uncondensed counter-ions (Figure 28). At present, the greater mobility of condensed counter-ions relative to that of the uncondensed counter-ions is not well understood. Kamcev et al. rationalized this observation by considering differences in the total distance traveled by the ions as well as their size. By diffusing along the polymer backbone, condensed counter-ions

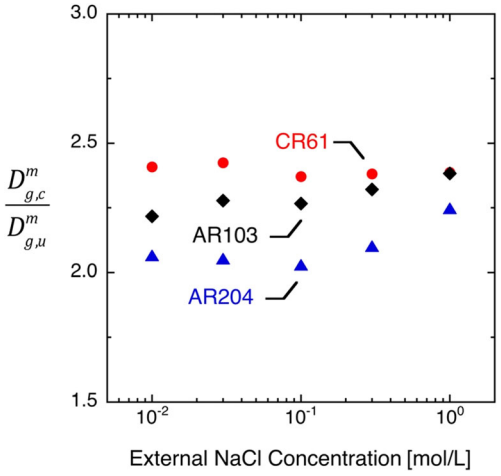

FIGURE 28 Ratios of fitted condensed counter-ion diffusion coefficients within the membrane to the predicted uncondensed counter-ion diffusion coefficients as a function of external solution salt concentration.[15] The data represent three membranes (CR61, AR103, and AR204) contacted by NaCl solutions. *Source*: Reproduced with permission from Reference 15, 2018, American Chemical Society

potentially travel a shorter distance to cross the membrane than uncondensed counter-ions. Additionally, if counter-ion condensation is accompanied by partial loss of hydration, the size of the condensed counter-ions would be smaller than that of the uncondensed counter-ion. Further investigation is necessary to elucidate the true nature of this phenomenon. With this example of condensed counter-ions diffusing about twice as fast as uncondensed counter-ions, and with the context that many commercial IEMs exhibit values of $f_c \sim 0.5$,[78,79] it is clear that this mode of transport should not be neglected when attempting to describe counter-ion mobility in IEMs.

Similarly to ξ, fitting α under one set of experimental conditions should allow the sequential prediction of the membrane performance under other conditions. Therefore, the Manning-Meares model is predictive of membrane salt permeability and semi-predictive of membrane ionic conductivity. Developing a predictive equation for α would be the final step in describing IEM ion transport based on just tortuosity, fixed charge group electrostatic friction, and counter-ion condensation.

3.2 | Experimental ion diffusion studies

3.2.1 | The Manning-Meares model assuming mobile condensed counter-ions

The original studies by Kamcev et al. detail the application of the Manning-Meares model to predict both the salt permeability (co-ion dominated transport) and ionic conductivity (counter-ion dominated transport) of several commercial IEMs. First, the coupled salt diffusion coefficients (Equation (33)) in CR61, AR103, and AR204 were predicted.[17] The salt permeability coefficients of each membrane were subsequently calculated for upstream solutions of 0.01–1 M salt and a downstream chamber filled with DI water. This procedure involved applications of both the Donnan-Manning model for predicting the ion concentrations and the Manning-Meares model for predicting the ionic diffusivities in the membranes. The predicted salt diffusion coefficients were in good agreement with the experimental data. Both modeled and measured values were approximately one order of magnitude lower than the values for aqueous solutions (Figure 29). The Manning-Meares model predicted a moderate decrease in diffusivity with increasing concentration. However, the results for NaCl in each membrane and for $MgCl_2$ in CR61 did not display any clear trends within the experimental uncertainties. When combined with the sorption coefficient into permeability predictions, the predicted values were somewhat lower than experimental salt permeabilities at the lower salt concentrations, but agreement improved at the higher salt concentrations. Much of the discrepancy at lower concentrations can be attributed to the partitioning component of the framework, as the Donnan-Manning model also under-predicted salt partitioning at these low concentrations (Figure 4C).

In a second study, the same membranes were utilized to study electric field-driven counter-ion transport.[15] The ionic conductivity of CR61, AR103, and AR204 were probed when equilibrated with 0.01–1 M NaCl. With the co-ion diffusion coefficients already predicted for use in the salt permeability study, the counter-ion diffusivities were fit extremely well with the single adjustable parameter α (Figure 30). The fact that a single value of α produced excellent agreement at all external salt concentrations in this study suggests that the functional form of the model is correct, even though it is not predictive regarding this specific quantity. Additionally, because the counter-ion diffusivity at each salt concentration is consistent with a single value of α, the Manning-Meares model may be used semi-predictively. That is, measuring α for a membrane at any of these concentrations would have allowed predictive modeling at other concentrations. Thus, this pair of studies demonstrate that the Manning-Meares model can precisely describe counter- and co-ion diffusivities in several commercial IEMs.

Ji et al. applied the Manning-Meares model to describe the salt permeability of several sodium salts (NaCl, NaBr, $NaNO_3$, and $NaClO_4$ at 0.1 and 0.5 M) in weakly charged AMPS-PEGDA membranes. The authors performed the experiments without an electric field, so

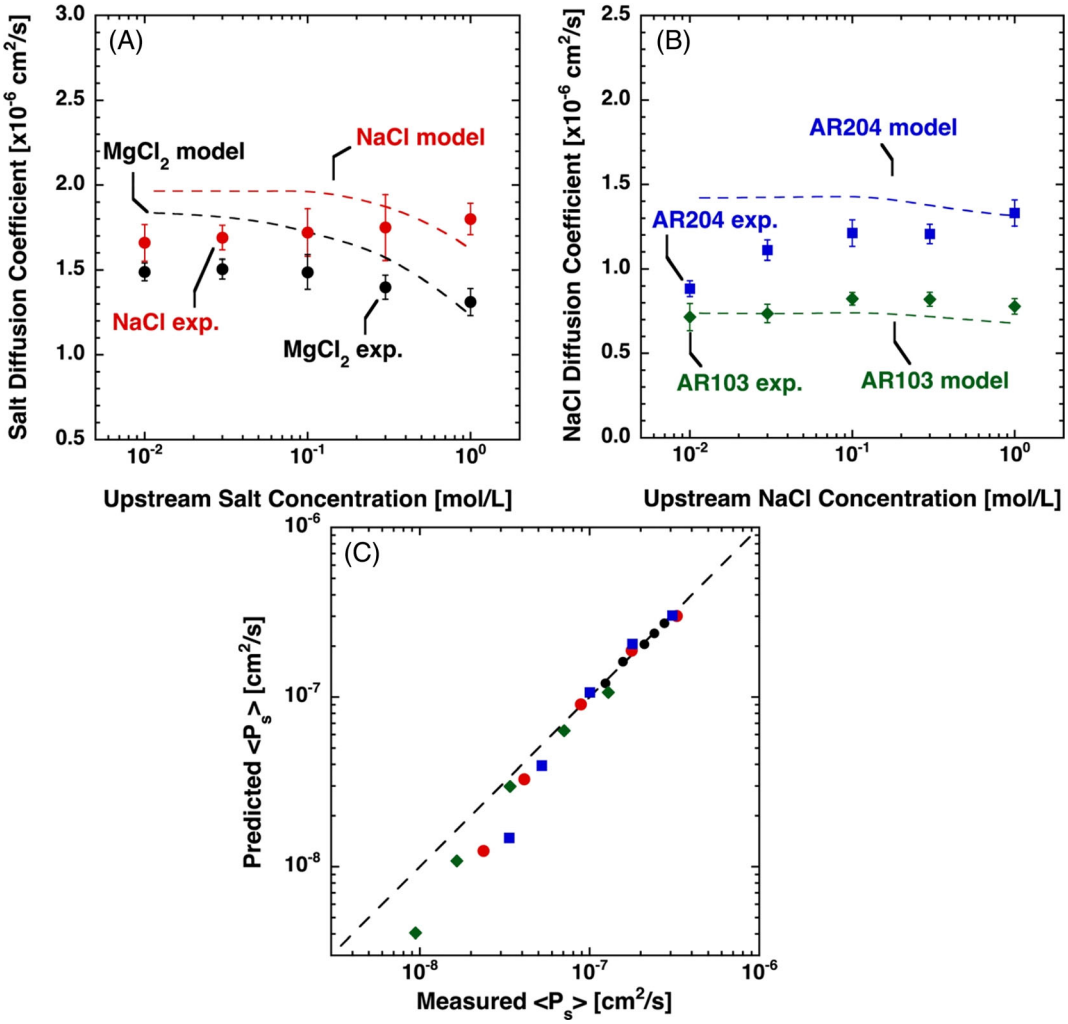

FIGURE 29 (A) and (B) Salt diffusion coefficients in IEMs as a function of external upstream salt concentration.[17] The symbols represent the experimental data, while the dashed lines represent predictions by the combined Donnan-Manning and Manning-Meares models. (A) NaCl and $MgCl_2$ permeability experiments were performed with CEM CR61. (B) NaCl permeability experiments were performed with AEMs AR103 and AR204. (C) Parity plot of salt permeability coefficients for NaCl (red circles) and $MgCl_2$ (black circles) in CR61 and NaCl in AR103 (green diamonds) and AR204 (blue squares). Salt permeability coefficients predicted by the Donnan-Manning/Manning-Meares models are plotted versus the experimentally measured salt permeability coefficients. *Source*: Adapted with permission from Reference 17, 2017, American Chemical Society

co-ion transport is expected to govern the overall salt permeation rate and the relevance of condensed counter-ions is expected to be minimal. Moreover, the charge density of the IEM was below the threshold for condensation—the Manning-Meares model is fully predictive for this scenario due to the absence of condensed counter-ions.[85] The Manning-Meares model predicted salt diffusion coefficients remarkably well for NaCl, but the predictions for NaBr, $NaNO_3$ and $NaClO_4$ deviated from the experimental data significantly (Figure 31). The authors attributed the discrepancy between modeled and experimental diffusivities to specific interactions between the polymer and co-ions (complexation, in the case of $NaClO_4$), which are not accounted for by the Manning-Meares model. Ji et al. also suggested that the co-ion shape (spherical for chloride and bromide, planar for nitrate, and tetrahedral for perchlorate) could impact co-ion diffusivity in the IEMs, though such effects are only expected to be important when the membrane's mesh size approaches the size of the solute. IEMs are typically not considered to sieve solutes as small as ions based upon their size. Further study regarding the IEM chemistry and mesh size would be necessary to refine these claims and understand co-ion specific effects.

Wang et al. studied the ionic conductivity of IEMs equilibrated with differing salts: they investigated AR103 and AR204 equilibrated with NaAc (sodium acetate) and NaLa (sodium lactate) between 0.1 and 1 M and at pH

values between 3.5 and 7.[83] The authors found good agreement between the modeled values and experimental results when using theoretical ξ values and fitted α values (Figure 32). The pH and concentration dependence of the modeled Ac^- diffusivities were predicted similarly well by utilizing the values of ξ fitted from their sorption analysis with the Donnan-Manning model; these values for ξ were below ξ_{crit}, so no additional adjustable parameter was needed for calculating the diffusivities for the ξ_{fit} conditions. Regarding the pH dependence, the membrane diffusivities of Ac^- under the acidic conditions were over-predicted by the Manning-Meares model. The authors postulated that the formation of acetate dimers can potentially explain the strong dependence of acetate diffusion coefficients on solution pH. This collection of fitted and semi-predictive Manning-Meares data demonstrate the robustness of the framework even with such uncommon salts as NaAc and NaLa.

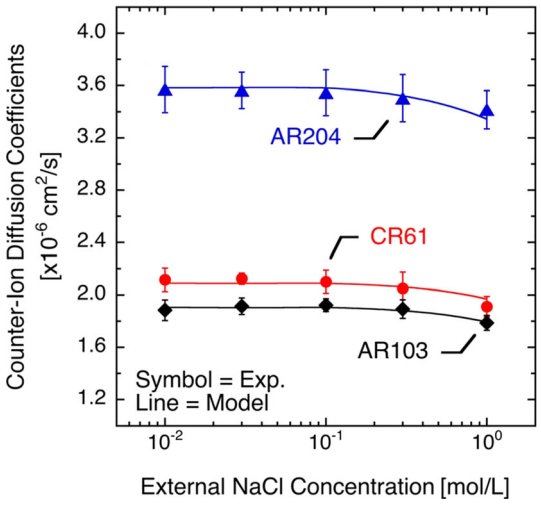

FIGURE 30 Counter-ion diffusion coefficients in IEMs CR61, AR103, and AR204 as a function of external solution NaCl concentration. The symbols represent the experimental data. The lines represent predictions by the Donnan-Manning/Manning-Meares models after fitting the adjustable parameter α. A single value of α was utilized for each membrane to produce the modeled values over the entire concentration range. *Source*: Adapted with permission from Reference 15, 2018, American Chemical Society

3.2.2 | The Manning-Meares model assuming immobile condensed counter-ions

The use of the complete Manning-Meares model for ion diffusion in IEMs is much less frequent than that of the Donnan-Manning partitioning model—this may be partially due to its more recent development, or also due to its non-predictive nature. To the best of our knowledge, the studies discussed in the preceding section are the only ones in the open literature that use the complete Manning-Meares model to describe ion diffusion in IEMs. The remaining experimental studies, discussed below, utilize the limited version of the treatment which assumes that condensed counter-ions are immobile. This assumption renders the framework fully predictive. However, as discussed previously, condensed counter-ions could contribute to the overall counter-ion diffusivity to a significant degree (Figure 28). This limited treatment is therefore expected to yield poor predictions of counter-

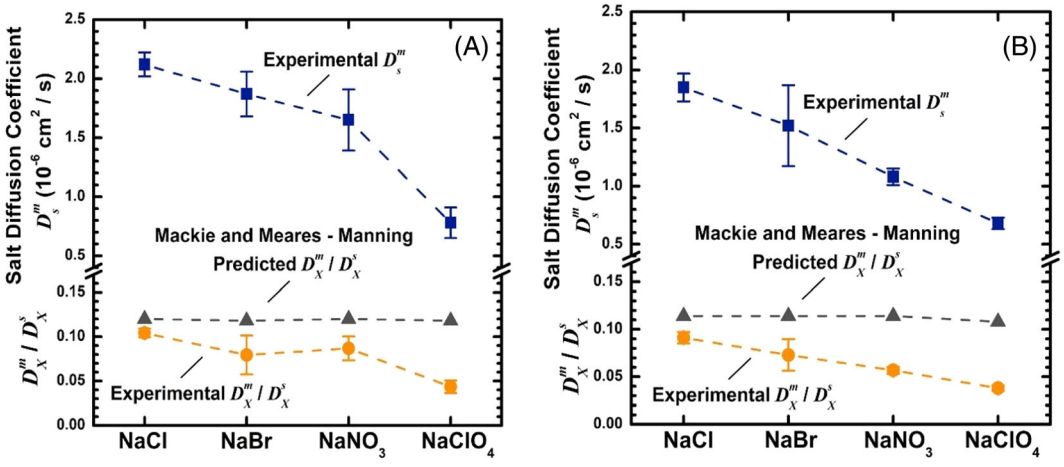

FIGURE 31 Diffusivities from salt permeability experiments performed with an AMPS-PEGDA membrane contacted by different salt solutions.[85] The blue squares represent the experimental results. The orange squares represent the ratio of experimental co-ion diffusivities in the membrane and in solution. The gray triangles represent predictions by the Manning-Meares model. (A) The upstream concentration in the permeability experiments was 0.1 M. (B) The upstream concentration in the permeability experiments was 0.5 M. *Source*: Adapted with permission from Reference 85, 2018, Elsevier

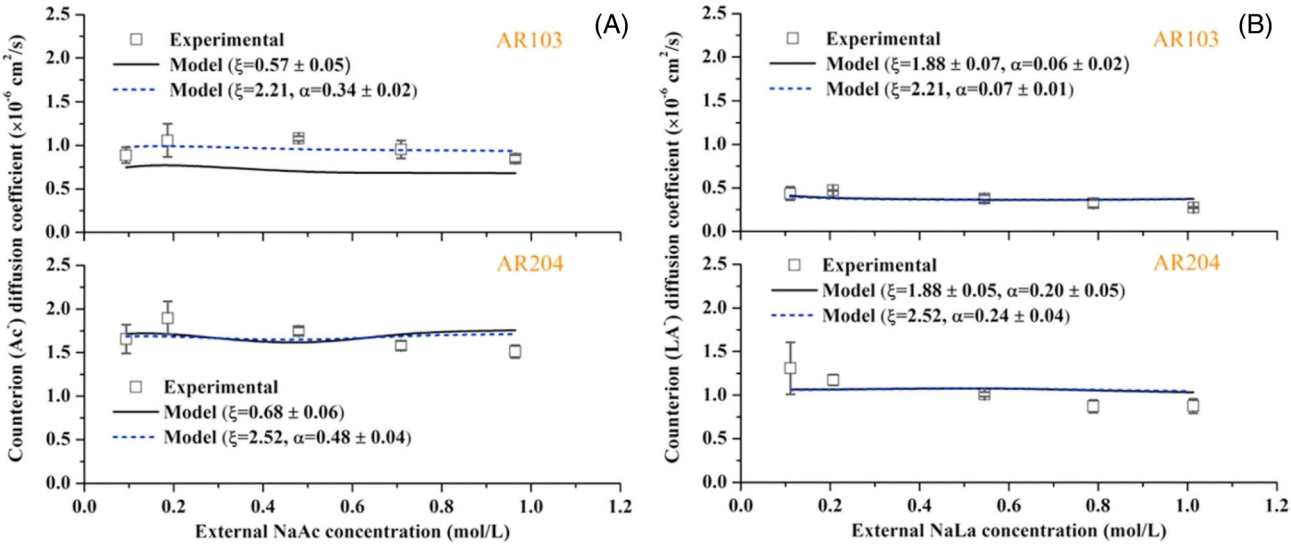

FIGURE 32 Counter-ion diffusion coefficients in AR103 and AR204 membranes contacted by (A) sodium acetate (NaAc) and (B) sodium lactate (NaLa) solutions.[83] The symbols represent the experimental data extracted from ionic conductivity measurements. The lines represent predictions by the Donnan-Manning/Manning-Meares models with the theoretical values for ξ (blue line) as well as the ξ values fitted using partitioning data (solid black). The fitted values for α are recorded in the legend. *Source*: Adapted with permission from Reference 83, 2020, Elsevier

ion diffusivity when significant fractions of the counter-ions are condensed.

Several researchers have utilized the Manning model to correct for nonideal effects toward the counter-ion activity when predicting the counter-ion transport selectivity of IEMs. Luo et al. studied the mobility ratios of Mg^{2+}/Na^{+} and K^{+}/Na^{+} counter-ions in CMX, SPEEK, and F9120 membranes.[118] The authors quantified the counter-ion transport selectivity of their mixed-salt equilibrated IEMs via two methods: (1) ionic conductivity measurements in the single salt limit and (2) ED experiments with both salts present. Ion activities, instead of concentrations, were notably employed in the calculation of ionic mobilities from ionic conductivity results through the classical Nernst-Einstein equation. The authors point out that this is inconsistent with typical applications of the Nernst-Einstein equation.[119] Luo et al. utilized Manning's equations in the limit of zero co-ions, such that the ratio of two counter-ion activity coefficients (the actual quantity which appears in their analysis) explicitly represents the ratio of uncondensed counter-ions. This analysis is therefore equivalent to assuming that only uncondensed counter-ions carry the current in the presence of an electric field, though this was not explicitly stated by the authors. The use of activities in the Nernst-Einstein equation is not as unusual with this added context: when condensation is the only non-ideality considered, the activity modification merely amounts to considering only the concentration of uncondensed counter-ions. By comparison, traditional activity considerations (such as Debye-Hückel, which describe effective changes in concentration instead of actual ones) would represent a much greater deviation from typical applications of the Nernst-Einstein equation. The exception to this interpretation is the membrane F9120, which was not expected to exhibit monovalent counter-ion condensation based on its ξ value being less than 1. Regardless, by including the nonideal effects in their counter-ion transport selectivity predictions, Luo et al. observed improved agreement between the predicted counter-ion selectivity and the selectivity measured via ED.[119] We add that they put forth considerable efforts to model reasonable values for b in these membranes, particularly for the perfluoro sulfonic acid polymer F9120. However, an additional test of the calculated b values through sorption experiments was not performed.

The improved agreement between the Mg^{2+}/Na^{+} transport selectivity obtained by Luo et al. after accounting for non-idealities[118] may be a coincidence, since the agreement between the predicted and measured ED selectivity worsened for two of the three membranes when considering K^{+}/Na^{+} transport. Their application of Manning's model is only strictly valid for monovalent ions, so this result should be more representative of its analytic capabilities. The case of counter-ion condensation in the presence of mixed-valence counter-ions was not discussed in the Donnan-Manning model for IEMs. Manning dealt with this question many years after introducing his theory, detailing how all higher-valent counter-ions should condense before ions of lesser

valence.[41] This indicates that the fraction of condensed Na^+ in a Na^+-form CEM would presumably be much greater than the same value in the presence of Mg^{2+}. Such effects were not considered in the framework proposed by Luo et al., although they would likely be highly relevant. In the assumptions invoked by Luo et al., where condensed counter-ions are immobile, the preferential condensation of multivalent ions should lead to an overprediction of the Mg^{2+}/Na^+ selectivity when compared with the ED data. If the assumption of immobile condensed counter-ions is relaxed—if condensed counter-ions diffuse considerably faster than uncondensed counter-ions, as reported by Kamcev et al.—then the reverse is true, and the Mg^{2+}/Na^+ transport selectivity would be under-predicted. The latter case is observed in Luo et al.'s data.[118] The strictly preferred condensation of multivalent counter-ions complicates the comparison of ideal divalent/monovalent transport selectivities. Because this same problem is not present for ideal monovalent/monovalent selectivities, the worsened agreement between the K^+/Na^+ data should be a better representation of this data analysis technique. A potential complication still exists in monovalent/monovalent analyses because ion-specific interactions may still lead to marginal preferences for condensation between monovalent counter-ions. For example, the MD simulations performed by Aryal and Ganesan demonstrated Na^+ to be preferentially condensed over K^+ (Section 2.3).[95]

To further test the activity-corrected ionic conductivity framework for counter-ion transport selectivity, Zou et al. performed a complementary study on anion transport in commercial AEMs (ASE, ACS, and FAA) contacted by mixed sodium salt solutions containing NO_3^-/Cl^- and SO_4^{2-}/Cl^- counter-ions.[119] The premises for these studies were similar, except the simple conductivity control of Luo et al. was now replaced with an expression that resembles Kohlrausch's law. Kohlrausch's law is generally used to predict the concentration dependence of ionic conductance in aqueous electrolyte solutions.[40] The Debye-Hückel-Onsager equation informed the theoretical basis for Kohlrausch's law, revealing that it accounts for the electrostatic interactions which restrict ionic mobility.[40] In the study by Zou et al., Kohlrausch's law was proposed to account for interactions between counter-ions of different identity in the membrane. The AEM modeling results were less conclusive than those of the original study[118] involving CEMs. The membrane FAA was not analyzed per Manning's framework, so the authors limit the discussion of condensation to just two membranes, ASE and ACS. Only considering uncondensed ions to be conductors improved the selectivity predictions under two conditions (SO_4^{2-} in ASE and NO_3^- in ACS) but worsened the predictions under the inverse conditions (NO_3^- in ASE and SO_4^{2-} in ACS). Zou et al. conclude that neither the nonideal Manning method nor the Kohlrausch's law method of estimating counter-ion transport selectivity is superior.

One advantage of fully predicting ion partitioning and diffusion in IEMs, which is enabled by the combined Donnan-Manning and Manning-Meares models, is that one may also predict process-based performance metrics. For IEMs, these metrics can include the permselectivity (Equation (3)), the membrane potential, or the current density of an ED stack. Although convenient, macroscopic quantities such as permselectivity can obfuscate the agreement between what is being modeled and what the collected data indicates. For example, a 0.2% error in a highly processed term such as permselectivity will lead to ~40% error in a simpler quantity such as the membrane selectivity, as defined by Equation (4).[18] Nevertheless, a membrane's permselectivity is a useful parameter to predict.

Kingsbury and Coronell employed the Manning-Meares model in a thorough experimental/modeling study of the permselectivity for several commercial IEMs: AMX, CMX, FAS-30, and FKE-30.[120] The authors developed a framework for predicting the apparent permselectivity of IEMs based on the extended Nernst-Planck equation. Their model accounted for the effects of non-idealities and water transport, both of which have been traditionally neglected in the broader literature.[121] Nonideal effects on ion partitioning in the IEMs were treated with the Donnan-Manning model. The Manning-Meares model (in its limited form, with the assumption that condensed counter-ions do not transport) was used to quantify diffusion coefficients in the IEMs. Finally, convective effects were accounted for through experimental measurements of water transport across the membranes. The authors compared the full version of the model to limited versions, in which some of the components were removed, seeking agreement between predicted and experimental permselectivity data at two extreme concentrations (0.5 and 4 M NaCl).

The full model predicted the experimental data well under conditions that resulted in high permselectivity (i.e., 0.5 M NaCl) but under-predicted the low permselectivity data (i.e., 4 M NaCl), as can be seen in Figure 33. Removing the contributions from Manning's model on partitioning and diffusion yielded better agreement between the modeled and experimental permselectivities at 4 M NaCl. These results suggest that the Donnan-Manning model does not perform well at such high concentrations. To add context to these results, we recall that Galizia et al. reported good predictions from the Donnan-Manning model for this concentration range of NaCl partitioning in CR61, but demonstrated

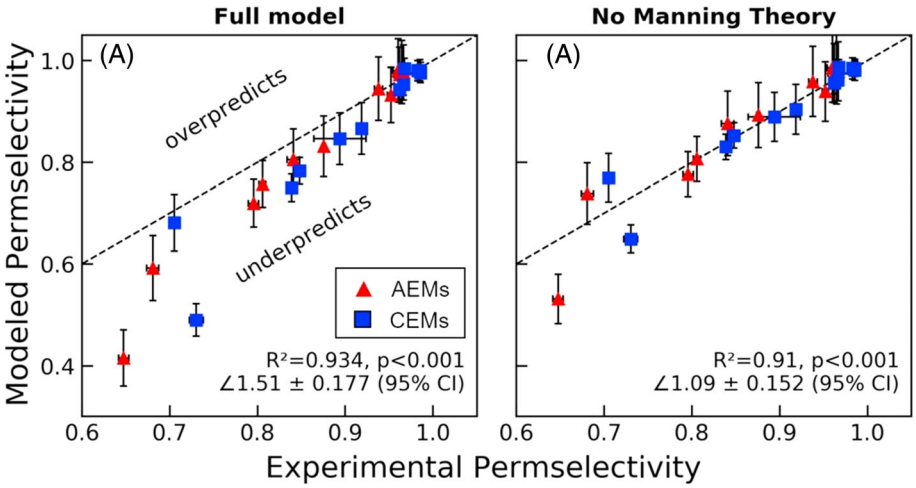

FIGURE 33 Parity plots of membrane permselectivity values predicted by Kingsbury and Coronell's framework and the experimentally measured values for AMX, CMX, FAS-30, and FKE-30 membranes.[120] Parity plots are displayed for (A) the full framework, which includes the Donnan-Manning model, the Manning-Meares model, and convection effects and (B) the framework without Manning's theory, which includes the ideal Donnan model, the Mackie and Meares tortuosity model, and convection effects. *Source*: Adapted with permission from Reference 120, 2021, Elsevier

that the ideal Donnan model was more accurate for such high concentrations of $CaCl_2$ partitioning in CR61.[47] The relatively poor agreement between modeled and experimental results observed by Kingsbury and Coronell for conditions with characteristically low IEM permselectivity suggests one of two conclusions: Potentially, the Donnan-Manning model does not fully capture the thermodynamic behavior of the studied IEMs at 4 M NaCl, perhaps due to their much lower water content relative to CR61. Alternatively, the Manning-Meares framework underestimates the ratio of counter- to co-ion diffusivity at 4 M NaCl. The authors concluded the latter, stating that the primary source of error in their full-model prediction was related to the poor prediction of counter-ion diffusion coefficients by the limited Manning-Meares model. Because Kingsbury and Coronell considered condensed counter-ions to be immobile, this is consistent with the idea that condensed counter-ions carry a significant fraction of the current across highly charged IEMs.[15]

Fan and Yip have also applied the limited Manning-Meares model (without condensed counter-ion transport) to ED and RED stacks.[122] They utilize the sorption predictions of the Donnan-Manning model in addition to the diffusion predictions of the Manning-Meares model to model the current density of an RED stack. The authors considered a 20-cell RED stack, outfitted with Fumasep FAD and FKE membranes and operated with feed solutions of 0.531 and 0.017 M NaCl. For all of the complexity that goes into such predictions, the combined framework successfully predicted the experimental current density of this RED stack (Figure 34). The predictions did not appear hampered by assuming condensed counter-ions to be immobile, despite the fact that the authors were predicting the results of electrically-driven experiments. Although the current density is the only experimentally validated prediction, Fan and Yip report additional data, using the framework to examine other ED process variables such as the current efficiency, the areal resistance, and the permselectivity of their modeled RED stack.

The complete version of the Manning-Meares diffusion model, which includes the contributions of condensed counter-ion diffusion, has not been tested against a broad set of materials and experimental conditions, so it is difficult to make generalized statements about the validity of this framework. Neglecting transport of condensed counter-ions appears to be acceptable for concentration gradient-driven transport, in which the co-ions govern the overall ion transport. In such scenarios, the salt permeability has been successfully predicted for multiple IEMs. The literature is inconclusive regarding electric field-driven transport, though results from the limited number of studies that used the complete diffusion model suggest that transport of condensed counter-ions is important in describing experimental results. Further investigation of electric field-driven ion transport in IEMs expected to exhibit condensation should illuminate the transport properties of condensed counter-ions.

3.3 | Computational ion diffusion studies

In this section, we highlight several computational studies which examine ion diffusion in IEMs in the context of counter-ion condensation. Without a consensus on which

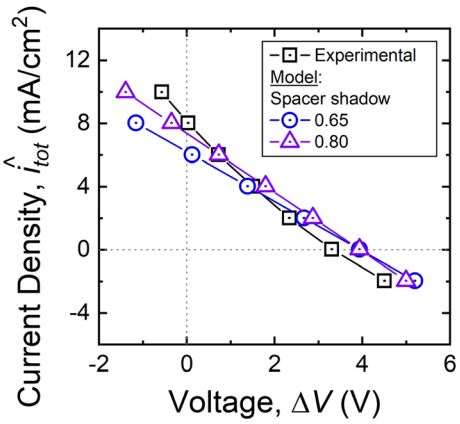

FIGURE 34 The current density of an RED stack plotted against the produced voltage.[122] The black squares represent experimental data based on a 20-cell stack with Fumasep FAD and FKE membranes and feed streams of 0.531 and 0.017 M NaCl. The blue circles and purple triangles represent predictions based on the Donnan-Manning/Manning-Meares models. The spacer shadow was not known, so two reasonable assumptions were used to predict the data. The choice of spacer shadow did not impact the accuracy of the predictions significantly. *Source*: Reproduced with permission from Reference 122, 2019, Elsevier

simulated counter-ions should be considered condensed (Section 2.3), the diffusivities of different populations of counter-ions become difficult to quantify and compare. Such uncertainties in defining counter-ion populations make it troublesome to query any specific assumptions of the Manning-Meares model, like the relative diffusivity of an uncondensed and condensed counter-ion. Nevertheless, we summarize recent progress in simulating ion diffusion in IEMs.

Motivated by experimental observations that Na^+ exhibited greater diffusivity than Cl^- in CEMs,[15] despite the reverse being true in solution, Aryal and Ganesan computed the diffusivities of counter- and co-ions in a styrenic CEM via molecular dynamics (MD) simulations. As was discussed in Section 2.3, Aryal and Ganesan identified various populations of counter- and co-ions in their MD simulations by considering the nearest neighbor of each mobile ion.[95–97] Across the series of manuscripts on this topic, which considered NaCl, KCl, and $MgCl_2$ salts, trends in ion diffusivities emerged between the different populations of counter- and co-ions. The authors reported that the diffusivities of condensed counter-ions are lower than those of uncondensed counter-ions. Furthermore, when co-ions ions enter the condensed layer alongside condensed counter-ions, the co-ions are also slowed compared with their free counterparts (Figure 35). It is interesting to note that, counterintuitively, the co-ions that enter the condensed layer are slowed to a greater extent than the condensed counter-ions, when compared with their respective free ions. Additionally, this population of counter-ion-coordinated co-ions in the condensation region around the polymer backbone dominated the simulated sorbed salts, making up the majority of the total co-ions in every case.[95–97] Taken together, the results of these simulations explained the greater diffusivity of Na^+ counter-ions relative to that of Cl^- co-ions in the CEM. The reversal is not caused by an increase in the diffusivity of condensed counter-ions, as suggested by Kamcev et al.,[15] but rather by a decrease in the diffusivity of condensed-conjugated co-ions. No quantitative comparison with experimental data was made, although Aryal and Ganesan invited this possibility by choosing simulation conditions similar to those used in the experimental study by Kamcev et al. Further studies are needed to reconcile the different explanations for enhanced counter-ion diffusivities in highly charged IEMs.

The mechanism of Li^+ counter-ion transport in an MD-simulated poly(allyl glycidyl ether-sulfonate) solution was investigated by Fong et al.[51] With battery separators as the intended use-case, these authors simulated fixed charge concentrations of 0.04–1 M using DMSO as the solvent. The counter-ions were described to be either free, in a solvent-separated ion pair (SSIP), or in a contact ion pair (CIP). These designations are analogous to uncondensed, territorially condensed, and site-wise condensed states, respectively (we discuss these distinctions further in Sections 2.1.1 and 2.3). Although the diffusivities of the various populations of counter-ions were not compared, Fong et al. highlighted the mechanism of transport for each population (Figure 36). As a baseline, the authors considered the free Li^+ ions to be taking moderately-sized diffusive steps at a moderate frequency. Compared with these free counter-ions, the SSIP (territorially condensed) Li^+ took smaller but more frequent diffusive steps, consistent with transport between densely packed, accessible regions along the polymer backbone. Meanwhile, the CIP (site-wise condensed) Li^+ took much larger diffusive steps than the free ions, but at a greatly reduced frequency. The method of diffusion for site-wise condensed ions is consistent with "hopping", wherein the random fluctuations of energy occasionally allow an ion to move from one fixed charge group to the next.

With this data, Fong et al. suggested that the condensed counter-ions contribute significantly to the conductivity of their system.[51] Such direct comparisons of the transport mechanism of each type of counter-ion indicate that both territorially and site-wise condensed counter-ions are able to execute diffusion steps. It would be interesting to probe the transport of site-wise condensed counter-ions in simulated aqueous conditions, where the solvation energy is much greater and therefore

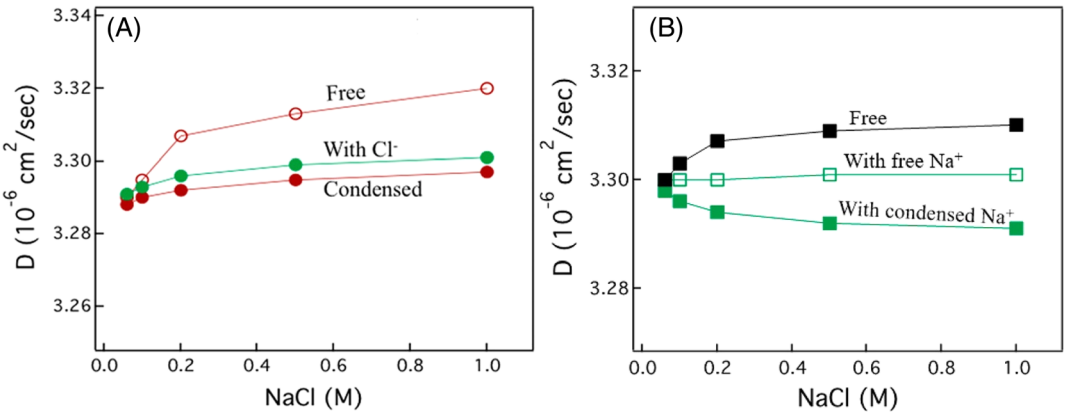

FIGURE 35 Simulated ion diffusivities in a styrenic CEM as a function of NaCl concentration.[96] (A) The diffusivity of free, condensed, and co-ion-coordinated counter-ions. (B) The diffusivity of free, counter-ion-coordinated, and condensed-counter-ion-coordinated co-ions. *Source*: Adapted with permission from Reference 96, 2018, American Chemical Society

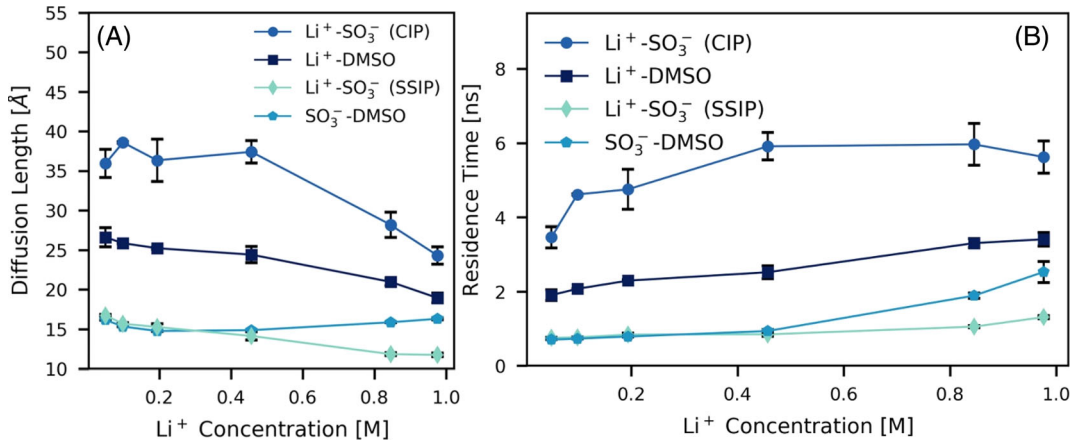

FIGURE 36 Simulated diffusion length and residence time of Li^+ counter-ions in poly(allyl glycidyl ether-sulfonate) dissolved in DMSO.[51] The counter-ion properties are distinguished based on the condensation state, listing the uncondensed (free or solvent-coordinated) Li^+, the territorially condensed (SSIP) Li^+, and the site-wise condensed (CIP) Li^+. Without a supporting membrane, the polymer's fixed charge groups also exhibited some minimal mobility. (A) Average length of a diffusive step. (B) Average residence time between diffusion steps. *Source*: Adapted with permission from Reference 51, 2019, American Chemical Society

the un-solvated site-bound counter-ions may face greater energy barriers to diffusion. Fong et al. also compared experimental data to their simulated conductivities, finding that their simulation over-predicted the ionic conductivities at all concentrations. However, the qualitative trends of the two data sets aligned well, suggesting that the simulation results capture the underlying phenomena occurring in the real system.

The MD simulation portion of Lei et al.'s study on block copolymer electrolytes (BCE), discussed in Section 2.3, also examined ion diffusion in the IEMs.[92] The authors studied ion partitioning and transport in a poly(styrene-b-pyridinium) BCE in contact with KI salt solutions between 0.0001 and 1 M. Different simulated ionic conductivity trends were observed depending on whether the membrane contacted solution droplets or humid air. The ionic conductivity decreased with increasing concentration when the BCE contacted humid air but increased with increasing concentration when the membrane contacted the salt solution. The authors also report a significant contribution toward conductivity from ions transporting via a hopping mechanism rather than a vehicular mechanism. Interestingly, the MD simulations yielded very different ionic conductivities depending on the driving force (or lack thereof). The ionic conductivities of membranes under equilibrium simulation conditions were much lower than those under an applied electric field. Under the electric field, the condensed counter-ions that transport via a hopping mechanism contributed to the overall transport, increasing the ionic conductivity tenfold. Such differences between the two simulated driving forces are very important and can be rationalized by assuming fixed charge groups (and therefore condensed counter-ions) are evenly

distributed. Without a large driving force, condensed counter-ions would not have enough thermal energy to execute their high-energy diffusion hopping steps. An applied electric field, however, provides this energy. We remind the reader that the simulations in this paper were performed under very low water content conditions ($\lambda \leq 6$), so site-wise condensation/ion-pairing is expected to significantly dominate territorial condensation—transport of territorially condensed counter-ions was not discussed in Lei et al.'s MD simulations.

Computational investigations are very relevant to modeling ion transport in IEMs because they have the ability to identify various populations of ions and permit researchers to monitor the diffusion of a single ion. The simulations results discussed in this section suggest that counter-ion condensation significantly affects the diffusion of counter-ions within IEMs. The simulations by Lei et al. are especially relevant because, although many MD simulations study self-diffusion under equilibrium conditions, these authors investigated electric potential driving forces. IEMs are generally used under an applied electric field, so this is an important condition to simulate. The mathematical treatment of the Manning-Meares model does not currently have any means to predict condensed counter-ion diffusion coefficients, so simulations may serve as a starting point for identifying the relevant membrane factors impacting condensed counter-ion diffusivity.

3.4 | Alternative membrane transport models

Competing models for ion diffusion coefficients are scarce—studies which predict ion diffusion are less common than those predicting ion sorption in IEMs. Two models have maintained the greatest prevalence in describing diffusion in solvent-swollen membranes: the Mackie and Meares tortuosity model and the Yasuda free-volume model.[123] The Yasuda model relates ion diffusivities to the fractional free volume of a membrane, which, according to Yasuda, is proportional to the water volume fraction.[124] Although there are proposed fundamental identities for the parameters appearing in the Yasuda model, it is frequently used with adjustable parameters because the actual values are unknown. The one-parameter Yasuda model is given by Equation (36):

$$\frac{D_i^m}{D_i^s} = \exp\left(B\left(1 - \frac{1}{\phi_w}\right)\right) \tag{36}$$

Here, B is an adjustable parameter. The Mackie and Meares model only considers tortuosity effects of the polymer, but does so predictively based upon the water volume fraction.[16,17,62] The Mackie and Meares model is discussed in greater detail as it applies to the Manning-Meares model in Section 3.1.

The Yasuda model has successfully described the transport of solutes in a wide variety of systems.[62,107,124–126] In general, experimental solute diffusivity data are described better by the Yasuda model than the Mackie and Meares model. Although appearing very different in their functional forms, and although they are derived by considering different phenomena, the Yasuda model and Mackie and Meares model predict a nearly identical relationship between diffusivity and water content. This analysis has been quantified by Galizia et al., where both models were reduced via a Taylor series.[125] The authors report that for high water content membranes ($\phi_w > 0.4$), a value of 1.5 for the Yasuda model adjustable parameter aligns the two models. Thus, the increased agreement of the single-parameter Yasuda model is primarily derived from the adjustable parameter, while the dependence of ion diffusion coefficients on membrane water content is not significantly different from that of the Mackie and Meares model.

Beyond considering just free volume and tortuosity effects, as the Yasuda model and Mackie and Meares model do, some interest has been given to the interaction of water and ions. Lei et al. suggested that this was the case based on their MD simulations in very low water content membranes, directly stating that solvation seems more relevant than condensation in the system they were studying,[92] although it is not currently clear how to predict data with such knowledge. Tran et al.[107] measured the freezable water contents of their membranes via DSC (see Section 2.4) and applied the one-parameter Yasuda model for ion diffusion coefficients in neutral, cationic, anionic, and zwitterionic membranes. By discounting water associated with ions or the polymer backbone, the freezable water content was thought to represent the actual volume of water available for ions to diffuse through. However, the authors observed worsened agreement between their modeled and experimental salt diffusion coefficients when using the freezable water content instead of the total water content. Tran et al. rationalized this result based on observed Nafion 117 proton conductivity at temperatures as low as −50 °C.[86] The authors claim that this observation supports the possibility of ion diffusion occurring through non-freezable water, and therefore such water should not be discounted.

The scarcity of alternative predictive models for ion diffusivities in IEMs is a testament to the difficulty of this task. The Mackie-Meares and the Yasuda models both represent common, generalizable models for solute diffusion in membranes, but neither allow for electrostatic interactions with the membrane, which seem to dominate the behavior of ions in IEMs. The Manning-Meares

model, though relatively new, has already brought the modeling of ion diffusion coefficients in IEMs to new frontiers.

4 | CONCLUSIONS

Manning's model for counter-ion condensation has become widespread within the literature studying ion partitioning and diffusion in IEMs. Through the Donnan-Manning model for ion partitioning and the Manning-Meares model for ion diffusivity, Manning's framework has become a ubiquitous predictor of experimental IEM transport properties. These models represent the most common method for predicting ion partitioning and are essentially the only method for predicting ion diffusion in these membranes a priori. The two parameters in these models which may be unknown, ξ and α, appear to be relatively constant for IEMs across a variety of experimental conditions. Thus, each model may be used semi-predictively with a calibrating data point even when the a priori prediction of these parameters is inadequate.

This review highlighted the expansive usage and discussion of Manning's framework applied to ion partitioning into IEMs. After presenting the equations and derivations of the Donnan-Manning model, we highlighted the wide variety of salts (i.e., monovalent electrolytes, divalent electrolytes, and organic acids) and membranes (i.e., commercial membranes, laboratory prepared membranes, heterogeneous membranes) which have been used to test the predictive capability of the Donnan-Manning model. NaCl partitioning into highly-charged, high-water-content IEMs was almost always described accurately. However, the model predictions were inadequate for some broad conditions: ions with complex associative behaviors, membranes with low charge densities, membranes with low water content, and membranes with complex or phase-separated morphologies were more likely to yield poor agreement between model and experiment. However, except for low charge density membranes, many of these non-predictable scenarios were described semi-predictively by the model. Molecular dynamics (MD) simulations have aided in understanding the phenomenon of counter-ion condensation, although no atomistic criterion for condensation has seen consistent use in these studies. Finally, several alternative models for IEM ion partitioning were highlighted, but these models have not seen the same extensive usage nor predictive power as the Donnan-Manning model.

This review also highlighted the usage and discussion of Manning's framework applied to ion diffusion into IEMs. The Mackie and Meares model was introduced to discuss the Manning-Meares model for ion diffusivities in IEMs, and the instances of its experimental application were compared. In general, researchers have restricted their usage of the Manning-Meares model to co-ions and uncondensed counter-ions only, with success in predicting NaCl permeabilities but inconclusive results for other salts. The condensed counter-ion diffusivity factor, α, has not been broadly applied or tested with experimental data. The importance of condensed counter-ion diffusion has been emphasized via MD simulations that address diffusivity alongside condensation. These studies frequently reported transport among condensed counter-ions and attributed significant fractions of membrane ionic conductivities to this population of counter-ions. Without any comprehensive alternatives to predicting ion diffusivity in IEMs, the characterization of condensed counter-ion transport represents a challenge at the forefront of our molecular understanding of IEMs.

When combined, the Donnan-Manning and Manning-Meares models have predicted membrane properties of interest, including their ionic conductivity, salt permeability, and permselectivity. As these models are applied to more systems, we anticipate further refinement to make both models more robust. Regardless, the successes of Manning's framework so far strongly support that counter-ion condensation plays an important role in the transport properties of IEMs.

ACKNOWLEDGMENTS

This material is based upon work supported by the National Science Foundation Graduate Research Fellowship under Grant No. DGE-1841052. This material is based upon work supported by the U.S. Department of Energy, Office of Science, Basic Energy Sciences under Award Number DE-SC0022040. The authors would like to express their gratitude to a collection of individuals for proofreading the manuscript and for discussing its contents. These individuals include: Cassidy Carey, José Díaz, Carolina Espinoza, Harsh Patel, Greg Reimonn, and Prof. Gerald Manning.

CONFLICT OF INTEREST

The authors declare no competing financial interest.

ORCID

David Kitto https://orcid.org/0000-0001-6863-2731
Jovan Kamcev https://orcid.org/0000-0003-0379-5171

REFERENCES

[1] T. Sata, *Ion Exchange Membranes*, Royal Society of Chemistry, Cambridge **2004**.

[2] F. Helfferich, *Ion Exchange*, Dover Science Books, New York **1995**.
[3] T. Luo, S. Abdu, M. Wessling, *J. Membr. Sci.* **2018**, *555*, 429.
[4] S. Adhikari, M. K. Pagels, J. Y. Jeon, C. Bae, *Polymer (Guildf).* **2020**, *211*, 123080.
[5] L. Gurreri, A. Tamburini, A. Cipollina, G. Micale, *Membranes (Basel).* **2020**, *10*, 1.
[6] P. Xiong, L. Zhang, Y. Chen, S. Peng, G. Yu, *Angew. Chem. Int. Ed.* **2021**, *60*, 24770.
[7] S. Jiang, H. Sun, H. Wang, B. P. Ladewig, Z. Yao, *Chemosphere* **2021**, *282*, 130817.
[8] S. P. Nunes, P. Z. Culfaz-Emecen, G. Z. Ramon, T. Visser, G. H. Koops, W. Jin, M. Ulbricht, *J. Membr. Sci.* **2020**, *598*, 117761.
[9] D. A. Salvatore, C. M. Gabardo, A. Reyes, C. P. O'Brien, S. Holdcroft, P. Pintauro, B. Bahar, M. Hickner, C. Bae, D. Sinton, E. H. Sargent, C. P. Berlinguette, *Nat. Energy* **2021**, *6*, 339.
[10] H. Luo, W.-A. S. Agata, G. M. Geise, *Ind. Eng. Chem. Res.* **2020**, *59*, 14189.
[11] P. Y. Apel, O. V. Bobreshova, A. V. Volkov, V. V. Volkov, V. V. Nikonenko, I. A. Stenina, A. N. Filippov, Y. P. Yampolskii, A. B. Yaroslavtsev, *Membr. Membr. Technol.* **2019**, *1*, 45.
[12] G. G. Eshetu, D. Mecerreyes, M. Forsyth, H. Zhang, M. Armand, *Mol. Syst. Des. Eng.* **2019**, *4*, 294.
[13] J. Kamcev, B. D. Freeman, *Annu. Rev. Chem. Biomol. Eng.* **2016**, *7*, 111.
[14] H. B. Park, J. Kamcev, L. M. Robeson, M. Elimelech, B. D. Freeman, *Science (80-.).* **2017**, *356*, 1138.
[15] J. Kamcev, D. R. Paul, G. S. Manning, B. D. Freeman, *Macromolecules* **2018**, *51*, 5519.
[16] J. S. Mackie, P. Meares, *Proc. R. Soc. London, Ser. A* **1955**, *232*, 498.
[17] J. Kamcev, D. R. Paul, G. S. Manning, B. D. Freeman, *ACS Appl. Mater. Interfaces* **2017**, *9*, 4044.
[18] J. Kamcev, *J. Polym. Sci.* **2021**, *59*, 2510.
[19] G. M. Geise, B. D. Freeman, D. R. Paul, *Polymer (Guildf).* **2010**, *51*, 5815.
[20] W. Xie, J. Cook, H. B. Park, B. D. Freeman, C. H. Lee, J. E. McGrath, *Polymer (Guildf).* **2011**, *52*, 2032.
[21] J. Kamcev, C. M. Doherty, K. P. Lopez, A. J. Hill, D. R. Paul, B. D. Freeman, *J. Membr. Sci.* **2018**, *566*, 307.
[22] J. Kamcev, M. Galizia, F. M. Benedetti, E.-S. Jang, D. R. Paul, B. D. Freeman, G. S. Manning, *Phys. Chem. Chem. Phys.* **2016**, *18*, 6021.
[23] G. S. Manning, *J. Chem. Phys.* **1969**, *51*, 924.
[24] G. S. Manning, *J. Chem. Phys.* **1969**, *51*, 934.
[25] G. S. Manning, *J. Chem. Phys.* **1969**, *51*, 3249.
[26] G. S. Manning, *Acc. Chem. Res.* **1979**, *12*, 443.
[27] G. S. Manning, *Ber. Bunsenges. Phys. Chem.* **1996**, *100*, 909.
[28] G. S. Manning, J. Ray, *J. Biomol. Struct. Dyn.* **1998**, *16*, 461.
[29] N. Kamo, Y. Toyoshima, H. Nozaki, Y. Kobatake, *Kolloid-Zeitschrift Zeitschrift für Polym.* **1971**, *248*, 914.
[30] S. Mafé, P. Ramírez, A. Tanioka, J. Pellicer, *J. Phys. Chem. B* **1997**, *101*, 1851.
[31] C. Arntsen, J. Savage, Y. L. S. Tse, G. A. Voth, *Fuel Cells* **2016**, *16*, 695.
[32] K. M. Beers, D. T. Hallinan, X. Wang, J. A. Pople, N. P. Balsara, *Macromolecules* **2011**, *44*, 8866.
[33] J. P. Gong, N. Komatsu, T. Nitta, Y. Osada, *J. Phys. Chem. B* **1997**, *101*, 740.
[34] J. Zhou, R. F. Childs, A. M. Mika, *J. Membr. Sci.* **2005**, *260*, 164.
[35] S. Takamuku, A. Wohlfarth, A. Manhart, P. Räder, P. Jannasch, *Polym. Chem.* **2015**, *6*, 1267.
[36] H. S. Dang, P. Jannasch, *J. Mater. Chem. A* **2016**, *4*, 17138.
[37] A. Wohlfarth, J. Smiatek, K. D. Kreuer, S. Takamuku, P. Jannasch, J. Maier, *Macromolecules* **2015**, *48*, 1134.
[38] J. Kamcev, D. R. Paul, B. D. Freeman, *Macromolecules* **2015**, *48*, 8011.
[39] G. S. Manning, *Eur. Phys. J. E: Soft Matter Biol. Phys.* **2011**, *34*, 34.
[40] J. O. Bockris, A. K. N. Reddy, *Modern Electrochemistry: Ionics*, Vol. 1. New York: Kluwer Academic Publishers; **1998**.
[41] G. S. Manning, *J. Phys. Chem.* **1984**, *88*, 6654.
[42] B. L. Rivas, I. Moreno-Villoslada, *J. Phys. Chem. B* **1998**, *102*, 6994.
[43] G. S. Manning, *Biophys. Chem.* **1977**, *7*, 95.
[44] G. S. Manning, *Q. Rev. Biophys.* **1978**, *11*, 179.
[45] A. Münchinger, K. D. Kreuer, *J. Membr. Sci.* **2019**, *592*, 117372.
[46] R. A. Robinson, R. H. Stokes, *Electrolyte Solutions*, Dover Publications, Inc.: Mineola, **1965**.
[47] M. Galizia, G. S. Manning, D. R. Paul, B. D. Freeman, *Polymer (Guildf).* **2019**, *165*, 91.
[48] N. Yan, D. R. Paul, B. D. Freeman, *Polymer (Guildf).* **2018**, *146*, 196.
[49] F. Oosawa, *Polyelectrolytes*, 1st ed., Marcel Dekker, Inc., New York **1971**.
[50] Y. Yu, Y. Li, N. Hossain, C. C. Chen, *Fluid Phase Equilib.* **2019**, *497*, 1.
[51] K. D. Fong, J. Self, K. M. Diederichsen, B. M. Wood, B. D. McCloskey, K. A. Persson, *ACS Cent. Sci.* **2019**, *5*, 1250.
[52] J. Ray, G. S. Manning, *Macromolecules* **1999**, *32*, 4588.
[53] G. S. Manning, *J. Phys. Chem. B* **2009**, *113*, 2231.
[54] A. V. Dobrynin, M. Rubinstein, *Prog. Polym. Sci.* **2005**, *30*, 1049.
[55] A. Deshkovski, S. Obukhov, M. Rubinstein, *Phys. Rev. Lett.* **2001**, *86*, 2341.
[56] A. Naji, R. R. Netz, *Phys. Rev. Lett.* **2005**, *95*, 3.
[57] C. Cametti, *Polymers (Basel).* **2014**, *6*, 1207.
[58] E.-S. Jang, J. Kamcev, K. Kobayashi, N. Yan, R. Sujanani, S. J. Talley, R. B. Moore, D. R. Paul, B. D. Freeman, *Macromolecules* **2019**, *52*, 2569.
[59] K. Chang, H. Luo, G. M. Geise, *Macromolecules* **2021**, *54*, 637.
[60] K. Chang, H. Luo, S. M. Bannon, S. Y. Lin, W. A. S. Agata, G. M. Geise, *J. Membr. Sci.* **2021**, *630*, 119298.
[61] K. Chang, G. M. Geise, *Ind. Eng. Chem. Res.* **2020**, *59*, 5205.
[62] H. Zhang, G. M. Geise, *J. Membr. Sci.* **2016**, *520*, 790.
[63] L. Brannon-Peppas, N. A. Peppas, *Chem. Eng. Sci.* **1991**, *46*, 715.
[64] J. Crank, G. S. Park, *Diffusion in Polymers*, 1st ed., Academic Press Inc., New York **1968**.
[65] N. Lakshminarayanaiah, *Transport Phenomena in Membranes*, 1st ed., Academic Press, Inc., New York **1969**.

[66] G. M. Geise, L. P. Falcon, B. D. Freeman, D. R. Paul, *J. Membr. Sci.* **2012**, *423–424*, 195.
[67] E. Glueckauf, R. E. Watts, *Proc. R. Soc. London, Ser. A* **1962**, *268*, 339.
[68] K. S. Pitzer In Annual Meeting of the Geological Society of America **1987**;
[69] H. T. Kim, W. J. Frederick, *J. Chem. Eng. Data* **1988**, *33*, 278.
[70] J. M. Simonson, K. S. Pitzer, *J. Phys. Chem.* **1986**, *90*, 3009.
[71] J. Kamcev, D. R. Paul, B. D. Freeman, *Desalination* **2018**, *446*, 31.
[72] D. H. Freeman, V. C. Patel, T. M. Buchanan, *J. Phys. Chem.* **1965**, *69*, 1477.
[73] G. E. Boyd, K. Bunzl, *J. Am. Chem. Soc.* **1967**, *89*, 1776.
[74] R. L. Gustafson, *J. Phys. Chem.* **1963**, *67*, 2549.
[75] R. L. Gustafson, *J. Phys. Chem.* **1966**, *70*, 957.
[76] M. Galizia, D. R. Paul, B. D. Freeman, *J. Membr. Sci.* **2020**, *612*, 118410.
[77] M. Galizia, F. M. Bendetti, D. R. Paul, B. D. Freeman, *J. Membr. Sci.* **2017**, *535*, 132.
[78] R. S. Kingsbury, S. Zhu, S. Flotron, O. Coronell, *ACS Appl. Mater. Interfaces* **2018**, *10*, 39745.
[79] A. Hassanvand, G. Q. Chen, P. A. Webley, S. E. Kentish, *Desalination* **2017**, *417*, 36.
[80] J. Wang, R. S. Kingsbury, L. A. Perry, O. Coronell, *Environ. Sci. Technol.* **2017**, *51*, 2295.
[81] C. L. Ritt, J. R. Werber, M. Wang, Z. Yang, Y. Zhao, H. J. Kulik, M. Elimelech, *Proc. Natl. Acad. Sci. U. S. A.* **2020**, *117*, 30191.
[82] G. Q. Chen, K. Wei, A. Hassanvand, B. D. Freeman, S. E. Kentish, *Water Res.* **2020**, *175*, 115681.
[83] Q. Wang, G. Q. Chen, S. E. Kentish, *J. Membr. Sci.* **2020**, *614*, 118534.
[84] Y. Yu, N. Yan, B. D. Freeman, C. C. Chen, *J. Membr. Sci.* **2021**, *620*, 118760.
[85] Y. Ji, H. Luo, G. M. Geise, *J. Membr. Sci.* **2018**, *563*, 492.
[86] A. Kusoglu, A. Z. Weber, *Chem. Rev.* **2017**, *117*, 987.
[87] J. Peng, T. A. Zawodzinski, *J. Membr. Sci.* **2020**, *593*, 117340.
[88] R. Sujanani, L. E. Katz, D. R. Paul, B. D. Freeman, *J. Membr. Sci.* **2021**, *638*, 119687.
[89] M. W. Verbrugge, R. F. Hill, *J. Phys. Chem.* **1988**, *92*, 6778.
[90] J. Kamcev, D. R. Paul, B. D. Freeman, *J. Mater. Chem. A* **2017**, *5*, 4638.
[91] M. V. Ramos-Garcés, K. Li, Q. Lei, D. Bhattacharya, S. Kole, Q. Zhang, J. Strzalka, P. P. Angelopoulou, G. Sakellariou, R. Kumar, C. G. Arges, *RSC Adv.* **2021**, *11*, 15078.
[92] Q. Lei, K. Li, D. Bhattacharya, J. Xiao, S. Kole, Q. Zhang, J. Strzalka, J. Lawrence, R. Kumar, C. G. Arges, *J. Mater. Chem. A* **2020**, *8*, 15962.
[93] M. Ballauff, A. Jusufi, *Colloid Polym. Sci.* **2006**, *284*, 1303.
[94] G. S. Manning, *Soft Matter* **2014**, *10*, 3738.
[95] D. Aryal, V. Ganesan, *J. Phys. Chem. B* **2018**, *122*, 8098.
[96] D. Aryal, V. Ganesan, *ACS Macro Lett.* **2018**, *7*, 739.
[97] D. Aryal, V. Ganesan, *J. Chem. Phys.* **2018**, *149*, 1.
[98] B. Vondrasek, C. Wen, S. Cheng, J. S. Riffle, J. J. Lesko, *Macromolecules* **2021**, *54*, 302.
[99] A. Katchalsky, I. Michaeli, *J. Polym. Sci.* **1955**, *15*, 69.
[100] K. B. Goh, H. Li, K. Y. Lam, *Electrochim. Acta* **2019**, *297*, 307.
[101] E. S. Jang, J. Kamcev, K. Kobayashi, N. Yan, R. Sujanani, T. J. Dilenschneider, H. B. Park, D. R. Paul, B. D. Freeman, *Polymer (Guildf).* **2019**, *178*, 121554.
[102] P. J. Flory, *Principles of polymer chemistry*, 1st ed., George Banta Publishing Company, Ithaca **1954**.
[103] J. C. Bray, E. W. Merrill, *J. Appl. Polym. Sci.* **1973**, *17*, 3779.
[104] J. E. Bara, C. J. Gabriel, T. K. Carlisle, D. E. Camper, A. Finotello, D. L. Gin, R. D. Noble, *Chem. Eng. J.* **2009**, *147*, 43.
[105] N. R. Richbourg, N. A. Peppas, *Prog. Polym. Sci.* **2020**, *105*, 101243.
[106] M. Zhong, R. Wang, K. Kawamoto, B. D. Olsen, J. A. Johnson, *Science (80-.).* **2016**, *353*, 1264.
[107] T. Tran, C. Lin, S. Chaurasia, H. Lin, *J. Membr. Sci.* **2019**, *574*, 299.
[108] B. Vondrasek, C. Wen, S. Cheng, J. S. Riffle, J. J. Lesko, *Macromolecules* **2021**, *54*, 6477.
[109] A. Breytus, D. Hasson, R. Semiat, H. Shemer, *Sep. Purif. Technol.* **2019**, *226*, 252.
[110] J. D. Wells, *Biopolymers* **1973**, *12*, 233.
[111] A. A. Rashin, B. Honig, *J. Phys. Chem.* **1985**, *89*, 5588.
[112] T. T. Duignan, X. S. Zhao, *Phys. Chem. Chem. Phys.* **2020**, *22*, 25126.
[113] B. Roux, H.-A. Yu, M. Karplus, *J. Phys. Chem.* **1990**, *94*, 4683.
[114] Y. Song, C. C. Chen, *Ind. Eng. Chem. Res.* **2009**, *48*, 7788.
[115] G. S. Manning, *J. Chem. Phys.* **1993**, *99*, 477.
[116] G. S. Manning, *Eur. Phys. J. E: Soft Matter Biol. Phys.* **2011**, *34*, 39.
[117] J. G. Wijmans, R. W. Baker, *J. Membr. Sci.* **1995**, *107*, 1.
[118] T. Luo, Y. Zhong, D. Xu, X. Wang, M. Wessling, *J. Membr. Sci.* **2021**, *629*, 119263.
[119] Z. Zou, L. Wu, T. Luo, Z. Yan, X. Wang, *J. Membr. Sci.* **2021**, *635*, 119496.
[120] R. S. Kingsbury, O. Coronell, *J. Membr. Sci.* **2021**, *620*, 118411.
[121] J. Kamcev, D. R. Paul, G. S. Manning, B. D. Freeman, *J. Membr. Sci.* **2017**, *537*, 396.
[122] H. Fan, N. Y. Yip, *J. Membr. Sci.* **2019**, *573*, 668.
[123] L. Masaro, X. X. Zhu, *Prog. Polym. Sci.* **1999**, *24*, 731.
[124] H. Yasuda, C. E. Lamaze, L. D. Ikenberry, *Die Makromol. Chemie* **1968**, *118*, 19.
[125] M. Galizia, D. R. Paul, B. D. Freeman, *Polymer (Guildf).* **2016**, *102*, 281.
[126] A. C. Sagle, H. Ju, B. D. Freeman, M. M. Sharma, *Polymer (Guildf).* **2009**, *50*, 756.

AUTHOR BIOGRAPHIES

David Kitto earned his bachelor's degrees in chemical engineering and chemistry from the University of Minnesota – Twin Cities in 2019. While there, he researched nonwoven polymer fiber processing under the guidance of Professor Chris Ellison. Since 2019, David has been a PhD student studying ion exchange membranes with Professor Jovan Kamcev at the University of Michigan – Ann Arbor. His work focuses on understanding transport and equilibrium properties of aqueous polymer

membranes through mathematical modeling and experimental investigation of ion-specific effects.

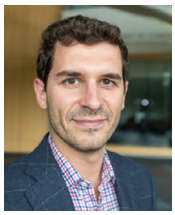

Prof. Jovan Kamcev is an Assistant Professor of Chemical Engineering and Macromolecular Science & Engineering at the University of Michigan. He completed his postdoctoral training in Chemistry at University of California, Berkeley under the guidance of Prof. Jeffrey Long. He earned his PhD in Chemical Engineering in 2016 from The University of Texas at Austin under the guidance of Profs. Benny Freeman and Donald Paul. His research group aims to develop next-generation polymeric materials (e.g., membranes and sorbents) for water treatment and energy generation/storage applications by implementing an integrative approach based on materials synthesis, advanced characterization, and modeling.

SUPPORTING INFORMATION

Additional supporting information may be found in the online version of the article at the publisher's website.

How to cite this article: D. Kitto, J. Kamcev, *J. Polym. Sci.* **2022**, *60*(21), 2929. https://doi.org/10.1002/pol.20210810